"Drug-Delivering" biopolymer – Caf1

Cheney Chen Hang Leung

Newcastle University

A thesis submitted for the degree of
Doctor of Philosophy in Chemistry

School of Natural and Environmental Sciences
Newcastle University

2023

Abstract of the Dissertation

"Drug-Delivering" biopolymer – Caf1

Tuneable Hydrogel System for Bio-applications

Cheney Chen Hang Leung

The thesis explores biopolymer-based hydrogel in the ever-growing "drug delivery" field – an approach to deliver pharmaceutical compounds to their targeted sites safely and effectively by tailoring the carrier for specific applications. This work reports the initial finding of Caf1 as a drug delivery vehicle to deliver drug molecules. Caf1 is a biopolymer produced by Yersinia pestis, the bacterium known for bubonic plague. The biopolymer act as a cloak for the bacterium shielding it from macrophages, and it has properties close to the extracellular matrix, which makes the material ideal for drug delivery due to its biocompatibility. A Caf1 protein polymer comprises several Caf1 subunits (monomers) linked together via donor strand exchange, where one subunit donates its N-terminal β-strand for acceptance on the adjacent subunit to form a polymer chain. This key mechanism is unique from this class of protein.

Herein, this thesis investigates the usability of crosslinked Caf1 hydrogels for drug delivery applications and the associated challenges that comes with it. Chapter 1 explores the use of biopolymers for drug delivery in literature and proposes strategies that utilise Caf1 polymer for "drug delivery" purposes. Chapter 2 explores the methodology to afford Caf1 hydrogel suitable for uploading model drugs from small molecules to large biomolecules and analyses the subsequence release profiles to further understand the mechanism that took place. Further, this work proposes several drug-loading approaches for loading biomolecules by utilising the unique reversible nature of Caf1 protein linkages where the Caf1 protein linkage can undergo thermal unfolding and reform. Chapter 3 proposes a stimulus-responsiveness mechanism for Caf1 hydrogel by modifying native Caf1 polymer with cysteine residues, inducing a cleavable disulfide bridge within the

hydrogel network, which will lead to the release of the model drug. Further, this chapter investigates a novel mosaic hydrogel consisting of two types of Caf1 subunit containing both Caf1WT and Caf1Cys subunits to improve the mechanical properties of a stimulus-responsiveness Caf1 hydrogel. Chapter 4 describes the term "nanogel" and exploits synthetic approaches to form such Caf1 nanogels, that can be functionalised with specific groups for specific application purposes. In conclusion, these findings laid a fundamental bedrock for the consequent development of Caf1 polymer; for release kinetics, drug loading, stimuli-responsive and nanoparticles, which showcases the versatility of Caf1 as an exciting novel material for biomedical purposes.

Acknowledgements

I would like to take this opportunity to thank all those who have contributed to the work in this thesis. Firstly, my thanks must go to my PhD supervisor Dr David Fulton for his constant guidance, patience, and encouragement, and most of all for providing such an inviting research environment, that has allowed me to develop into a scientist. For this opportunity and mentorship, I am truly grateful.

I have also been fortunate to work alongside and collaborate with some remarkably talented scientists during my time at Newcastle. I would like to thank Dr Gema Dura for her continuous support and belief, whose work ethic has been truly inspirational. I would like to thank her for her mentorship and friendship.

Thank you to Prof. Jeremy Lakey and his research group at Newcastle University for providing the Caf1 proteins, without it this project would have not been possible. I thank Dr Dan Peters and Dr Helen Waller who have been so generous with their time and guidance on protein synthesis and purification.

Thanks to all my friends I have met whilst working in the Chemical Nanoscience laboratory. Dr Liam Mistry, Pablo Rojas-Martinez, Dr Milene Dalmina, Dr Patrick Higgs, Dr Osama El-Zubir, without them my PhD would have never been so gratifying.

I would also like to acknowledge my fellow peers in Chemistry, Biology and Pharmaceuticals for their ingenuity and help during my PhD. Also, all the technical staff for their support in both hardware and software.

Last but never the least, my deepest thank my partner Lydia Tam for her sacrifices that have allowed me to pursue with my education. Thanks to my parents Kam Chuen and Yuk King, my brothers Luke and David without their support this would have not been possible. You have played a huge part during these few years, for which I am very grateful.

Table of Contents

Table of Figures

Table of Tables

Abbreviations

μg	Micrograms
μL	Microlitre
AFM	Atomic Force Microscopy
BSA	Bovine serum albumin
Caf1	Capsular antigen fraction 1
Da	Dalton
DLS	Dynamic light scattering
DMF	Dimethylforaminde
DMSO	Dimethylsulfoxide
E. coli	Escherichia coli
FITC	Fluorescein isothiocyanate
GA	Glutaraldehyde
GSH	Glutathione
G'	Storage modulus
G"	Loss modulus
h	Hour
IEP	Isoelectric point
Ka	Association constant
LVE	Linear viscoelastic range
mg	Milligram
min	Minute
MHz	Megahertz
mL	Millilitre
mM	Millimolar
Mn	Number average molecular weight
Mw	Weight average molecular weight
MW	Molecular weight
MWCO	Molecular weight cut-off
NMR	Nuclear magnetic resonance
NG	Nanogels
NPs	Nanoparticles
PBS	Phosphate-buffered saline
PD	Polymer dose
PDI	Polydispersity index
PEG	Poly(ethylene) glycol
PEG-SG	Poly(ethylene) glycol – Succinimidyl Glutarate
PEG-SH	Poly(ethylene) glycol – Sulfhydryl

ppm	Parts per million
rt	Room temperature
SDS-PAGE	Sodium dodecyl sulfate-polyacrylamide gel electrophoresis
TEM	Transmission electron microscopy
UV	Ultraviolet
UV-Vis	Ultraviolet-visible
ZP	Zeta potential

Chapter 1
Natural polymer in drug delivery

Table of Contents

1.1. Overview

Hydrogels are of interest in the field of drug delivery because of their ability to prolong drug release and their capacity to be tailored into any practical size or shape according to the requirements. Recently, interest in biopolymer-based hydrogels has increased due to their excellent levels of biocompatibility. This chapter reviews a selection of literature examples showcasing hydrogels' advantages for drug delivery applications. Biopolymer Caf1 secreted from Y. pestis is considered a good candidate to produce biomaterial due to its definable bioactivity, economical production, and ability to form hydrogels. A strategy to exploit the Caf1 polymer for drug delivery and applications is proposed.

1.2. Introduction

Recent advancements in hydrogel research have led to a phenomenal outbreak in biomedical application developments[1] such as cellular therapies,[2] imaging,[3,4] tissue engineering,[5] drug delivery[6] and other novel applications. The ever-increasing emergence of drug resistance in communicable and non-communicable diseases has also highlighted the need for more efficient drug delivery systems to prolong therapeutics' effectiveness and targeted delivery.[7] The fine tunability of characteristics of hydrogels offers a promising approach to fulfilling those requirements since hydrogels can be fabricated using different biodegradable and biocompatible polymers which are responsive to external stimuli, such as changes in pH, temperature and ion content.[8] In addition, drug delivery using hydrogels has also helped to tackle the issues associated with patient compliance, drug toxicity, and adverse side effects caused by prolonged therapy.[9] Herein, this chapter will review selected literature examples of hydrogels applied in the field of drug delivery.

1.2.1. What is a hydrogel?

Hydrogels are three-dimensional networks of polymeric materials that retain a large quantity of water. Hydrogels are mainly separated into two categories **(Figure 1.1)**, "physical" hydrogels and "chemical" hydrogels.10 Physical crosslinking occurs under mild conditions, which is ideal for entrapping labile compounds such as proteins. However, a physical hydrogel is mostly mechanically weak and can be disrupted by

changes in exterior conditions (pH, temperature, and ionic strength) when compared to a chemically crosslinked hydrogel. Chemical crosslinking hydrogels can be obtained by several methods, such as photo-polymerisation of poly(ethylene glycol) (PEG) (meth)acrylates.[10]

Polymer chains

crosslink

Chemical Hydrogel
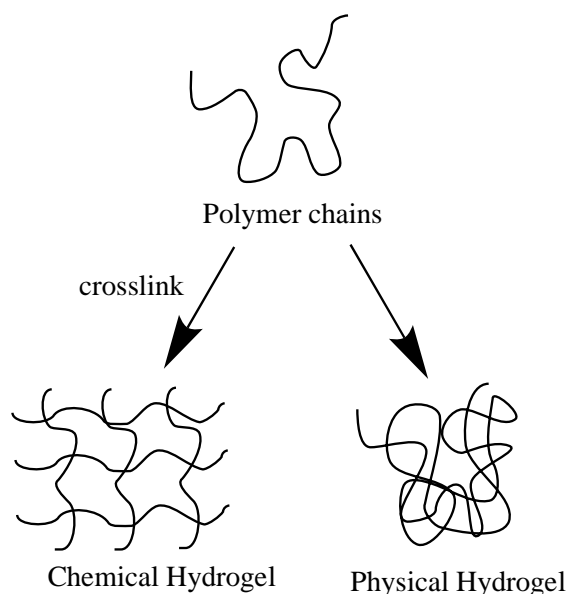
Physical Hydrogel

Figure 1.1, Schematic diagram indicates different types of crosslinking with hydrogel networks,[1] namely chemical and physical hydrogels.

Hydrogels have existed as a topic of academic and industrial research for more than half a century; the history of hydrogels can be separated into three generations.[11,12] First-generation hydrogels were developed using various crosslinking procedures to crosslink polymer chains into water-filled networks.[13] Second-generation hydrogels, inspired by the work of Katchalsky[14] on the possibility of transferring chemical energy into mechanical work, consist of materials capable of responding to specific stimuli, such as variations in pH, temperature or change in concentration of particular molecules in solutions.[15] The third generation of hydrogel research comprises the investigation and development of stereo-complex materials that consist of complementing stereoregular polymers that "interlock" through physical interactions.[15] The progression in hydrogel research has led to an increase in the development of "smart hydrogels'; polymeric matrices with a wide range of tuneable properties and stimuli-responsiveness properties. Hydrogels can be prepared by *in* situ formulation via covalent crosslinking between polymers with complementary

functional groups under physiological conditions with minimal toxicity.[16,8] Double network hydrogels that consist of the combination of various chemical and structural properties exhibit responsiveness to external stimuli, including pH, temperature, ionic concentration, UV, magnetic fields, electrical fields and chemicals where the systems change their structural and volume phase transition in response to external stimuli.[15] The combination of these features leads to hydrogels with tailored properties such as mechanical stability and release kinetics for the desired applications and the enormous potential for hydrogels applications.[11]

1.2.2. What is drug delivery?

Drug delivery describes technologies involved in transporting a pharmaceutical compound to its target site. The subject covers a wide range of moving parts, from formulations; manufacturing techniques; to storage solutions. While it might seem complicated at first glaze, the aim of drug delivery remained the same. The principles for the studies around the subject of drug delivery are to optimise efficacy and safety and to improve patient convenience and compliance. Among the developed technologies with recent advancements in drug delivery development, hydrogels have gained a vast interest due to their wide range of tuneable physical properties such as controllable degradability, protect labile drugs from degradations and induced physiochemical interactions between the hydrogel network and dug cargo to control drug release **(Figure 1.2)**.[9,17] These flexibility in the design of hydrogel have led to successful research in delivering small-molecule drugs, macromolecular drugs and cells.
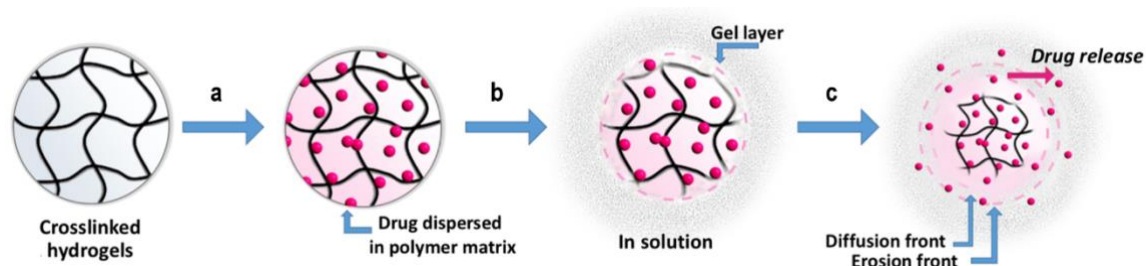
Figure 1.2, Scheme showing drug uptake and release with a model drug from Caf1-based hydrogels. **(a)** Drug uptake within the polymer matrix. **(b)** The outer layer of the gel becomes softened and swells. **(c)** Drug release at a time at 0 h. The drug is diffused from the polymer matrix, and/or gel erosion leads to drug release.

For the past several decades, the development of hydrogel drug delivery systems has been aided by advances in material chemistry, polymer physics, fabrication techniques and the fundamental understanding of tissues and cell biology.[18] More than 14,832 papers on hydrogel drug delivery systems have been published (according to a search for "hydrogel drug delivery" in PubMed, June 2023), demonstrating that the field is very active. Although recent research has demonstrated the possibility of multiple drugs release,[9] obtaining the release of chemically distinct molecules at different rates and side effects remains challenging. It is hypothesised that an ideal drug delivery system can precisely release drugs in response to stimuli change or upon demand. In recent research, many systems demonstrated on-demand drug release, but only a few have demonstrated low baseline release where no trigger has been applied to induce drug release. Additionally, the ability to exhibit triggered release repeatedly has been of great interest.[19] Resulted in a growing development of drug delivery systems that provide reliable, robust stimuli responses that necessitate new chemical strategies and control principles. Furthermore, any drug delivery depot will eventually become exhausted of its drug cargo, and a method to reload the depot with the same or different drug could be useful in many settings. Although drug-polymer interactions are typically exploited to allow for drug loading and controlled release, they may also be used to reload drug delivery depots that are already present in the body.[20] This concept depends on a very high specificity of the drug-polymer bond, which ensures that the drug does not bind indiscriminately to other molecules in the body. Although still at an early stage, both complementary base pairing using DNA molecules and bio-orthogonal click chemistries have been used to reload hydrogels many times, to differentially load two or more hydrogels present in the body with distinct drugs and to slow tumour growth.[21–23]
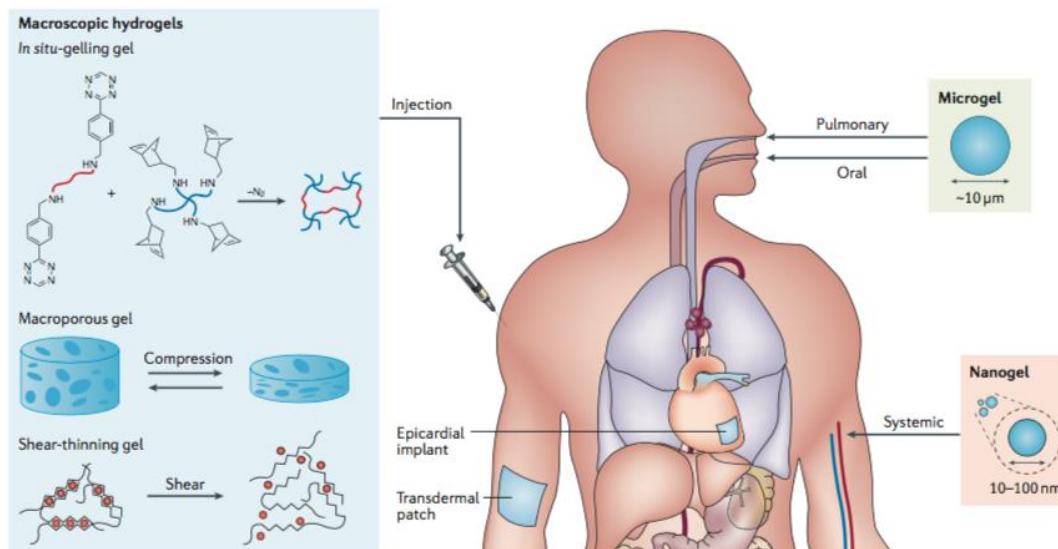
Figure 1.3, Macroscopic design determines the delivery route. Macroscopic hydrogels are used for transepithelial delivery and placement inside the body. Injectable macroscopic hydrogels including in-*situ*-gelling hydrogels with shear-thinning and macroporous hydrogels that can undergo reversible dramatic volumetric change. Microgels that are used for oral, pulmonary and intrabody delivery and nanogels are suitable for the systemic administration of drugs. Reproduced with permission from ref. 9, copyright of Springer Nature 2016.

The flexibility in the formation of hydrogels enabled them to be cast or formed into any shape and size according to the requirements of the delivery route into the human body. Hydrogel delivery systems can be classified into three main categories based on their size: macroscopic hydrogels, microgels and nanogels **(Figure 1.3)**. A novel application is to utilise the shear-thinning properties of the hydrogels that loses its three-dimensional structure upon on application of shear stress, that behave like low-viscosity fluids under shear stress during administration via injection, and quickly recover their initial structure after removal of shear stress. These types of hydrogels can be approached using reversible physical crosslinks or dynamic covalent bonds, as shown by the work of Lee *et al.*[24] on hyaluronic acid/Pluronic (poloxamer triblock polymer) hydrogels. The hydrogels could be injected *in vivo* in a solution state at room temperature, but immediately becomes a robust gel at body temperature. Their work shows the potential use of a physical hydrogel in drug delivery. Another class of hydrogel known as "In *situ*-gelling" hydrogels are systems that can be injected in a liquid state and undergo a sol-gel transition (The term "sol-gel transition" describes a

material that transitions from a liquid state colloidal solution (sol) into a solid/semisolid state nonfluid colloidal material (gel)) inside the body due to the temperature-responsive polymer used.[25] In addition, macroporous hydrogels can be used; these are hydrogels with interconnected pores that can mechanically collapse and recover reversibly. Despite having many advantages, such as simple fabrication and good mechanical properties, interlinked pores may significantly reduce the diffusion length for drug release, and the volume fraction of polymers could potentially lead to rapid release and limited drug loading capacity.[26,27]

Progress in bioelectronics and emerging areas such as gene editing highlight new opportunities for controlled drug delivery by utilising microelectronics and membrane reservoirs.[9,28] It is hypothesised that the conjunction of bioelectronics with hydrogel can lead to the creation of next-generation bioelectronics that can monitor the human body continuously and regulate it by releasing the required therapeutics accordingly. Hydrogels are used as carriers in drug delivery systems because of their capacity to encapsulate and release drug molecules.[29–31] A efficient drug delivery means controlling the drug release rate and avoiding aggregation, where the drug cargo becomes permanently trapped within the network.[32,33] The physical properties of the network, such as shape, volume and size distribution, influence the behaviour of porous medium. Pores are formed during hydrogel synthesis by phase separation or as small pockets within the network. The average pore size, the pore size distribution, and the pore interconnections are important factors of a hydrogel matrix that are often described by the parameter known as "tortuosity".[1] Tortuosity, τ, is a determinant used in continuum models to estimate effective flow and transfer phenomena inside the porous materials, it is a ratio that defines the convoluted pathways of actual flow through a porous medium. The tortuosity of material is investigated by determining the permeability, K, of porous material using the Kozeny-Carman relationship **(Equation 1.1)**,[34] where the Kozeny-Carman constant, C_{KC}, describes the shape factor of the material, and porosity, φ, and specific surface area, S. In a porous medium, a drug molecule within the network would naturally diffuse away from the entrapped network driven by an osmotic effect. The lesser porosity compared to the surface area a material has the lesser permeable it will become as shown in **Equation 1.1**, lower

permeability will impede molecular movement and lead to slower molecular diffusion.[28,34]

$$K = \frac{1}{C_{KC}} \frac{\varphi^3}{S^2 \tau^2} \qquad \textbf{(Equation 1.1)}$$

Drug molecule diffusion rate within the porous material is restricted by hydrogel thickness, the ratio of the pore volume fraction and tortuosity.[34] These factors are influenced by the composition and crosslink density of the hydrogel polymer network.[35] The drug molecule's size and shape, its relative hydrophilic and hydrophobic character, and the availability of 'free' water molecules to hydrate and dissolve the drug molecule are important factors governing solute permeation through hydrogel matrices. The uniformity of a drug-loaded within a hydrogel depends upon the size, shape, net charge, and the total available "*free*" water within a hydrogel network.[35,36] The release of a drug molecule from a hydrogel is governed mainly by pore size fraction, interconnections between polymer chains, size of the cargos, the crosslink density of the networks, and the interactions between drug molecules and polymer chains.[31] Thus, in designing a hydrogel network for the controlled release of a drug, it will be necessary to 'match' the polymer composition and crosslink density and mesh size with the particular size and composition of the drug molecule to be delivered (**Figure 1.4**).

The basic understanding of drug release mechanisms for hydrogel systems has been studied using mathematical modelling.[37,38] However, many parameters in existing models are unknown and remain to be quantified. In particular, the modelling of *in vivo* drug release has been explored to an insufficient extent despite its significance,[39] this is due to the unpredictable condition in a physiological environment. An integrated understanding of drug release and transport through the local tissues will be able to facilitate the development of drugs and drug delivery systems.
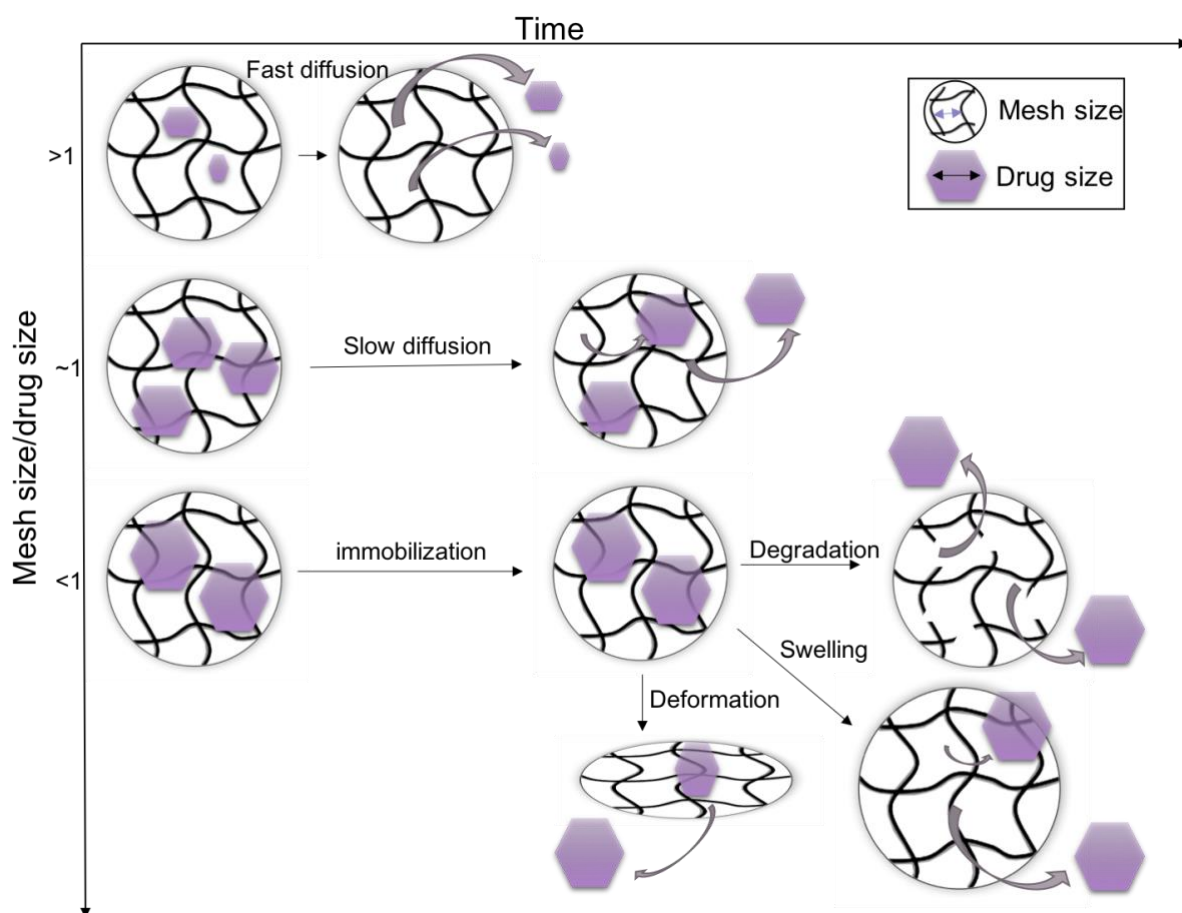
Figure 1.4, Mesh size mediates drug diffusion rate. A small drug relative to the mesh size diffuses rapidly through the hydrogel, resulting in a short release duration. As the size of the drug approaches the mesh size, the drug release slows dramatically. When the drug is larger than the mesh size, the drugs are physically entrapped inside the network. The immobilised drug can be released through enlargement of the network by its degradation, swelling or deformation. The arrow refers to the diffusion pathway of drugs. Reproduced with permission from ref. 8, copyright of Springer Nature 2016.

A hydrogel's water: polymer ratio determines solute molecules' absorption and diffusion characteristics. As a dry hydrogel begins to hydrate, the first water molecules[40,41] entering the matrix will hydrate the most polar groups, known as '*primary bound waters'*. As the network swells, it exposes hydrophobic groups that interact with water molecules, leading to "*secondary bound waters*". The combination of the two interactions is known as "*total bound water*". The network will then absorb the additional water in a process driven by osmotic force, causing the network to swell toward infinite dilution. This swelling is opposed by the covalent or physical crosslinks, leading to an elastic network retraction force, and thus, the hydrogel will reach an

equilibrium state which depends on the gelation conditions. The additional water absorbed is often referred to as "*free water*" or "*bulk water*"[1] that fills the space between the network chains, pores, macrospores or voids. As the network swells to infinite volume, any degradable network chains or crosslinks present will begin to disintegrate and dissolve at a rate depending on its composition.[29] The swelling property can be evaluated by measuring the dry weight and swollen weight of the gel **(Equation. 1.2)**,[1] the evaluation can be used as a measurement of stability.

$$Swelling\ index = \frac{Swollen\ weight - dry\ weight}{Dry\ weight} \times 100 \qquad \textbf{(Equation 1.2)}$$

1.2.3. An example of drug delivering physical hydrogel

Hydrogels described as 'reversible' or 'physical' gels, encompass systems where chains are linked together by molecular entanglements and secondary forces, including ionic, H-bonding or hydrophobic forces.[42] In 2019, Björnmalm et al.[43] reported an in vivo forming hydrogel via metal-phenolic gelation. The gelation of TiTannic gels occurs by mixing polyphenols with group IV metal ions (Figure 1.5a), the hydrogel is made up of a network of polyphenols stabilised by metal ion (TiIV). The group demonstrated the titanium accumulation in mice's distal tissues (Figure 1.5b) remained low over the period of 14 weeks (Figure 1.5c), and the gel exhibited a sustained release of corticosteroid, dexamethasone up to 10 days (Figure 1.5d) compared with Pluronic F127. The drug release was measured using liquid chromatography, for TiTannic gels > 75 % of the drug was released over 6 days, and the drug remained detectable for up to 28 days. Additionally, the capacity to form a hydrogel in vivo demonstrated that it could be an interest in drug delivery applications.
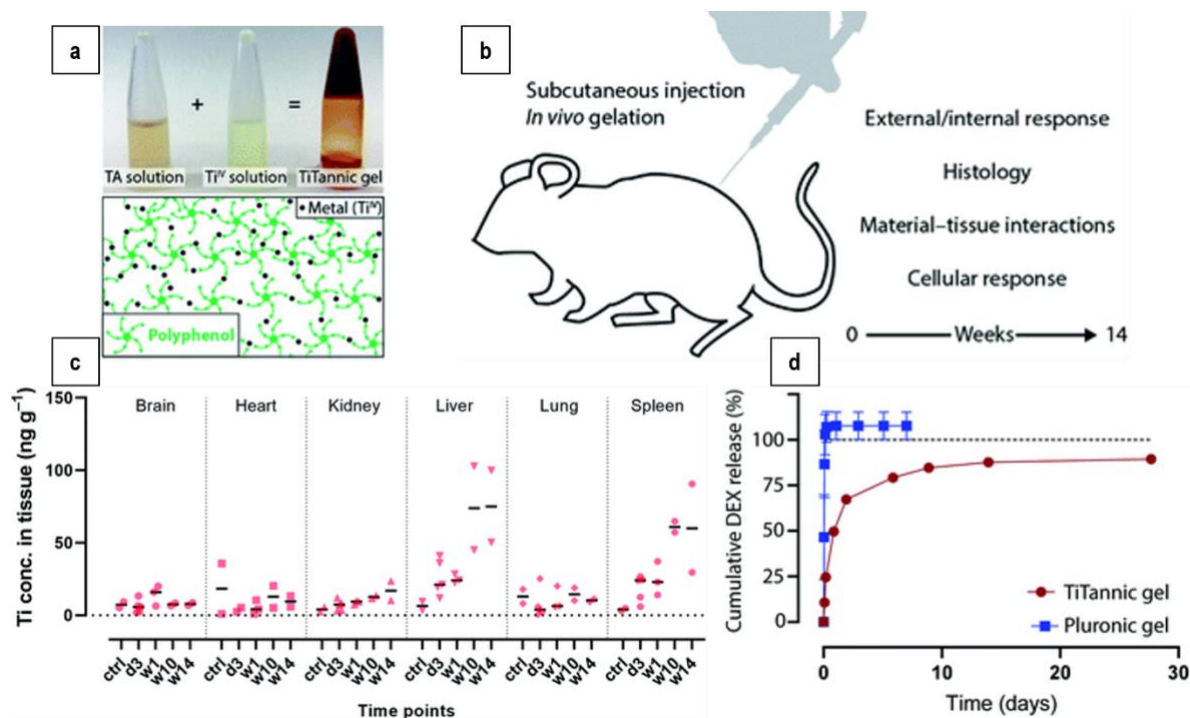
Figure 1.5, (a) Photographs showing that upon mixing TA solution with a TiIV solution, a TiTannic gel is formed. Followed by the schematic illustration below showing hydrogel structure is stabilised by metal-phenolic coordination. **(b)** Illustration showing an overview of in vivo biocompatibility and immunogenicity study up to 14 weeks. **(c)** Biodistribution studies from animal works show low titanium levels are detected in most distal mice tissues after 14 weeks. **(d)** The cumulative release of dexamethasone (DEX) from TiTannic gel and Pluronic gel revealed the release rate from the Pluronic gel compared to TiTannic gel. Reproduced with permission from ref. 43, copyright of Chemical Science 2019.

1.2.4. Example chemically crosslinked hydrogels

An early example of hydrogels described as 'chemical' or 'permanent' gels whose networks of covalently crosslinked polymers is the synthetic hydrogels of Wichterle and Lim, based on copolymers of HEMA with the crosslinker ethylene glycol dimethacrylate (EGDMA).[13] Their work showed the potential application for HEMA hydrogels because of their hydrophilic characteristics and potential to be biocompatible.[44] This important and influential early work started a golden era of research. Pioneering work by Lim *et al.* in 1980[45] showed the potential applications of calcium alginate microcapsules utilised for drug delivery, as well as the utilisation of natural polymers such as collagen and shark cartilage in a hydrogel matrix for dressing for artificial burns.[12] Such hydrogels have become especially attractive in the new field

of 'tissue engineering' as matrices for repairing and regenerating a wide variety of tissues and organs,[46,47] as well as to deliver therapeutics in a controlled manner.

As an alternative method to administrate high dosages of drugs, hydrogel-forming microneedles (MN) are of great interest to replace the typical syringe and needles.[48–50] Microneedles are micron-scale polymeric needles situated in perpendicular orientation on a base plate where the drug-containing reservoir is located. Through pain-free application to the skin, the MNs imbibe interstitial skin fluid and swell, creating a channel into the skin layer and permitting drug delivery into circulation.

Hutton *et al.*[51] reported a microneedles formulation composed of 500 mg of an aqueous blend of 20 % w/w Gantrez® S-97, 7.5 % w/w PEG 10 000 and 3 % w/w Na_2CO_3 crosslinked at 80 °C for 24 h **(Figure 1.6 a & b)**. The group demonstrated the use of 'super-swellable' MNs were used to deliver FITC-dextran and fluorescein sodium *in vitro* **(Figure 1.6c)** using neonatal porcine skin as test subjects. The hydrogel benefited from low density and bigger pores combined with the capacity to swell greatly, this causes the creation of larger micro-conduits within the skin, which leads to a more efficient drug delivery. The release of FITC-dextran shows little difference between the four formulations during the 0 - 6 h period. The MN swells to its maximum capacity at 6 h during this period. After this period, it was observed that the formulation containing the highest molecular weight of the FITC-based compound decreased the permeability across the skin between 6 - 24 h, likely caused by FITC-dextran entrapped within the hydrogel's crosslinked network. In summary, the work has demonstrated that low molecular weight biomolecules will permeate through the skin greater than larger monoclonal antibodies (mAbs) with microneedles.

It is also worthwhile to note that the swelling rate depends on the thermodynamic affinity between the materials and the solvent in crosslinked hydrogel network. Chemical hydrogels are not homogeneous, containing regions of low water swelling and high crosslink densities that form 'clusters' dispersed within regions of high swelling and low crosslink density. Hydrophobic aggregation of crosslinking agents can lead to high crosslink density clusters,[9,10] the formation depends on the solvent compositions, temperatures, and solid concentrations during gel formation. During gelation, phase separation can occur, and voids or macrospores can form that are filled with water. In chemical gels, defects in network structure can be caused by free

chain ends or chain loops. These inhomogeneities resulted in encapsulated cargo molecules that are not dispensed homogeneously and thus are not ideal for drug delivery as they may cause unwanted 'burst' or rapid drug release,[52] however, the effect of inhomogeneities is lesser in comparison to physical gels with the extensive domain of drug entrapped pockets[31].
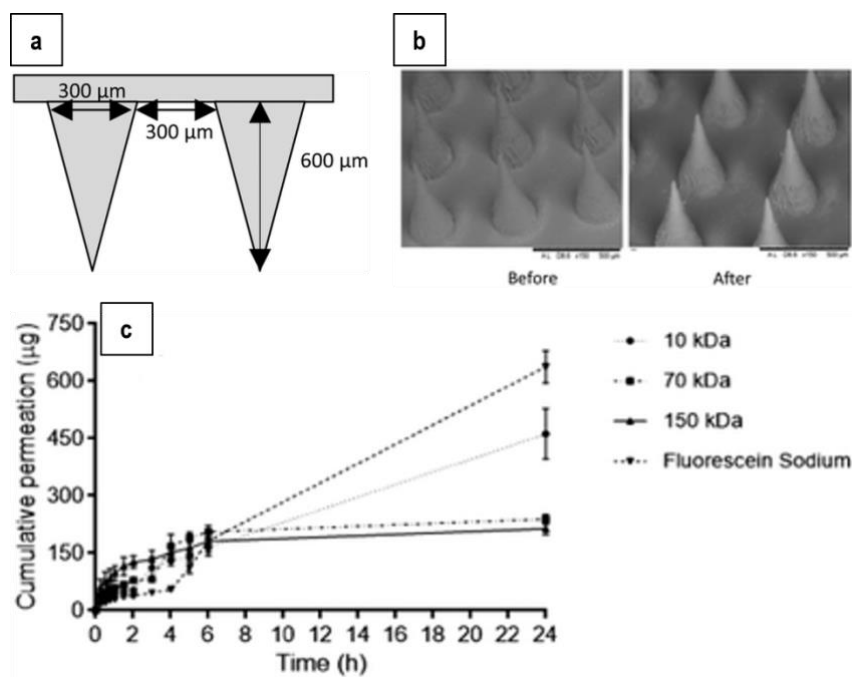
Figure 1.6, (a) Schematic representation of conical-shaped needles as a mould for the formation of 'Super-swelling' MN hydrogel, 600 μm in height, 300 μm interspacing and 300 μm width. **(b)** SEM imaging of the 'Super-swelling' MN hydrogels before and after application of 30 N force for 30 s. **(c)** In vitro permeation profiles of FITC–dextran 10 kDa, 70 kDa, 150 kDa and fluorescein sodium through dermatomed (350 μm) neonatal porcine skin over 24 h using 'super swellable' hydrogel-forming MN hydrogels. With all formulations achieved a release of above 150 μg after 6 h of release and followed by a sustained release. Reproduced with permission from ref. 51, copyright of Journal of Materials Chemistry, 2020.

1.2.5. Stimuli-responsive hydrogel system

Stimuli-responsive hydrogels are systems which imitate a physical response (changing in volume, refractive index, and hydrophilicity-hydrophobicity) upon changes in conditions such as pH, temperature, ionic forces, redox, environment, etc.[53] Jung et al.[54] demonstrated that a thermo-sensitive injectable hydrogel formed by combining of hyaluronic acid with Pluronic F127, a thermo-sensitive hydrogel which exhibits sustained piroxicam (PX) release over 200 h. *In vivo,* data suggest this PX-loaded

hydrogel presents superior drug bioavailability in physiological conditions compared to piroxicam on its own. Work by McAvan et al. has revealed[55] the controlled release of albumin protein upon hydrogel (complex of S-tert-butylmercapto-L-cysteine N-carboxahydride) interaction with the reducing agent glutathione. These stimuli-responsive materials hold great promise as biomaterials that are capable of drug delivery and suggest their potential use for tissue regeneration, aiding cell growth and proliferation through the release of protein growth factors.

Salama *et al.* have demonstrated[56] the potential use of a pH-sensitive hydrogel for bone tissue engineering by using a chitosan-g-poly(3-sulfopropyl methacrylate)-based hydrogel that induces rod-like hydroxyapatite formation. This hydrogel mimics the composition of native bone and also exhibits controlled protein release. In 2018, Jalababu *et al.* presented[57] a possible hydrogel candidate as an anti-cancer drug carrier **(Figure 1.7)**.
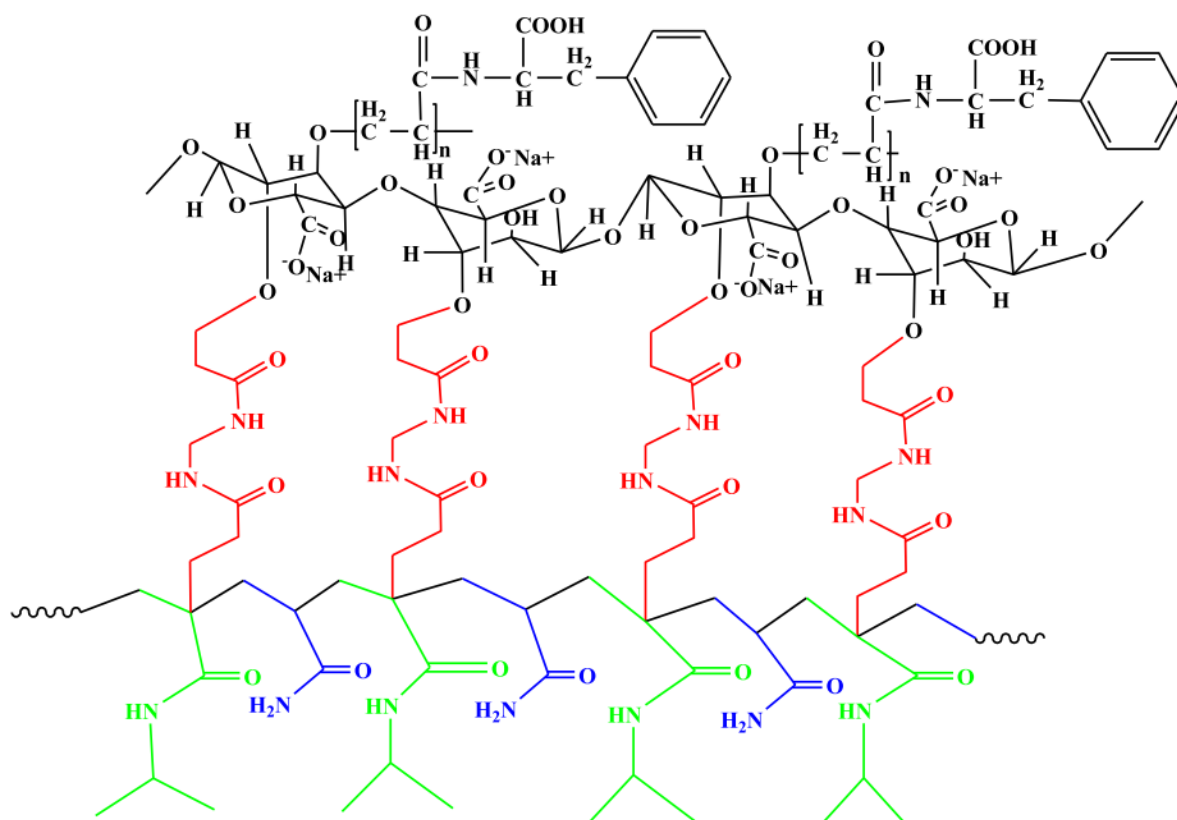
Figure 1.7, Chemical structure of NaAla-g-PAPA-co-(PINIPAAm-co—PAAm) [SPAM].[57]

The group utilised hydrogels based upon NaAla-g-PAPA-co-(PINIPAAm-co—PAAm) **(Figure 1.7)** as a pH and temperature-responsive interpenetrating polymer network, and the in-vitro release studies have shown a diffusion-based release of the anti-cancer drug imatinib mesylate over two days. This example is a much-improved system to deliver medication over an extended period compared to the conventional tablet. New hydrogels have been discovered that may be suitable for drug delivery. For example, Xie *et al.* in 2018[19] obtained a pH-sensitive hydrogel by crosslinking Chinese quince seed gum and poly (N, N-diethalacryl amide-co-methacrylic acid), and the resulting hydrogel formed was studied with a model protein drug that underwent sustained release over 10 hours.

1.2.6. Nanogels drug delivery

Microgels and nanogels are small hydrogel particles formulated for minimally invasive drug delivery. The size of hydrogels determines the manner of their transport and adherence when introduced into blood vessels, airways, or the gastrointestinal tract. Nanogels are particularly appealing for the delivery of nucleotide-based drugs such as plasmids DNA used for gene therapy.[58] Macroscopic hydrogels are usually implanted surgically into the body or placed in contact with the body for transepithelial drug delivery.[9] Drug delivery for epithelial barriers including skin, intestinal epithelium and mucosa have been exploited. Despite the epithelial being impenetrable to macroscopic hydrogels, they can be permeable to the drug release from the hydrogels.

In 2013, Steinhiber *et al.,*[59] presented a biodegradable dendritic polyglycerol nanogel by nanoprecipitation process **(Figure 1.8)**. The work shows that nanogel formed using this new approach can encapsulate proteins with an efficacy of almost 100 %. The release of proteins was released upon the change in pH as the nanogel began to degrade over time.[60]
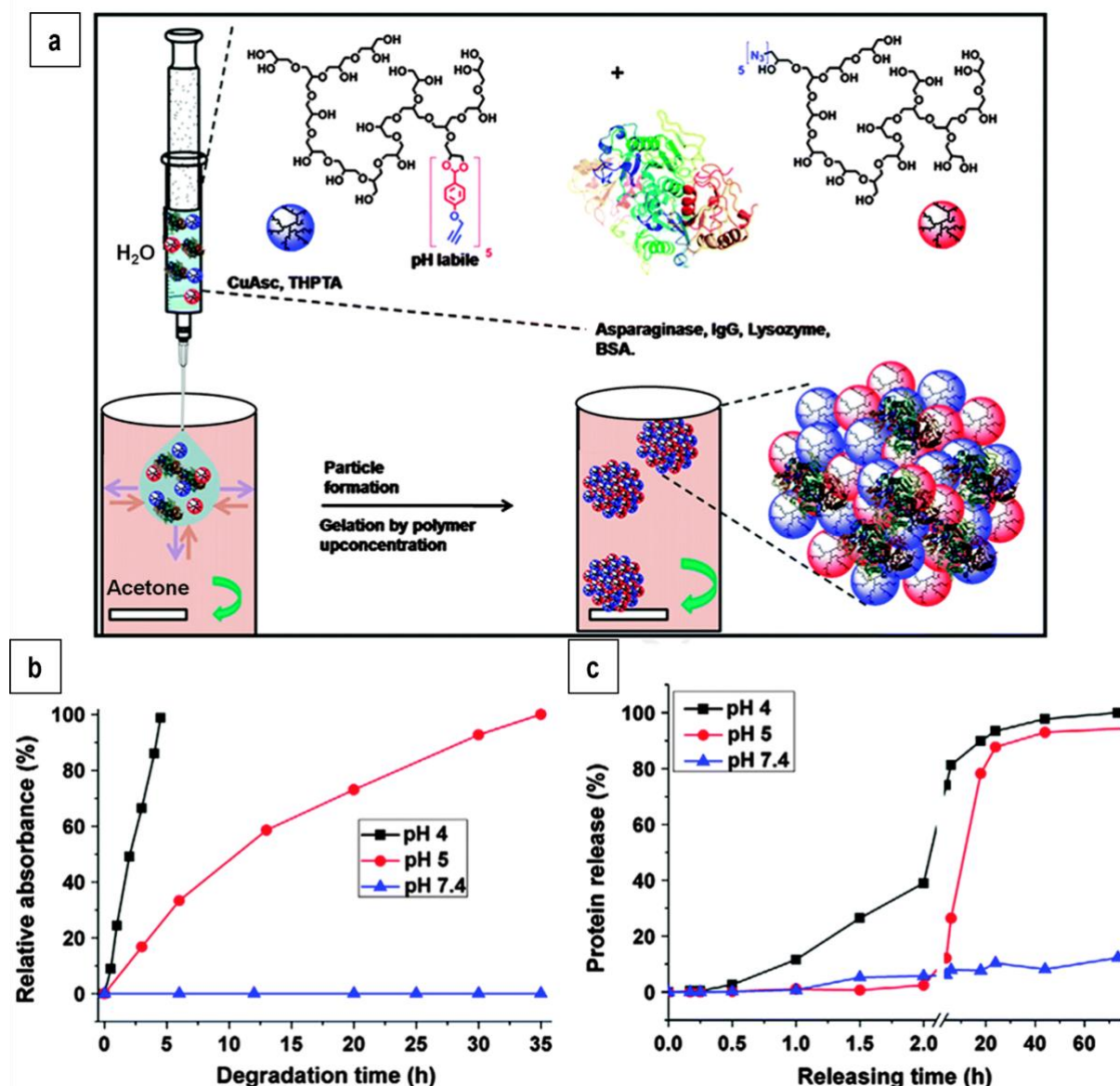
Figure 1.8, (a) The nanoprecipitation process prepared the dendritic polyglycerol nanogels. Injection of an aqueous solution of azide functionalised polyglycerol shown in red, alkyne functionalised polyglycerol in blue. The formation of a particle occurs after the aqueous phase diffuses into the organic phase (acetone), crosslinked by CuAAC via upconcentration. **(b)** Degradation of polyglycerol nanogels at different pH over time (h) measured via UV-vis measurement. **(c)** Cumulative release of proteins from nanogel network at different pH determined by HPLC. Reproduced with permission from ref. 60, Royal Society of Chemistry 2015.

1.2.7. Biopolymer – Caf1 protein polymer

There is a vast and diverse range of polymer compositions used to fabricate hydrogels.[61] The compositions can be divided into natural polymer-based hydrogels, synthetic polymer hydrogels, and combinations of the two classes. Hydrogels

fabricated from synthetic polymers such as poly (vinyl alcohol) and natural polymers such as alginate, collagen and chitosan are widely used as wound dressing. These biocompatible polymers are also highly appealing for drug delivery.[9] Hydrogels such as type I collagen have been used successfully as three-dimensional substrates for cell culture[62] and as a surgically implanted hydrogel[9] because the scaffolds more closely mimic *in vivo* conditions than traditional cellular monolayers which have gained widespread popularity for tissue engineering due to the abundance of collagen in the natural extracellular matrix (ECM). Polymeric compound that is native in biology (such as collagen, fibrin, and elastin) have been successfully extracted from ECM to form cross-linked hydrogels.[63,64] Due to their biocompatibility, these materials have been of great interest in the field of biomaterials such as drug delivery, cell growth, cell movements, cell adhesions and other cell functions.[65]
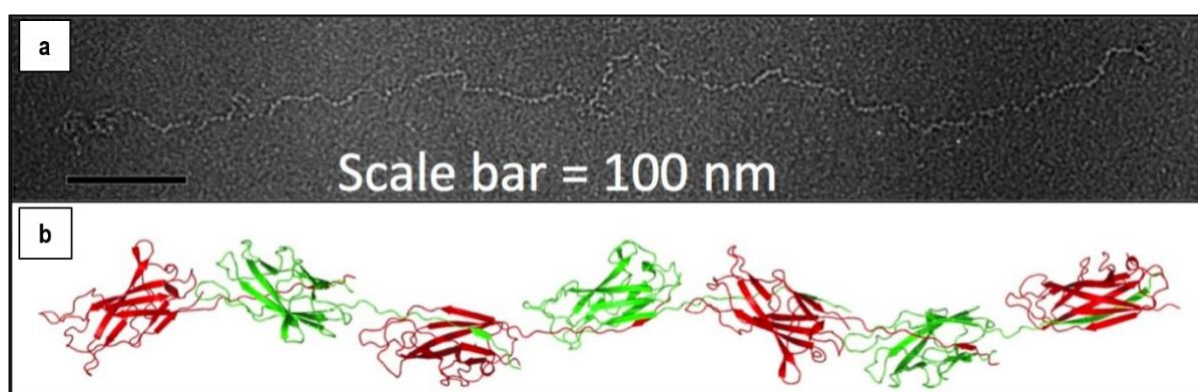
Figure 1.9, (a) The Caf1 polymer chain as seen using an electron microscope, **(b)** schematic model of Caf1. Reproduced with permission from ref. 67, copyright of Advanced Materials 2014.

Herein, we proposed using a biopolymer - Capsular antigen fraction 1 (Caf1) for drug delivery. Caf1 is a protein-based fimbria isolated initially from the plague bacterium *Yersinia pestis*,[66] whose role is to form an enveloping hydrogel around the bacterium to inhibit interactions with host cells and to help the bacterium evade the immune system[67], acting as "cloaking device" forming a gelatinous capsule around the bacterial surface.[68] Knight et al. have uncovered the mechanism by which Caf1 polymers are synthesised,[69] aided by a chaperone and usher protein. Caf1 monomer is an incomplete immunoglobulin domain comprising a 2-layer sandwich of β-sheets over a

hydrophobic core, with a β-strand facing outward, exposing a deep hydrophobic cleft. This β-strand is known as the N-terminal donor strand, which binds to an adjacent acceptor cleft Caf1 subunit, completing the immunoglobulin fold. This design is remarkably unique, transforming an inherently monomeric protein into strong polymer chains **(Figure 1.9)**.[66,70] This Caf1-Caf1 interaction is highly in kinetic and thermodynamic stability, even in harsh conditions such as extremes of pH, high salt concentrations and detergents.[71] Ulusu and coworkers have observed Caf1 protein polymer by electron microscopy to achieve lengths of >1μm, composed of more than 250 ~15 kDa subunits.[67] In polymer biogenesis, the subunits polymerise through a process called donor strand exchange, with chaperone and usher proteins mediating the donation of the N-terminal β-strand to complete the immunoglobulin-like fold of the next subunit in the chain.[67] The interactions linking the subunits together display dissociation constants $K_D < 10^{-14}$ M, and dissociation half-life $>10^8$ years which means the polymer is extremely kinetically inert. The protein is thus robust, resists both thermal and proteolytic degradation, and it is highly soluble in aqueous solutions. Most importantly, it retains its biological ability to prevent mammalian cell attachment because Caf1 can be expressed in *E. Coli*. (Escherichia coli), its manufacturing process can be easily scaled-up. These advantageous properties are difficult to design into a protein polymer de novo.[67] Furthermore, our group have demonstrated that Caf1 has the capacity to switch between its polymeric and monomeric forms reversibly and thermally. [72] The Caf1 polymer has a melting temperature of ~85 ºC, where the acceptor moiety unfolds, leading to the loss of tertiary structure and releasing the donor strand, leading to the loss of polymeric quaternary structure. Our group demonstrated upon cooling the Caf1 protein refolds and reform of its polymeric quaternary, this feature was observed with SDS-PAGE and CD spectroscopy.[67] It is hypothesised that these unique properties of Caf1 can be used in multiple applications such as drug/cell encapsulation, wound healing and 3D printing.

Caf1-based biocompatible materials are an ideal candidate as a polymer building block for drug delivery applications. One of which is to develop Caf1-based hydrogels by crosslinking polymer chains with crosslinkers via covalent bonds. The formation of these hydrogels can be characterised by rheology techniques measured in storage

modulus (G') – the energy required to distort the material; loss modulus (G'') – energy lost as the material returns to its original shape; Tan delta (Tan δ) – the ratio of the loss modulus to the storage modulus.[73,74] Nanoscaled nanogels can be characterised by dynamic light scattering (DLS) that determines the size distribution of small particles or polymers in solution. The technique utilises the Brownian motion rules that describe particles scattered in laser light at different intensities, and from that the particle size is based on the Stokes-Einstein relationship.[75,76] The 3-D hydrogel network is porous in nature, enabling the encapsulation and release of drug molecules. In vitro studies such as dissolution tests can be used to determine the rate at which drug molecules are released from these hydrogel networks, mathematical modelling such as zero-order; first-order; Hixson-Crowell; Higuchi; Korsmeyer-Peppas can be used to understand further the kinetics and mechanism that took place during drug release.[6,77,78]

1.3. Conclusion

In conclusion, advances in biomaterials have broadened the repertoire of hydrogels designed for controlled drug delivery. With an expanding arsenal of materials and target applications and increasing fundamental understanding, the impact of hydrogel drug delivery systems is expected to grow in importance for years to come. Hydrogel drug delivery systems are likely to change the scale, efficacy, and cost of therapeutics and continue to improve health care. The project aim is to investigate the possibilities of Caf1-based hydrogels in drug delivery applications.

1.4. Experimental Approach

The objective of this work was to investigate the possibilities of Caf1-base hydrogels in drug delivery applications. Investigations in this work began with producing a well-characterised Caf1 hydrogel[79] (Chapter 2) by rheology and developed methods to upload and release model drug molecules from small to large biomolecules into the hydrogel network **(Figure 1.10a)**. The rate of drug cargo release was determined by following cargo released using UV spectroscopy, and the associated release mechanism was ascertained. In Chapter 3, the production of stimuli-responsive Caf1 hydrogel is explored by introducing a cysteine motif to the Caf1 polymer, that allows for the formation of disulfide bonds which break upon reduction and trigger the release of small molecules **(Figure 1.10b)**. The success of disulfide bond formation will be evaluated by rheology and SDS-PAGE. Further, several approaches are introduced with the aim of producing a new type of mosaic Caf1 hydrogel, and the mechanical property of this hydrogel will be tested against other systems by rheology. Investigation toward Caf1 nanogel is reported in Chapter 4, which details a successful method to produce Caf1 nanogel **(Figure 1.10c)** that has the potential for drug release and cell encapsulation with minor modifications to the Caf1. Furthermore, DLS is used to evaluate the success in producing Caf1 nanogel where a uniform and stable Caf1 nanogel should be observed.
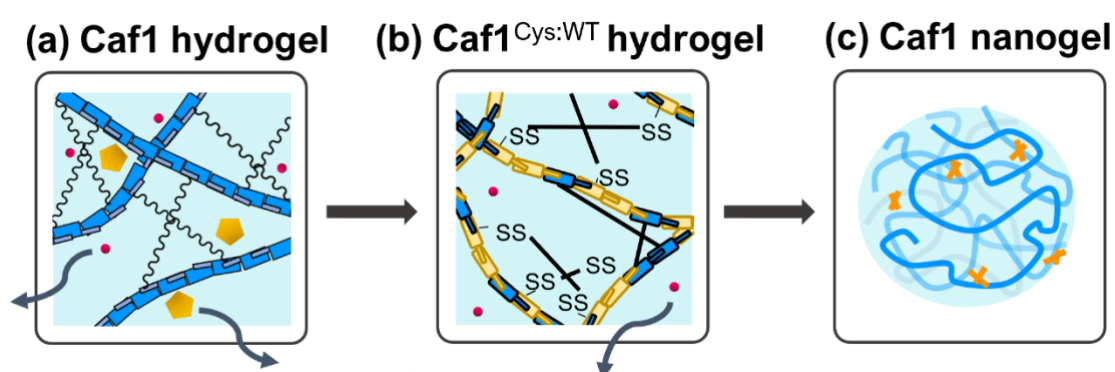
Figure 1.10, Schematic illustration of **(a)** Caf1 hydrogel formed by crosslinking between Caf1 polymer with PEG-SG via amide bonds, the hydrogels were loaded with small molecules and macromolecule payloads and the release mechanism that took place was analysed. **(b)** Formulation of mosaic Caf1$^{Cys: WT}$ hydrogel comprised of amide bonds and disulfide bridges, small molecules were uploaded for drug release studies. **(c)** Formation of chemically crosslinked nanoscale hydrogel – Caf1 nanogels.

1.5. References

1.   Yahia, Lh. History and Applications of Hydrogels. Journal of Biomedical Sciencies 04, 1–23 (2015).
2.   Miele, E. et al. Nanoparticle-based delivery of small interfering RNA: Challenges for cancer therapy. Int J Nanomedicine 7, 3637–3657 (2012).
3.   Ye, F. et al. Real-time UV imaging of drug diffusion and release from Pluronic F127 hydrogels. European Journal of Pharmaceutical Sciences 43, 236–243 (2011).
4.   Wu, W., Shen, J., Banerjee, P. & Zhou, S. Chitosan-based responsive hybrid nanogels for integration of optical pH-sensing, tumor cell imaging and controlled drug delivery. Biomaterials 31, 8371–8381 (2010).
5.   Park, H. et al. Effect of Swelling Ratio of Intectable Hydrogel Composites on Chondrongenix Differentiation of Encapsculated Rabbit Marrow Mesenchymal Stem Cells In Vitro (Author Manuscript). Biomacromolecules 10, 541–546 (2010).
6.   Lee, P. I. Kinetics of drug release from hydrogel. Journal of Controlled Release 2, 277–288 (1985).
7.   Panyam, J. & Labhasetwar, V. Biodegradable nanoparticles for drug and gene delivery to cells and tissue. Adv Drug Deliv Rev 55, 329–347 (2003).
8.   Singh, N. K. & Lee, D. S. In situ gelling pH- and temperature-sensitive biodegradable block copolymer hydrogels for drug delivery. Journal of Controlled Release 193, 214–227 (2014).
9.   Li, J. & Mooney, D. J. Designing hydrogels for controlled drug delivery. Nat Rev Mater 1, 1–18 (2016).
10. Hiemstra, C., Zhong, Z., van Steenbergen, M. J., Hennink, W. E. & Feijen, J. Release of model proteins and basic fibroblast growth factor from in situ forming degradable dextran hydrogels. J Control Release. 122, 71–78 (2007).
11. Ullah, F., Othman, M. B. H., Javed, F., Ahmad, Z. & Akil, H. M. Classification, processing and application of hydrogels: A review. Materials Science and Engineering C 57, 414–433 (2015).
12. Hoffman, A. S. Hydrogels for biomedical applications. Adv Drug Deliv Rev 64, 18–23 (2012).
13. Wichterle, O. & Lím, D. Hydrophilic Gels for Biological Use. Nature 185, 117–118 (1960).
14. Kuhn, W., Hargitay, B., Katchalsky, A. & Eisenberg, H. Reversible dilation and contraction by changing the state of ionization of high-polymer acid networks. Nature 165, 514–516 (1950).
15. Buwalda, S. J. et al. Hydrogels in a historical perspective: From simple networks to smart materials. Journal of Controlled Release 190, 254–273 (2014).
16. Upadhyay, A., Kandi, R. & Rao, C. P. Injectable, Self-Healing, and Stress Sustainable Hydrogel of BSA as a Functional Biocompatible Material for Controlled Drug Delivery in Cancer Cells. ACS Sustain Chem Eng 6, 3321–3330 (2018).
17. Appel, E. A., Forster, R. A., Rowland, M. J. & Scherman, O. A. The control of cargo release from physically crosslinked hydrogels by crosslink dynamics. Biomaterials 35, 9897–9903 (2014).
18. Liu, H. et al. A functional chitosan-based hydrogel as a wound dressing and drug delivery system in the treatment of wound healing. RSC Adv 8, 7533–7549 (2018).
19. Xie, A. J., Yin, H. S., Liu, H. M., Zhu, C. Y. & Yang, Y. J. Chinese quince seed gum and poly (N,N-diethylacryl amide-co-methacrylic acid) based pH-sensitive hydrogel for use in drug delivery. Carbohydr Polym 185, 96–104 (2018).
20. Kearney, C. J. et al. Switchable Release of Entrapped Nanoparticles from Alginate Hydrogels. Adv Healthc Mater 4, 1634–1639 (2015).

21. Senapati, S., Mahanta, A. K., Kumar, S. & Maiti, P. Controlled drug delivery vehicles for cancer treatment and their performance. Signal Transduct Target Ther 3, 7 (2018).

22. Kar, M. et al. Responsive Nanogels for Anti-cancer Therapy. in Nanogels for Biomedical Applications vols 2018-Janua 210–260 (The Royal Society of Chemistry, 2017).

23. Bahrami, B. et al. Nanoparticles and targeted drug delivery in cancer therapy. Immunol Lett 190, 64–83 (2017).

24. Lee, Y. et al. Thermo-sensitive, injectable, and tissue adhesive sol-gel transition hyaluronic acid/pluronic composite hydrogels prepared from bio-inspired catechol-thiol reaction. Soft Matter 6, 977–983 (2010).

25. Censi, R., Fieten, P. J., Di Martino, P., Hennink, W. E. & Vermonden, T. In situ forming hydrogels by tandem thermal gelling and Michael addition reaction between thermosensitive triblock copolymers and thiolated hyaluronan. Macromolecules 43, 5771–5778 (2010).

26. Giray, S., Bal, T., Kartal, A. M., Kizilel, S. & Erkey, C. Controlled drug delivery through a novel PEG hydrogel encapsulated silica aerogel system. J Biomed Mater Res A 100 A, 1307–1315 (2012).

27. Sheikhpour, M., Barani, L. & Kasaeian, A. Biomimetics in drug delivery systems: A critical review. Journal of Controlled Release 253, 97–109 (2017).

28. Delplace, V. et al. Controlled release strategy designed for intravitreal protein delivery to the retina. Journal of Controlled Release 293, 10–20 (2019).

29. Larrañeta, E., Stewart, S., Ervine, M., Al-Kasasbeh, R. & Donnelly, R. Hydrogels for Hydrophobic Drug Delivery. Classification, Synthesis and Applications. J Funct Biomater 9, 13 (2018).

30. Diego Caccavo, Sara Cascone, Gaetano Lamberti, A. A. B. and A. L. Swellable Hydrogel-based Systems for Controlled Drug Delivery. doi:10.5772/58459.

31. Hoare, T. R. & Kohane, D. S. Hydrogels in drug delivery: Progress and challenges. Polymer (Guildf) 49, 1993–2007 (2008).

32. Varghese, J. S., Chellappa, N. & Fathima, N. N. Gelatin-carrageenan hydrogels: Role of pore size distribution on drug delivery process. Colloids Surf B Biointerfaces 113, 346–351 (2014).

33. Ulubayram, K., Eroglu, I. & Hasirci, N. Gelatin microspheres and sponges for delivery of macromolecules. J Biomater Appl 16, 227–241 (2002).

34. Llarena, Z. M. A review: Permeability, porosity, tortuosity and physicochemical properties of controlled release oral dosage formulations. International Journal of Research in Pharmaceutical Sciences 8, 41–48 (2017).

35. Lin, H. et al. Transport and structural characteristics of crosslinked poly(ethylene oxide) rubbers. J Memb Sci 276, 145–161 (2006).

36. Yao, F. & Weiyuan, J. K. Drug Release Kinetics and Transport Mechanisms of Non-degradable and Degradable Polymeric Delivery Systems. Expert Opinion Drug Delivery 7, 429–444 (2010).

37. Grassi, M., Lamberti, G., Cascone, S. & Grassi, G. Mathematical modeling of simultaneous drug release and in vivo absorption. Int J Pharm 418, 130–141 (2011).

38. Moore, T., Croy, S., Mallapragada, S. & Pandit, N. Experimental investigation and mathematical modeling of Pluronic(®) F127 gel dissolution: Drug release in stirred systems. Journal of Controlled Release 67, 191–202 (2000).

39. Mathew, A. P., Uthaman, S., Cho, K. H., Cho, C. S. & Park, I. K. Injectable hydrogels for delivering biotherapeutic molecules. Int J Biol Macromol 110, 17–29 (2018).

40. Coyle, F. M. & Martin, S. J. Dynamics of Water Molecules in Polymers. Dynamics pf Water Molecules in Polymers 69, (1996).

41. Hatakeyama, H. & Hatakeyama, T. Interaction between water and hydrophilic polymers. Thermochim Acta 308, 3–22 (1998).

42. Montembault, A., Viton, C. & Domard, A. Rheometric study of the gelation of chitosan in aqueous solution without cross-linking agent. Biomacromolecules 6, 653–662 (2005).

43. Björnmalm, M. et al. In vivo biocompatibility and immunogenicity of metal-phenolic gelation. Chem Sci 10, 10179–10194 (2019).

44. Huglin, M. R. Hydrogels in medicine and pharmacy Edited by N. A. Peppas, CRC Press Inc., Boca Raton, Florida, 1986 (Vol. I), 1987 (Vols 2 and 3). Vol. 1 Fundamentals, pp. vii + 180, £72.00, ISBN 0-8493-5546-X; Vol. 2 Polymers, pp. vii + 171, £72.00, ISBN 0-8493-5547-8; British Polymer Journal 21, 184–184 (1989).

45. Lim, F. & Sun, A. M. Microencapsulated Islets as Bioartificial Endocrine Pancreas. Science (1979) 210, 908–910 (1980).

46. Ahmed, T. A. E., Dare, E. V. & Hincke, M. Fibrin: A versatile scaffold for tissue engineering applications. Tissue Eng Part B Rev 14, 199–215 (2008).

47. O'Brien, F. J. Biomaterials & scaffolds for tissue engineering. Materials Today 14, 88–95 (2011).

48. Aditya, A. et al. Kinetics of collagen microneedle drug delivery system. J Drug Deliv Sci Technol 52, 618–623 (2019).

49. Ita, K. Transdermal delivery of drugs with microneedles—potential and challenges. Pharmaceutics 7, 90–105 (2015).

50. Yin, Z. et al. Swellable silk fibroin microneedles for transdermal drug delivery. Int J Biol Macromol 106, 48–56 (2018).

51. Hutton, A. R. J., McCrudden, M. T. C., Larrañeta, E. & Donnelly, R. F. Influence of molecular weight on transdermal delivery of model macromolecules using hydrogel-forming microneedles: Potential to enhance the administration of novel low molecular weight biotherapeutics. J Mater Chem B 8, 4202–4209 (2020).

52. Sriwongjanya, M. & Bodmeier, R. Effect of ion exchange resins on the drug release from matrix tablets. European Journal of Pharmaceutics and Biopharmaceutics 46, 321–327 (1998).

53. Molina, M. et al. Stimuli-responsive nanogel composites and their application in nanomedicine. Chem Soc Rev 44, 6161–6186 (2015).

54. Jung, Y. seok, Park, W., Park, H., Lee, D. K. & Na, K. Thermo-sensitive injectable hydrogel based on the physical mixing of hyaluronic acid and Pluronic F-127 for sustained NSAID delivery. Carbohydr Polym 156, 403–408 (2017).

55. McAvan, B. S., Khuphe, M. & Thornton, P. D. Polymer hydrogels for glutathione-mediated protein release. Eur Polym J 87, 468–477 (2017).

56. Salama, A. Chitosan based hydrogel assisted spongelike calcium phosphate mineralization for in-vitro BSA release. Int J Biol Macromol 108, 471–476 (2018).

57. Jalababu, R., Veni, S. S. & Reddy, K. V. N. S. Synthesis and characterization of dual responsive sodium alginate-g-acryloyl phenylalanine-poly N -isopropyl acrylamide smart hydrogels for the controlled release of anticancer drug. J Drug Deliv Sci Technol 44, 190–204 (2018).

58. Soni, K. S., Desale, S. S. & Bronich, T. K. Nanogels: An overview of properties, biomedical applications and obstacles to clinical translation. Journal of Controlled Release 240, 109–126 (2016).

59. Steinhilber, D. et al. Surfactant free preparation of biodegradable dendritic polyglycerol nanogels by inverse nanoprecipitation for encapsulation and release of pharmaceutical biomacromolecules. J Control Release. 169, 289–295 (2013).

60. Zhang, X., Malhotra, S., Molina, M. & Haag, R. Micro- and nanogels with labile crosslinks-from synthesis to biomedical applications. Chem Soc Rev 44, 1948–1973 (2015).

61. Parhi, R. Cross-linked hydrogel for pharmaceutical applications: A review. Adv Pharm Bull 7, 515–530 (2017).

62. Antoine, E. E., Vlachos, P. P. & Rylander, M. N. Review of Collagen I Hydrogels for Bioengineered Tissue Microenvironments: Characterization of Mechanics, Structure, and Transport. Tissue Eng Part B Rev 20, 683–696 (2014).

63. Wei, W. et al. Colloids and Surfaces B : Biointerfaces A novel thermo-responsive hydrogel based on salecan and poly (N-isopropylacrylamide): Synthesis and characterization. Colloids Surf B Biointerfaces 125, 1–11 (2015).

64. Kharkar, P. M., Kiick, K. L. & Kloxin, A. M. Designing degradable hydrogels for orthogonal control of cell microenvironments. Chem Soc Rev 42, 7335–7372 (2013).

65. Matricardi, P., Meo, C. Di, Coviello, T. & Alhaique, F. Recent advances and perspectives on coated alginate microspheres for modified drug delivery. Expert Opin Drug Deliv 5, 417–425 (2008).

66. Waksman, G. & Hultgren, S. J. Structural biology of the chaperone–usher pathway of pilus biogenesis. Nat Rev Microbiol 7, 765–774 (2009).

67. Ulusu, Y. et al. Thermal stability and rheological properties of the 'non-stick' Caf1 biomaterial. Biomedical Materials 12, 051001 (2017).

68. Soliakov, A., Harris, J. R., Watkinson, A. & Lakey, J. H. The structure of Yersinia pestis Caf1 polymer in free and adjuvant bound states. Vaccine 28, 5746–5754 (2010).

69. Zavialov, A. V. et al. Structure and Biogenesis of the Capsular F1 Antigen from Yersinia pestis. Cell 113, 587–596 (2003).

70. Roque, A. I. et al. Reversible non-stick behaviour of a bacterial protein polymer provides a tuneable molecular mimic for cell and tissue engineering. Advanced Materials 26, 2704–2709 (2014).

71. Schreiber, G. Kinetic studies of protein-protein interactions. Curr Opin Struct Biol 12, 41–47 (2002).

72. Dura, G. et al. Exploiting Meltable Protein Hydrogels to Encapsulate and Culture Cells in 3D. Macromol Biosci 22, 2200134 (2022).

73. Franck, A. Understanding rheology of structured fluids. Book of TA instruments 1–11 (2004).

74. Picout, D. R. & Ross-Murphy, S. B. Rheology of biopolymer solutions and gels. ScientificWorldJournal 3, 105–121 (2003).

75. Khoee, S. & Asadi, H. Nanogels: Chemical Approaches to Preparation. Handbook of Encapsulation and Controlled Release 1271–1309 (2015) doi:doi:10.1201/b19038-60.

76. Vashist, A. et al. Chapter 1: Journey of Hydrogels to Nanogels: A Decade after. RSC Smart Materials 1–8 (2018) doi:10.1039/9781788010481-00001.

77. Zhu, W. Release Kinetics Model Fitting of Drugs with Different Structures from Viscose Fabric. 3282 (2023).

78. Colombo, P., Bettini, R., Catellani, P. L., Santi, P. & Peppas, N. A. Drug volume fraction profile in the gel phase and drug release kinetics in hydroxypropylmethyl cellulose matrices containing a soluble drug. European Journal of Pharmaceutical Sciences 9, 33–40 (1999).

79. Dura, G., Waller, H., Gentile, P., Lakey, J. H. & Fulton, D. A. Tuneable hydrogels of Caf1 protein fibers. Materials Science and Engineering C 93, 88–95 (2018).

Chapter 2

Caf1 hydrogel drug delivery from small molecule to macromolecule

Table of contents

2.1. Overview

The design of an efficient drug cargo carrier for the controlled delivery of therapeutic proteins is highly desirable in the development of biotherapeutics. Despite recent achievements in drug delivery systems, controlled protein delivery remains challenging on account of their intrinsic properties, including their large sizes and surface charges. In this study, demonstration of the hydrogels based on the polymer Capsular antigen fragment 1 (Caf1) can be used to efficiently encapsulate proteins within a chemically crosslinked hydrogel network up to 100 h of drug release availability. Caf1 polymers consist of protein subunits linked together into polymer through non-covalent interactions, that inherit a unique reversible property upon thermal unfolding of the Caf1 between its polymeric form and monomeric form.

In this chapter, Caf1 hydrogels were synthesised by crosslinking PEG-SG via amide bonds. A small molecule, Rhodamine-B, was loaded into the hydrogel, and the kinetic release was measured against Pluronic F-127 hydrogel. In comparison, Rhodamine-B experienced a slower release rate with the Caf1 hydrogel than in Pluronic F-127 hydrogel which was due to its matrix hydrophilic composition. The rate of release can be tuned by altering the crosslink density of the hydrogel formulation, the release rate can be reduced significantly as pore size decrease and approach the size of the cargo which limits the cargo mobility. Further, protein biomolecules (BSA, DNase, Trypsin) were loaded into the Caf1 hydrogels by two different approaches, the "melt" and "abs" approaches utilise the reversible nature of Caf1 protein. The cross-linkage between Caf1 and PEG-SG remained intact during the refolding process while providing a window for drug loading via yielded "*melt*" Caf1 hydrogels or through achieving cargo loading via the "abs" (absorption) approach. While the release from these approaches both are diffusion controlled, to "*melt*" static interaction between the protein cargos and the hydrogel matrix resulted in a faster release rate compared to cargos loaded via the "*abs*" approach, that suggest the proteins were not homogeneously dispersed in comparison to the "*melt*" approach. This work suggests that the 'meltable' feature of Caf1 hydrogels may present an improved method of loading and delivering protein cargos into cross-linked hydrogel networks whilst avoiding the need for biorthogonal cross-linking chemistries.

2.2. Introduction

In the past few decades, hydrogels have been in use for several biomedical applications, such as drug delivery systems, wound healing, and in-situ gels.[1,2] Hydrogels are a three-dimensional cross-linked network of polymers, which are made up of large amounts of water.[3] The large body of water can be used to host a wide variety of drug cargo, from small molecules to large molecules. Hydrogels are smart, environmentally sensitive, and compatible with biological systems[4]. The flexibility of these hydrogels has attracted a growing interest in drug delivery systems. Hydrogels based upon natural protein polymers are vastly interested in the scientific community. In comparison to synthetic polymers, it possesses inherent advantages of superior bioavailability, biocompatibility and biodegradability with low toxicity by-products.[5,6] One of the which is the use in delivery for therapeutic proteins such as growth factors, cytokines, recombinant proteins, and monoclonal antibodies which can be found in many pharmaceutical applications today.[7] Recent studies have demonstrated the potential use of gelatine-based hydrogel in the sustained release and protection of the cargo from denaturation.[8,9] In another study, fluorescein-isothiocyanate labelled BSA was used as a model cargo encapsulated within a recombinant human gelatine nanoparticle.[10–13] It is anticipated that the growth for protein-based therapeutics will be significant in the coming years.[5] It is also anticipated that with this growth, there will be an increasing need to master controlled delivery methods for protein-based therapeutics. These are arguably underdeveloped compared to delivery methods for conventional small molecule therapeutics, where decades of work have been studied in developing controllable drug delivery.[14] These developments take advantage of conventional polymeric and liposomal delivery agents that afford the virtues of drug protection,[8,15,16] site targeting[14,17,18] and toxicity reduction[19]. However, on account of the intrinsic properties of proteins, such as their large sophisticated three-dimensional shapes that present; hydrophilic, lyophobic, and electrostatic charges together with susceptibility to degradation, it remains a challenging task to deliver proteins efficiently.[20]

With small molecule drug cargos, it is relatively simple to load and deliver the drug in high quantity in a chemically crosslinked hydrogel by simple partitioning of a concentrated aqueous drug solution, allowing the cargo to diffuse through the pores

concentrated aqueous drug solution, allowing the cargo to diffuse through the pores of the hydrogel network to afford a homogenous distribution, while shielding the drug payload from changes in exterior condition. However, this process is inefficient in the case of large macromolecular drugs which have diffusive limitations to their partitioning into a hydrogel phase.[14,21–23] These results in highly non-homogenous cargo distributions throughout the hydrogel network, leading to unpredictable release kinetics.[24] Alternatively, cargo loading can be performed by introducing the payload to the hydrogel cross-linking step in cargo solutions. However, this requires the application of highly selective biorthogonal chemistries to ensure that the functional groups upon the protein cargos do not also react with the polymer components of the hydrogel network. There is a need for methodologies that will allow the efficient encapsulation of therapeutic protein cargos within the chemically cross-linked hydrogel networks. To address this challenge, it is hypothesised that hydrogels composed of the protein polymer Capsular antigen fragment 1 (Caf1) could be utilised as a vehicle to encapsulate model protein cargos within chemically cross-linked networks, leading to a homogenous dispersion of cargo and better control of release kinetics.

Herein, the drug-delivering properties of Caf1 hydrogels were explored in this chapter. Caf1 wild type (Caf1WT) protein polymer was crosslinked with PEG-SG crosslinker via an amide bond to yield Caf1 hydrogel. The mechanical properties of Caf1 hydrogels were analysed and benchmarked with the Pluronic F-127 hydrogels. Small molecule Rhodamine-B was loaded "direct" into Caf1 hydrogel. Pluronic F-127 hydrogel and the release of Rhodamine-B were studied over time. Release profiles of Rhodamine-B from Caf1 hydrogel and Pluronic F-127 hydrogel were plotted, and the profiles were further analysed with kinetic models to determine release mechanisms that have taken place. The crosslink density of Caf1 hydrogel was explored with the aim of reducing the Rhodamine-B release rate, and the relationship between pore size and cargo size was investigated with FITC labelled BSA (BSA-FITC). Two cargo loading methods were developed protein loading via Caf1 hydrogel "absorption" and protein loading via "meltable" Caf1 hydrogel. These methods were introduced to reduce any undesired crosslinking between proteins with PEG-SG. Three protein cargos were selected: Deoxyribonuclease (DNase); Bovine Serum Albumin (BSA); and Trypsin (Try), to study

the effects of surface charge/size on the rate of release. The results were evaluated with kinetic models to gain a better insight into the mode of release mechanism.

2.3. Results and Discussion

2.3.1. Caf1 hydrogel synthesis

Caf1 polymers **(Figure 2.1)** comprise Caf1 subunits linked via non-covalent donor strand exchange, as described in the previous chapter. The wild-type Caf1^{WT} polymers were supplied by the Jeremy Lakey group at Newcastle University. Wild-type Caf1 polymers **(Figure 2.1)** consist of several surface lysine residues that can react with succinimidyl glutarate of PEG-SH to form an amide bond and thus yield Caf1 hydrogels.
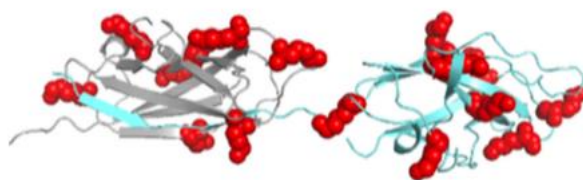
Figure 2.1, Structure of Caf1 protein dimer showing two successive monomers and surface lysine residues in **red** spheres. Each Caf1 subunit displays seven surface lysine residues.[25,26]

Caf1 hydrogels **(Figure 2.2a)** were synthesised by crosslinking polyethene glycol succinimidyl glutarate (4-Arm PEG-SG) **(Figure 2.2b)** with Caf1^{WT} protein polymer (note: wild type Caf1^{WT} is referred to Caf1 in this thesis). The activated ester group of the PEG polymer were reacted with lysine residues presented in the Caf1 protein at room temperature in an aqueous solution to afford transparent hydrogels without the need for further purification.
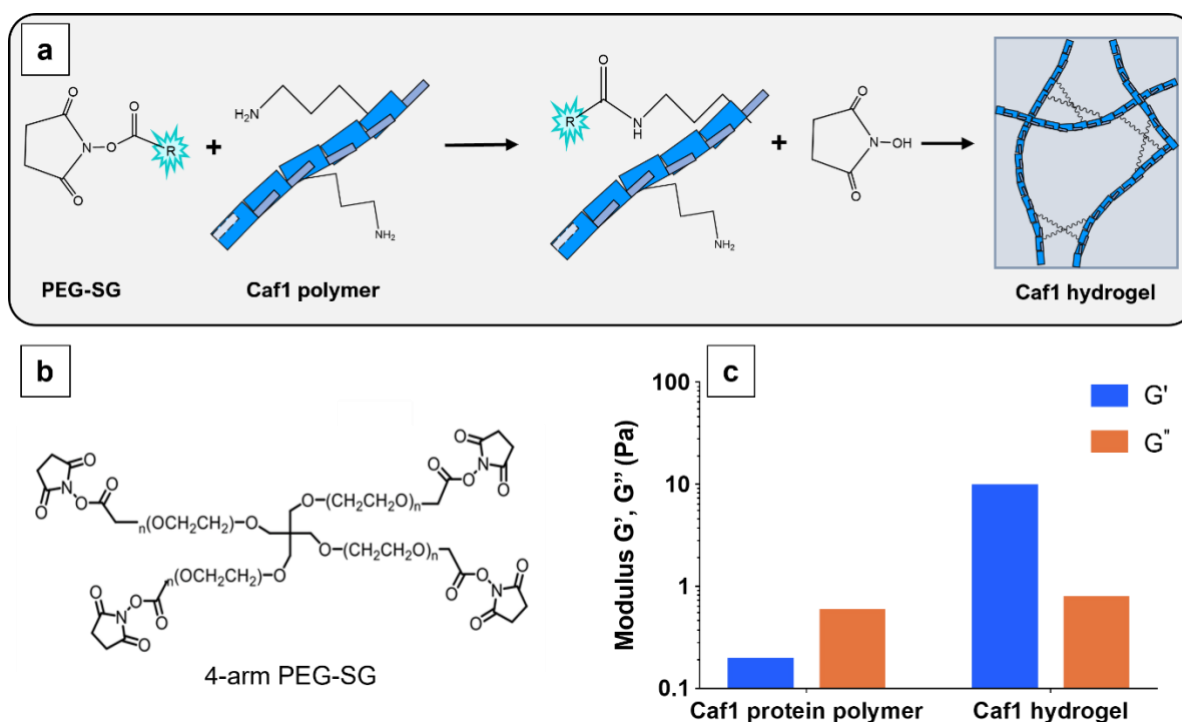
Figure 2.2, (a) Schematic representation of Caf1 hydrogels synthesis. **(b)** Chemical structures of succinimidyl glutarate PEG (PEG-SG) variants, 4-Arm (4-Arm PEG-SG) (20kDa) crosslinker. **(c)** Time sweeps of Caf1 protein polymer (2 %w/v) and Caf1 hydrogel (2 %w/v) with G' and G'' as the functions.

Caf1 hydrogels were prepared by reacting 2 % (w/v) of Caf1 polymer (100 μL) with 2 % (w/v) of 4-Arm PEG-SG (100 μL), the resultant hydrogel was analysed by rheometer to determine the storage modulus (G') and loss modulus (G''). Storage modulus G' is a measure of stored deformation energy, and loss modulus represents the dissipated deformation energy through internal friction when flowing.[27,28] Material is described as viscoelastic solids with G' > G'' when storage modulus is higher than loss modulus, resulting from links within the material such as chemical bonds or physical-chemical interactions. In contrast, viscoelastic liquids have a higher loss modulus than storage modulus (G'' > G') due to the lack of strong interaction between individual molecules. Herein, rheology studies were carried out to determine whether cross-linkage between Caf1 and PEG-SG occurred. The result **(Figure 2.2c)** of Caf1 hydrogel showed that G' (10.0 Pa) is dominant over G'' (0.8 Pa), which indicates that a chemically crosslinked network has been formed.[26,29] Caf1 hydrogel is more elastic and viscous in nature at room temperature in comparison to the non-crosslinked Caf1 protein polymer **(Figure 2.2c)**, where G'' (0.6 Pa) is more dominant over G' (0.2 Pa). The crosslinked Caf1

hydrogel formed can hold a large volume of water, where drug cargo is anticipated to be loaded within the cavity of the hydrogel network.
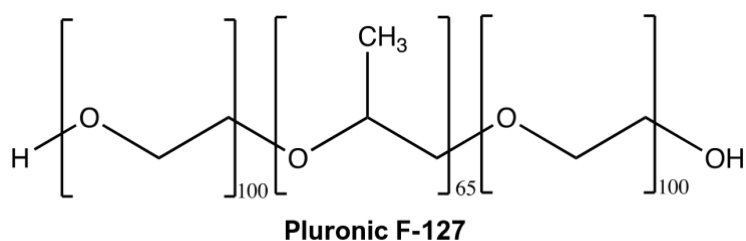
Figure 2.3, Chemical structure of Pluronic F-127, composed of a triblock PEO-PPO-PEO structure. PEO (poly(ethylene oxide)) is hydrophilic, and the central block PPO (poly(propylene oxide)) is hydrophobic.

The synthetic polymer Pluronic F-127 **(Figure 2.3)** was prepared as a benchmark hydrogel, allowing for the comparison of cargo release from the Caf1 hydrogel. The Pluronic F-127 polymers were soluble in water, the hydrogel was prepared by dissolving 20 % (w/v) in water at room temperature, it is important to note that below the 20 % threshold, hydrogel is less likely to form.[29] The Pluronic F-127 polymers **(Figure 2.4a)** form into a micelle[30,31] at pH 7.4 where the hydrophobic central block, PPO aggregate together in PBS and the PEO tail (hydrophilic) facing outward from the micelle, which resulted in a physical hydrogel held together by non-covalent bonds. It is speculated that the Caf1 hydrogel **(Figure 2.4b)** network is composed of hydrophobic and hydrophilic regions.
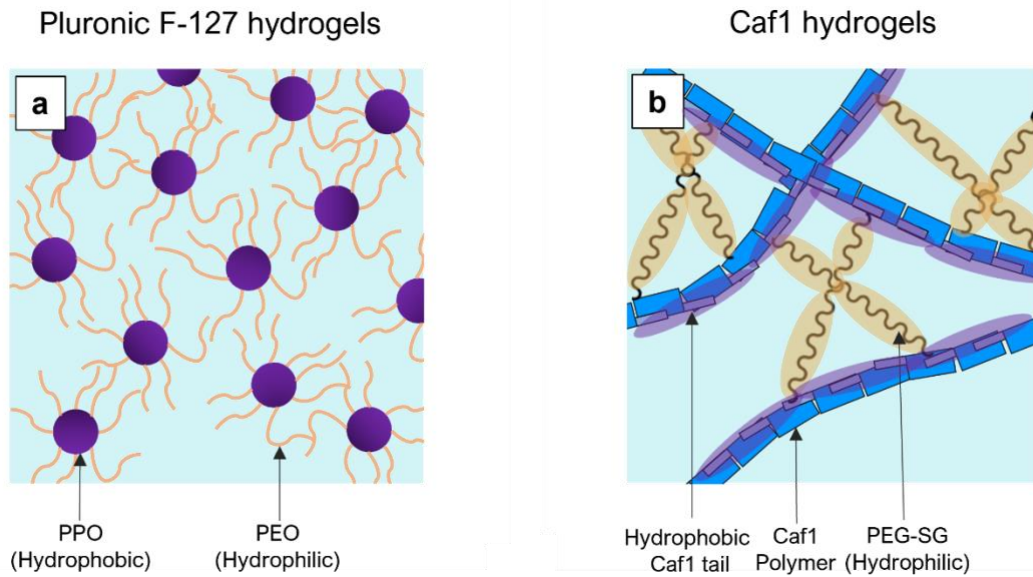
Figure 2.4, (a) Schematic illustration of Pluronic F-127 hydrogels yielded from micelles aggregation linked by non-covalent bonds. The Pluronic F-127 micelles are composed of a PPO head, shown in **purple**, and a PEO tail, shown in **yellow**. **(b)** Illustration of Caf1 hydrogels showing regions of hydrophobic Caf1 protein tail group in **purple** and hydrophilic PEG-SG in **yellow**.
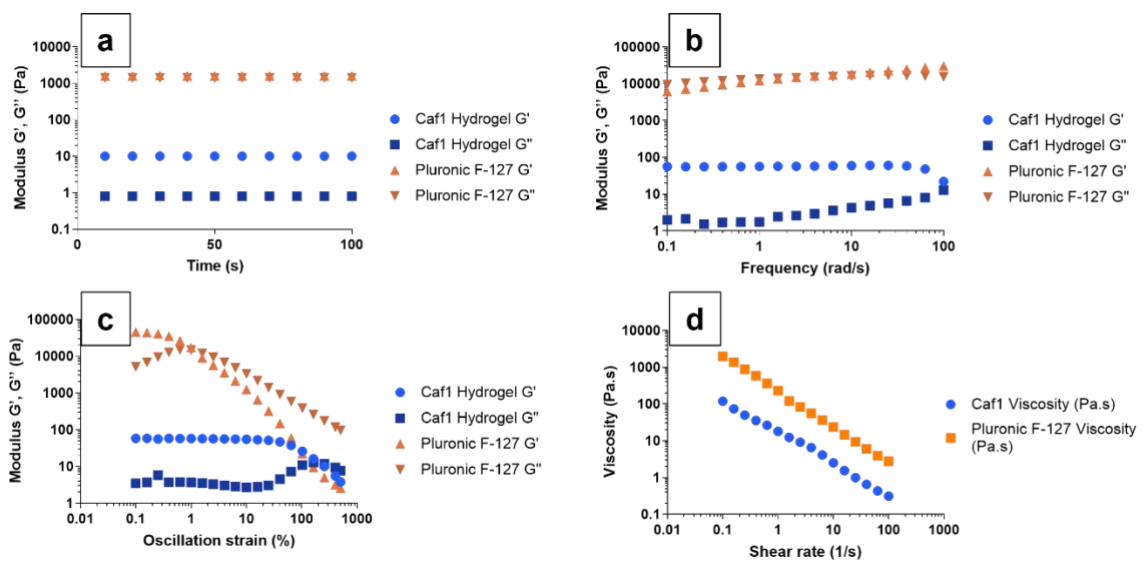
Figure 2.5, (a) Time sweep of 2 % (w/v) Caf1 hydrogel and 20 % (w/v) Pluronic F-127 hydrogel with G' and G'' as the functions. **(b)** Frequency sweep of Caf1 hydrogel and Pluronic F-127 hydrogel with G' and G'' as the functions. **(c)** Oscillation sweeps of Caf1 hydrogel and Pluronic F-127 hydrogel with G' and G'' as the functions. **(d)** Flow sweep of Caf1 hydrogel and Pluronic F-127 hydrogel with shear rate as the functions.

As anticipated, the rheological properties of crosslinked Caf1 hydrogel **(Figure 2.5a, blue)** show that G' is dominant over G'', indicating crosslinking between Caf1 and PEG-SG has occurred and yielded hydrogel. Like Caf1 hydrogel, the Pluronic F-127 hydrogel also displays more elastic properties than viscous properties **(Figure 2.5a, orange)**, which indicates a gel-like material formed as G' is more dominant over G''. To gain better insight into the network structure, the frequency sweep of Caf1 hydrogel **(Figure 2.5b, blue)** was conducted, the result showed that the microstructure of the network is altered at higher frequencies compared to static condition, where G' is more dominant than G'', suggests a defined network and intersection at higher frequencies as polymers entangle. The frequencies sweep **(Figure 2.5b, orange)** of Pluronic F-127 hydrogel, shows G'' is more dominant over G' at stationary and crossed over at ~1 rad/s, suggesting a network of entangled polymer chains.[32] The oscillation sweep revealed the linear viscoelastic region (LVE) **(Figure S2.1)** of Caf1 hydrogel **(Figure 2.5c, blue)** extends to 100% strain; Pluronic F-127 hydrogel **(Figure 2.5c, orange)**, on the other hand, extends to 1% stain. The shear flow properties of Caf1 hydrogel **(Figure 2.5d, blue)** and Pluronic F-127 hydrogel **(Figure 2.5d, orange)** were also studied. Viscosity was measured as a function of shear rate. Steady shear viscosity was measured at shear rates between 0.1 and 100 s^{-1}. Shear-thinning behaviour for both hydrogels was observed as viscosity decreased when a steady shear was applied, and thus the hydrogels displayed a non-Newtonian behaviour. The rheological studies show that both Caf1 and Pluronic F-127 have yielded hydrogels at 2 % (w/v) and 20 % (w/v) retrospectively **(Figure 2.5a)**, that both obtained a higher storage modulus than loss modulus. Despite that, the two are fundamentally different in nature, where one is chemically crosslinked (Caf1) hydrogel and the other a physical (Pluronic F-127) hydrogel, as highlighted by the difference in strain uptake **(Figure 2.5b & c)**.

2.3.2. Small molecule cargo delivery

To evaluate the potential application for the use of Caf1 hydrogels as a drug delivery platform, the release of small molecules was carried out initially to establish the groundwork needed to use Caf1 hydrogels for drug delivery applications. Rhodamine-B **(Figure 2.6a)** was selected as a model cargo because the fluorescence dye can be detected easily by UV and fluorescence spectroscopy.

Caf1 protein polymer and PEG-SG were mixed in a solution of Rhodamine-B (0.001 %w/v). The Caf1 hydrogel was formed, ensuring most of the Rhodamine-B was encapsulated within the hydrogel **(Figure 2.6b)**. Fresh buffer (1.0 ml) was then added on top of the gel, removed after a set time, and the concentration of Rhodamine-B was determined. The procedure is repeated at predetermined time intervals. Concentration was determined based on the calibration plot of Rhodamine-B using a UV spectrophotometer (NanoDrop One, ThermScientificic, UK).

Rhodamine-B (RhdB) release was plotted as cumulative release vs time **(Figure 2.6ci)**, the concentrations of Rhodamine-B were converted into masses, and each point was calculated as the released percentage (%) of the sum of Rhodamine-B mass determined at the time interval and mass found at previous time intervals over total loaded mass. Cumulative released is thus the fraction of total available drug released in percentage terms **(Equation 2.1)**.

$$Fraction\ n: (M_n + M_{n-1})/M_{Total} \quad \textbf{(Equation 2.1)}$$

The release profiles **(Figure 2.6ci)** revealed a quick initial release of Rhodamine-B from both gels recorded (Caf1 hydrogels and Pluronic F-127), with 100 % of Rhodamine-B being released from the Pluronic F-127 hydrogel and 58 % from the Caf1 hydrogel after 2 h **(Figure 2.6cii)**, followed by sustained release of Rhodamine-B between 4 - 60 h was observed from the Caf1 hydrogel network, even though the 2 %w/v Caf1 gel has a lower polymer concentration in comparison with 20 % F-125 gel. The difference between the two release types is due to the interaction between the polymer that made up the hydrogel network and the model drug Rhodamine-B. Rhodamine-B is hydrophilic in pH 7.4, therefore it will be most likely to be found in the hydrophilic regions of the hydrogels in an amphiphilic system such as Pluronic F-127 hydrogel **(Figure 2.4a)** and Caf1 hydrogel **(Figure 2.4b)**. The Pluronic F-127 hydrogel Rhodamine-B was mostly found in the PEO tail of the micelle which was also made up of most of the gel network. It is also anticipated that some of the Rhodamine-B were entrapped within the centre of the micelle. Thus, it resulted in a fast release rate of up to 75% and with the remaining 25% entrapped. Jeong et al.[33] observed similar behaviour when the group followed the release of ketoprofen and spironolactone

(hydrophobic) from a physical hydrogel composed of PEG-PLGA-PEG. Ketoprofen was released over two weeks, followed by a first-order release profile, while spironolactone was released over two months with an S-shaped release profile. The group believe that Ketoporfen was released by diffusion, while spironolactone was released firstly by diffusion, followed by degradation because of different hydrophilic and hydrophobic domains. On the other hand, it is anticipated that Caf1 hydrogel also consists of both hydrophilic and hydrophobic domains. The bi-phasic release of Rhodamine-B is likely the result of the fast initial release of Rhodamine-B encapsulated within the hydrophilic domains in the Caf1 hydrogel, followed by a slower release of Rhodamine-B from the hydrophobic domains in the Caf1 hydrogel.
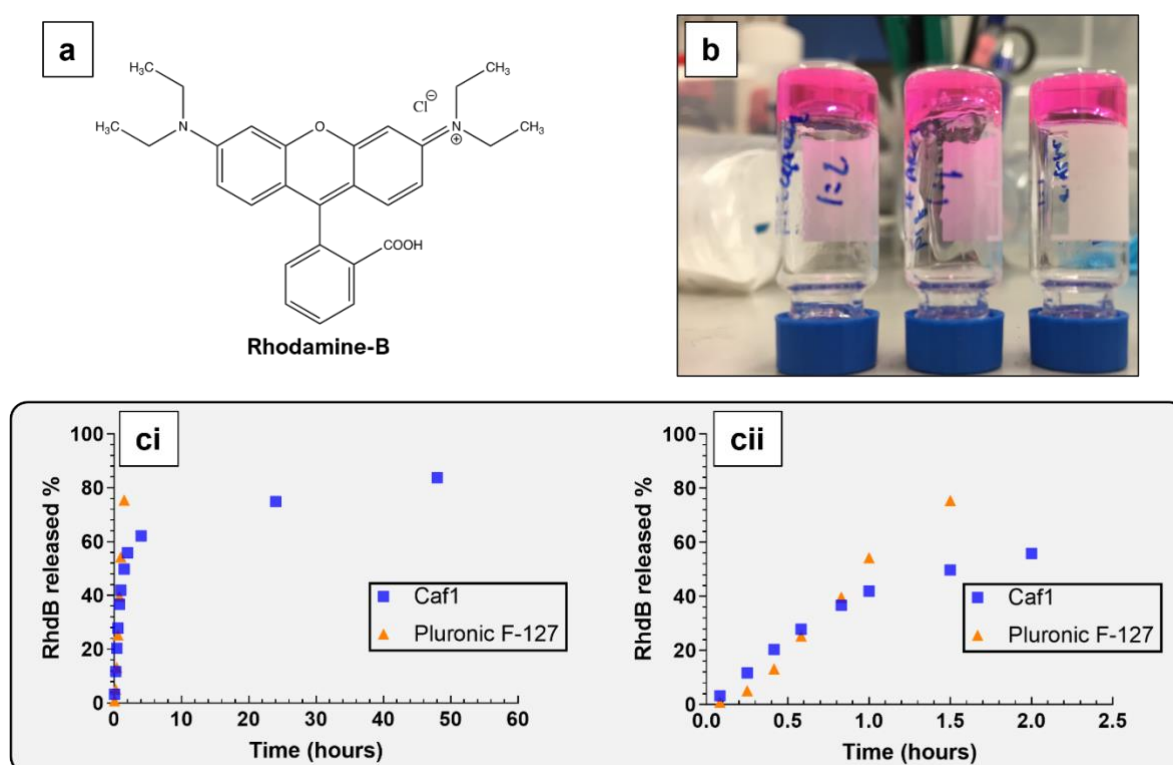
Figure 2.6, (a) Chemical structure of Rhodamine-B, the fluorescence dye at 554 nm (UV). **(b)** Images of Rhodamine-B encapsulated within the 2 %w/v Caf1 hydrogels (1:1). **(ci)** Cumulative Rhodamine-B release profiles from Caf1 hydrogels (blue) and 25 %w/v Pluronic F-127 hydrogels (orange) 0-60 h, and a close-up **(cii)** inset of Rhodamine-B release profile up to 0-2.5 h.
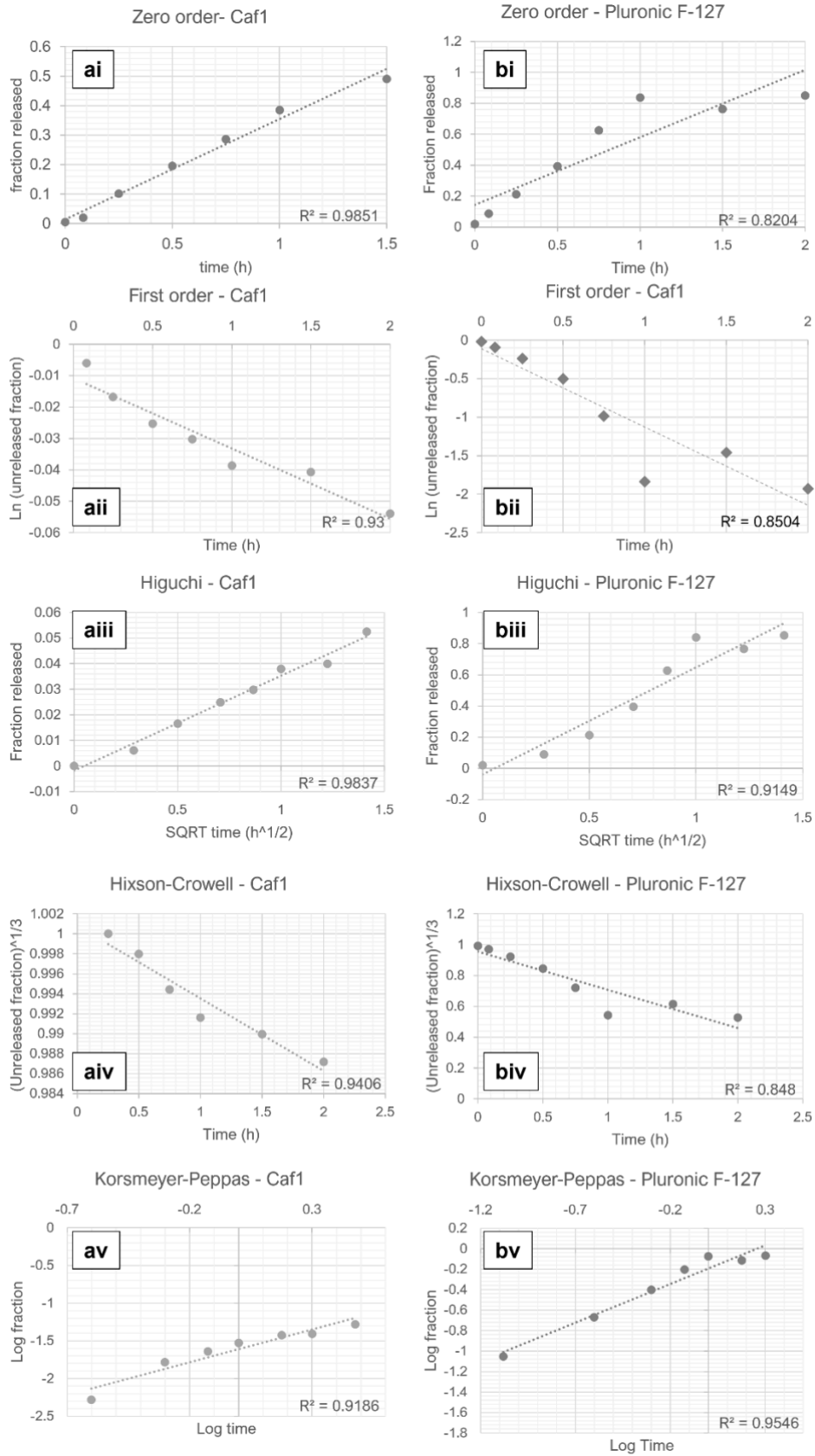
Figure 2.7, Release of Rhodamine-B **(Figure 2.6cii)** from Caf1 **(a)** and Pluronic F-127 **(b)** hydrogels plotted to fit kinetic models based on **Equation 2.7 – 2.11**: **(i)** Zero order; **(ii)** First order; **(iii)** Higuchi; **(iv)** Hixson-Crowell and **(v)** Korsmeyer-Peppas.

Table 2.1, Coefficient of determination derived from kinetic models for Rhodamine-B release from Caf1 and Pluronic F-127 hydrogels **(Figure 2.7)**.

Kinetic Model	Coefficient of determination (R^2)	
	Caf1	Pluronic F-127
Zero-order	0.9851	0.8204
First order	0.9300	0.8504
Higuchi	0.9837	0.9150
Hixson-Crowell	0.9406	0.8480
Korsmeyer-Peppas	0.9186	0.9546
k	1.6117	0.1939
n	0.8684	0.7560

The release profiles were fitted to mathematical models for drug release in the range of M_t/M_∞ = 0.6,[34] i.e., 60% of the total encapsulated drug has been released. Mathematical models were used to analyse the release profile to gain insights into the nature of the release mechanism. How well the data fit a given model can be determined from the calculated coefficient of determination R^2, where values of R^2 = 0.9-1.0 suggests an excellent fit to the model. The coefficient of determinations results was calculated from kinetic models **(Table 2.1)**, indicating that both Caf1 and Pluronic F-127 systems followed first-order release kinetic in the initial 60% of drug release. This suggested that the drug release rate depends on the drug concentration in hydrogels. The results indicate that the coefficient of determination shows that Caf1 and Pluronic F-127 hydrogels are 0.9851 and 0.8204 in the zero-order release kinetic model. In comparison, R^2 of first-order release kinetic (0.9300 Caf1 hydrogel and 0.8504 Pluronic F-127 hydrogel), whose coefficient of determinations suggests that drug release rate is independent of drug concentration.[35] This observation suggests the drug release rate in Pluronic F-127 systems is driven by osmotic effects, where the concentration gradient drives the release of Rhodamine-Bt. The release of RhdB from Caf1 hydrogel is not dependent on the changes in a concentration gradient, where RhdB is released at a constant pace. The Higuchi model is based on drug release as diffusion based on Fick's law. The Hixson-Crowell model describes drug release by dissolution rather than diffusion, where the dissolution of the network leads to changes

in the surface area of hydrogels and the size of the drug cargos.[36] The results from these two models indicated that both release profiles from Caf1 and Pluronic F-127 gels are based on diffusion, as the coefficient of determination is closer to 1.0 in Higuchi than Hixson-Crowell models. Korsmeyer-Peppas model describes drug release considering both diffusion and network swelling. The Caf1 and Pluronic F-127 hydrogels both afford a diffusion exponent (n = 0.8684 and 0.7560) higher than 0.5, indicating it follows non-Fickian diffusion where diffusion and swelling occur. Whereas a Fickian diffusion (n < 0.5) indicates constant diffusion has occurred defined by Fick's Law. In conclusion, the majority of Rhodamine-B release from Caf1 and Pluronic hydrogels are driven by diffusion following first-order kinetic.

2.3.3. Effect of porosity on drug release

Further release studies were performed to investigate the effect of crosslink density on the Rhodamine-B release rate. The crosslink density of the Caf1 hydrogels network can be tuned by altering the concentration of polymer and/or crosslinker.[37] It is hypothesised that by reducing pore sizes, the rate of drug release will be affected, as the decrease in porosities leads to reduce in drug motilities and alter the underlying mass transport mechanism and promotes a slower release rate. Thus, the relative drug release rates can be tuned by modifying the pore size of the networks.

Table 2.2, Formulation and mechanical properties of Caf1 hydrogels with increased crosslink density.

ENTRY	Caf1 (%w/v)	4-Arm PEG-SG (%w/v)	8-Arm PEG-SG (%w/v)	G′ (Pa)	G′′ (Pa)	Ge (Pa)	Mesh size* (nm)	Crosslinking density**
1	2	2	-	13.87	1.28	12.86	67.57	0.005
2	2	-	2	39.53	3.31	48.14	47.66	0.019
3	2	4	-	70.99	4.16	58.32	39.21	0.023

* Mesh size calculated using **Equation 2.2**

** Crosslink density calculated using **Equation 2.3**
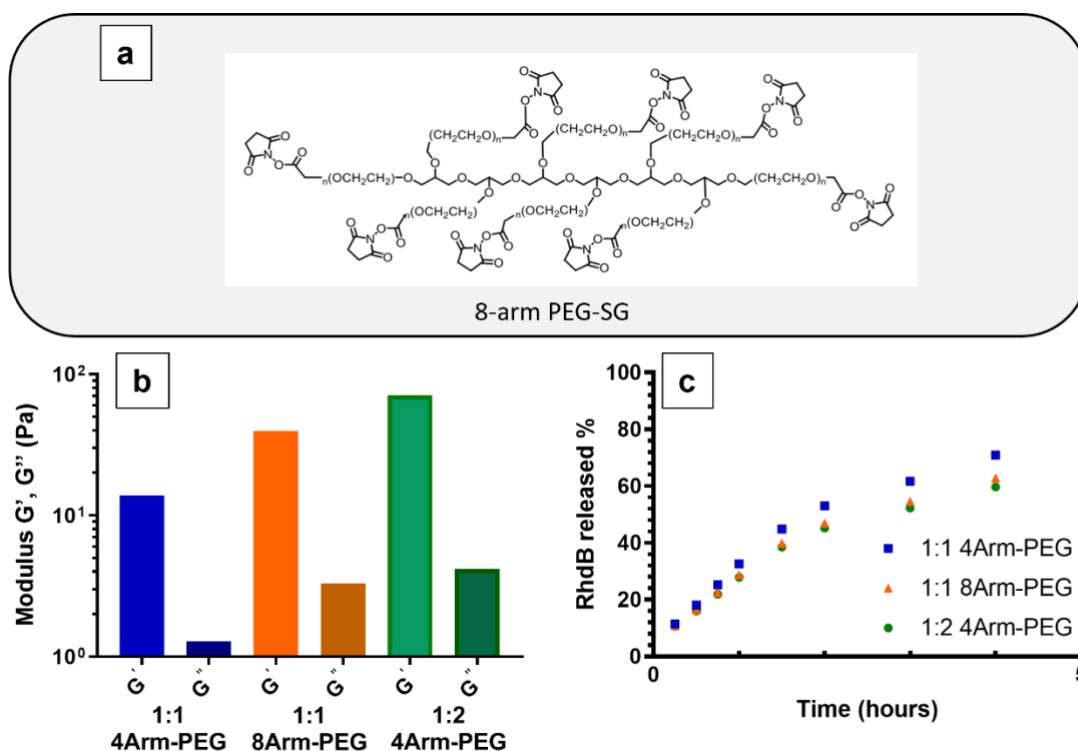
Figure 2.8, (a) Chemical structure of 8-Arm PEG-SG (MW: 20 k). **(b)** Rheological properties of Caf1-hydrogels as crosslink density increases the storage modulus (G') as the cross-linker density increases. **(c)** The cumulative release of Rhodamine B from the Caf1-hydrogels reduced as the size of the pores decreased; 1:2 4 Arm-PEG is the most efficient in prolonging drug release.

To test this hypothesis, Caf1 hydrogels possessing a number of crosslinked networks were prepared. Three gels were prepared with 4-Arm PEG-SG (1:1 2 %w/v Caf1) **(Table 2.2, Entry 1)**, 8-Arm PEG-SG **(Figure 2.8a)** (1:1 2 %w/v Caf1) **(Table 2.2, Entry 2)** and 4-Arm PEG-SG (1:2 2 %w/v Caf1) **(Table 2.2, Entry 3)**. Rheological studies **(Figure 2.13b)** of Caf1 hydrogels showed that the difference between storage modulus (G') and loss modulus (G'') increased as either the polymer concentration increased or increase in crosslinker concentration or the number of structural arms of PEG which all will contribute to an increase cross-link density. An increase in crosslink density in the hydrogel was prepared from 8-Arm PEG-SG (1:1) **(Table 2.2, Entry 2)**, obtained a storage modulus of 393.13 Pa, showed an increase in strength compared with 4-Arm PEG-SG (1:1) **(Table 2.2, Entry 1)** of 138.42 Pa. Moreover, an increase in the concentration of short-chained 4-Arm PEG-SG (1:2) **(Table 2.2, Entry 3)**

crosslinker increased the crosslink points and hence improved the strength of the network, a storage modulus of 670.55 Pa was measured.

$$\xi = \left(\frac{G'N_A}{RT}\right)^{-\frac{1}{3}} \qquad \textbf{(Equation 2.2)}[38]$$

$$n_e = \frac{G_e}{RT} \qquad \textbf{(Equation 2.3)}[38]$$

The relationship between stiffness and mesh size is described by the equation above **(Equation 2.2)**, where the average mesh size (ξ, nm) describes the distance between the crosslinking points; R is the gas constant (8.314 J/L mol); T is the absolute temperature (310 K), and N_{Av} is the Avogadro constant (6.022×10^{23}). Furthermore, the crosslinking density of the hydrogels can be evaluated using **Equation 2.3**, the crosslinking density (n_e, mol/m^3) defined as the number of elastically active junctions in the network per unit of volume, calculated with the plateau value of storage modulus (G_e, Pa) measured with frequency sweeps. This results **(Figure 2.8b)** in a crosslink density increase, the difference between G' and G'' also increases, and thus pore size decreases. Release profiles of Rhodamine-B **(Figure 2.8c)** show that the release rate decreases. It is likely the result of the decrease in hydrogel mesh size, and thus, reduces the size of diffusion pathways and prolongs the time needed to free it from the hydrogel network.

2.3.4. Macromolecule delivery

The well-studied Bovine Serum Albumin (BSA) was chosen as a model protein to provide information on the release rate of macromolecules. BSA is a serum albumin (blood albumin) protein derived from cows.[39,40] It is hypothesised that its rate of release will be slower on account of the size difference between BSA and Rhodamine-B. The BSA protein contains 583 amino acid residues with a molecular weight of 66.5 kDa, translating to approximately a diameter of 14 nm[41] compared to Rhodamine-B. To improve the fluorescent level of BSA for release experiment studies, BSA was reacted with fluorescein isothiocyanate (FITC) **(Figure 2.9a)**, a fluorescence dye that can be observed by UV and fluorescent spectroscopy **(Figure 2.9a)**. The addition of FITC to BSA allows for detection at its peak at 525 nm **(Figure 2.9b)**, whereas the Caf1, BSA and PEG are detected below 300 nm **(Figure 2.9c)**.
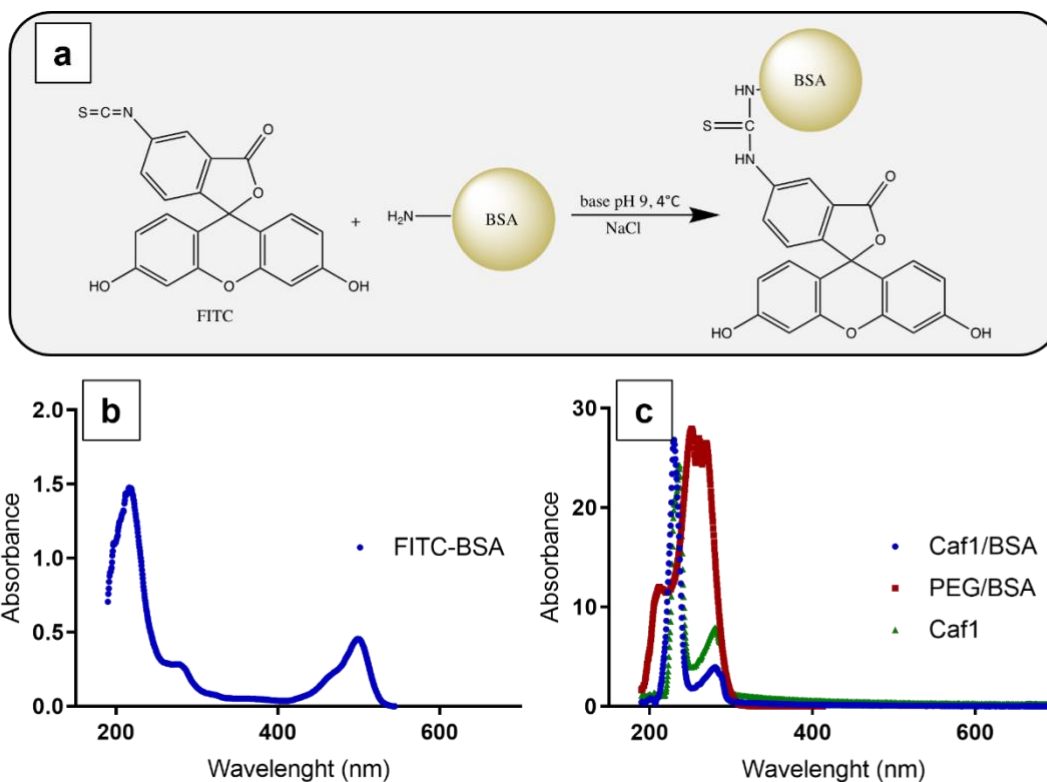
Figure 2.9, (a) Reaction scheme of bovine serum albumin (BSA)-fluorescein isothiocyanate (FITC) conjugation. **(b)** UV absorbance spectroscopy of FITC-BSA and **(c)** Caf1-BSA, PEG-SG interacted with BSA, and Caf1.
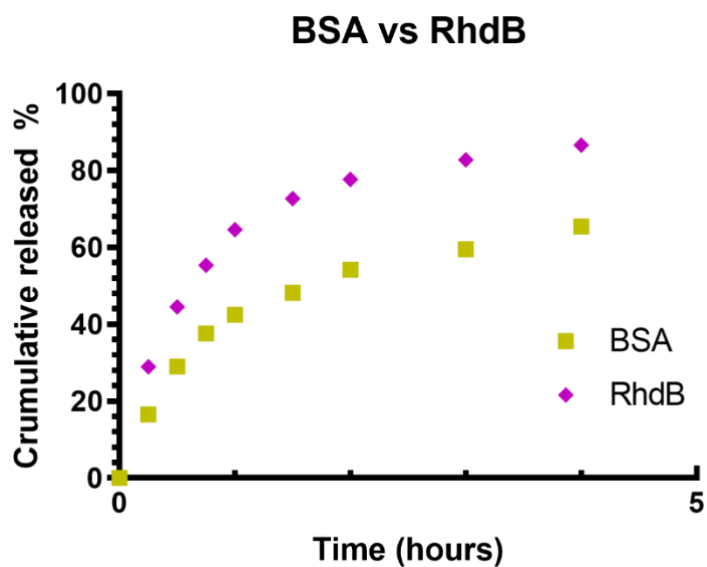
Figure 2.10, BSA and Rhodamine-B (RhdB) release profiles from Caf1 hydrogels (2 %w/v) up to 5 h.

FITC-labelled BSA and RhdB were loaded into the Caf1 hydrogels directly during the crosslinking step, as mentioned previously in this chapter, and the release of these model cargos was measured. As expected, the results **(Figure 2.10)** show that BSA has a reduced release efficiency when compared with Rhodamine-B, as the larger BSA molecule diffuses through the gel slower than, the smaller Rhodamine-B molecule. The overall release rate thus depends upon the size of the cargos; a small drug relative to the network mesh size diffuses rapidly through the hydrogel, resulting in a short release duration. As the size of a drug approaches the mesh size, the drug release is slowed.[42]

Despite the encouraging results, it is important to point out that the experimental setup has a flaw where BSA is possibly crosslinked with PEG-SG instead of Caf1. This is because the amide bond formation is not selective, and thus, PEG-SG can react with lysine residues on BSA (60 lysine residues per protein) and/or Caf1 proteins to form cross-linkages. It resulted in retained BSA within the hydrogel network and/or faster release rate due to weaken the mechanical properties of the Caf1 hydrogel network. Therefore, alternative approaches were investigated to eliminate this design flaw and load biomolecules into the hydrogels.

2.3.5. Preparation Caf1 hydrogels and loading of model biomolecule cargos
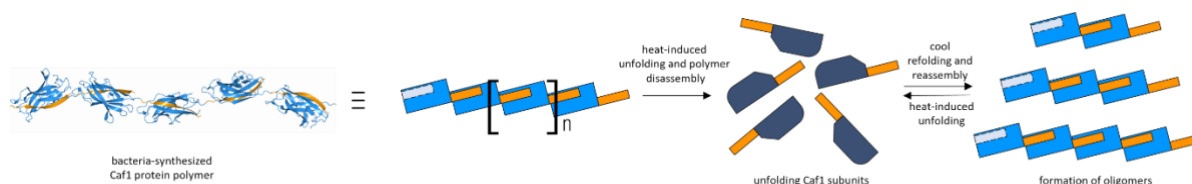
Figure 2.11, Model of a Caf1 polymer (generated from PDB entry 1P5U)[29]. The N-terminal donor strands (coloured **orange**) are complexed by the acceptor clefts (coloured **blue**) of adjacent sub-units. Caf1 subunits undergo a reversible thermal unfolding and refolding.

In this part of the study, three macroscopic protein cargos loading approaches were drafted by utilising the refolding properties of the Caf1 protein **(Figure 2.11)**. As discussed in the previous chapter, the Caf1 protein possess a unique property which allows the protein polymers to thermally interconvert between its polymeric and monomeric forms. More importantly, this property is retained even when the Caf1

protein is chemically crosslinked. By captivating this unique property of Caf1, it is theorised that it can help to reduce the undesired cargo proteins' interaction with the PEG-SG crosslinker. With this in mind, the "*melt* Caf1 hydrogel" approach **(Figure 2.12)** of cargo loading was drafted, where *native* Caf1 hydrogel was prepared by crosslinking Caf1 protein polymers with the 20 kDa *N-hydroxy succinic* acid-terminated multi-arm PEG cross-linker as mentioned previously. The prepared aqueous solutions of protein cargo were then added into the molten hydrogel, where the Caf1 protein had to undergo thermal unfolding and converted into its monomeric forms, the mixture was allowed to reset, while this window allowed for protein cargos encapsulation to take place. Another approach (*abs* Caf1 hydrogel) **(Figure 2.12)** was investigated by the absorption of aqueous solutions of protein cargo into the fully dehydrated hydrogel. It is also good to note that the dehydrated hydrogel used for *abs* Caf1 hydrogel undergoes a cycle of thermal refolding (Caf1 hydrogel that has been subject to one complete cycle of melting and resetting), to ensure a good comparison with the *melt* Caf1 hydrogel. As studies from our research group have demonstrated that mechanical strength decreases (slightly lowered stiffness and increased critical strain) after a cycle of thermal refolding in comparison to the original *native* Caf1 hydrogel **(Figure 2.2a & S2.2)**. It was speculated that this difference most likely arises because of differences in network topologies, with the *refolded* -Caf1 networks having more dangling ends than the more regular *native* Caf1 networks, and therefore is likely to be relatively more porous.
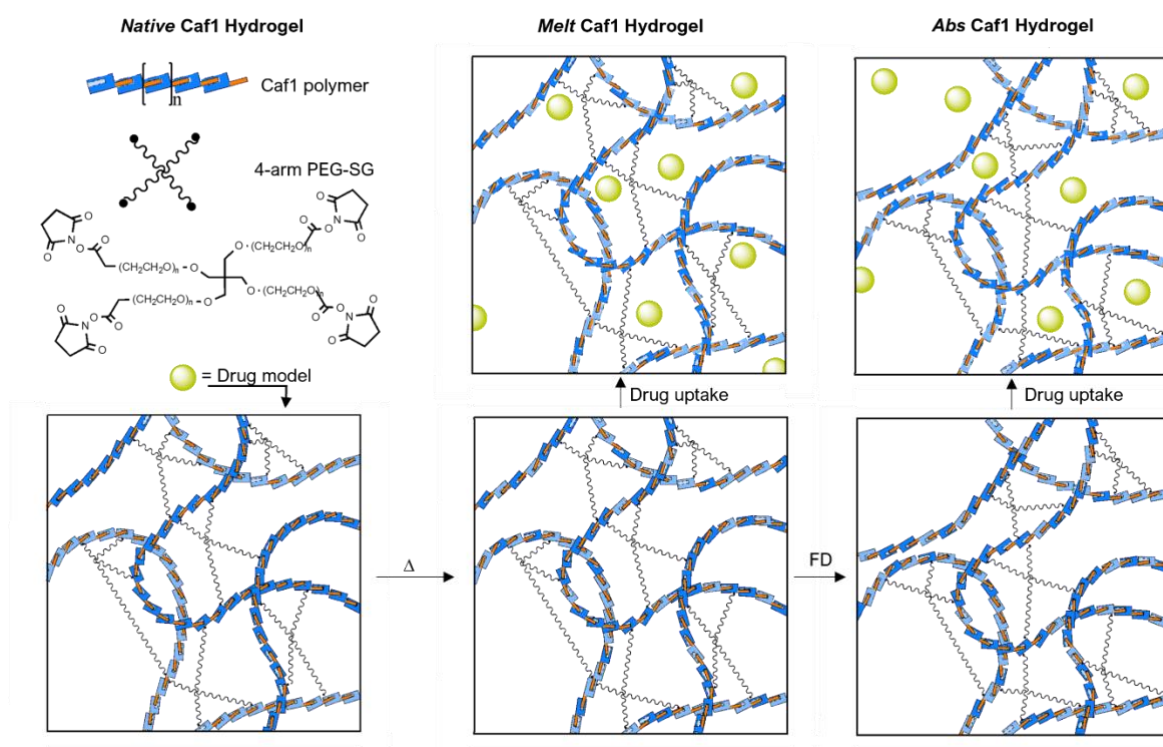
Figure 2.12, The crosslinking of native Caf1 polymer with a commercially available 20 kDa N-hydroxy succinic acid-terminated PEG cross-linker to form a native Caf1 hydrogel. Cargo loading is performed by one of two approaches: Approach (1) "melt Caf1 hydrogel". The native Caf1 hydrogels were melted through the application of heat, followed by immediate cooling and the addition of the protein cargo. Subsequent cooling afforded the protein-encapsulated hydrogels. Approach (2) "abs Caf1 hydrogel". The hydrogel was through the application of heat followed by immediate cooling, and the gel was allowed to reset. This step is required to ensure changes in the network topology that occur during the melting resetting process and are consistent between both cargo loading approaches. The hydrogel was then freeze-dried to eliminate water, aqueous solutions of protein cargos were added, and the cargo was allowed to absorb into the hydrogel networks.

To study the new cargo loading approaches, three proteins (BSA, Trypsin, and Deoxyribonuclease) **(Figure 2.13)** were selected because of their different size and/or surface charges **(Table 2.3)**. By altering the concentrations and ratios of *native* Caf1: PEG-SG cross-linker, it is possible to tune the rheological properties of the resulting Caf1 hydrogels, thus, changing the overall release rate. Building on this knowledge, the relationship between the rate of release and the pore size is further investigated where proteins were loaded in both *melt* and *abs* Caf1 hydrogels at a difference Caf1:PEG-SG ratio (1:1, 1:2). As established above, the release rate reduces as it approaches near or bigger than the pore size of the hydrogel network. Thus, it is

anticipated that the release rate will be slower as the pore size reduces with the hydrogel containing Caf1:PEG-SG at a 1:2 ratio (5:10 %w/v), compared to the hydrogel containing lower crosslinker contained at 1:1 ratio (5:5 %w/v). Although a wide variety of hydrogel formulations are available, in this study, it was decided to work with Caf1 polymer concentration of 5 %w/v as exploratory work as these particular formulations showed efficiency at re-gelation after melting (unfolding). These formulations also allow two different cross-linking densities to be explored.

DNase   BSA   Trypsin
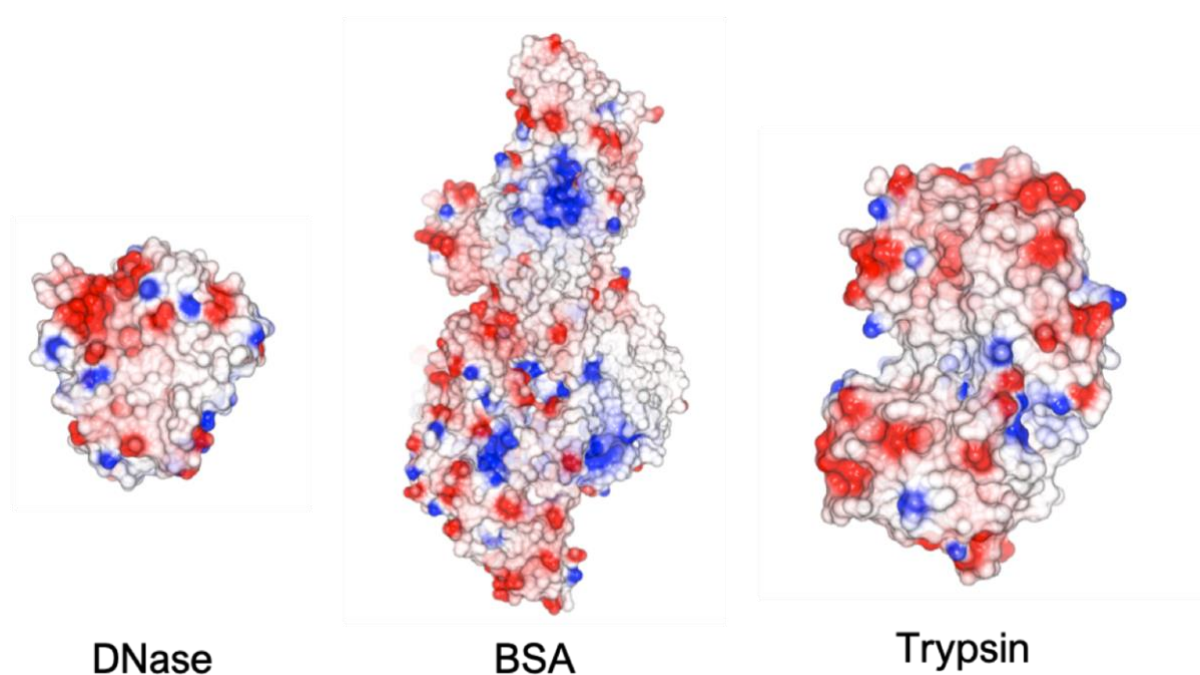
Figure 2.13, A range of protein cargos model selected. Deoxyribonuclease (DNase, 4.5 nm, 4.9 - 5.22, 3dni); Bovine serum albumin (BSA, 14 nm, 4.8 - 5.4, 3v03); Trypsin (11.6 nm, 9.3 - 10.5, 1fon). Electrostatic surface potentials are coloured in **red** (negative charges), blue (positive charges), and white represents neutral residues.

Table 2.3, Macromolecule proteins molecular weight, isoelectric point, and hydrodynamic diameter.[43]

	Molecular weight (kDa)	Isoelectric point	Hydrodynamic diameter (nm)
DEOXYRIBONUCLEASE	31	4.9 – 5.22	4.5
BSA	66	4.8 – 5.4	14
TRYPSIN	23.4	9.3 – 10.5	11.6

Native Caf1 hydrogels were prepared in the same way as mentioned above, that Caf1 protein polymer (5 %w/v) was dissolved in PBS buffer (200 µL) with mild heating (40 °C) for 5 min and mixed with 4-Arm PEG-SG (5 or 10 %) dissolved in bicarbonate solution (200 µL), the hydrogels were allowed to set overnight before the next step. The protein cargos (BSA, Trypsin, Deoxyribonuclease) were labelled with FITC, so that they can be measured by UV or fluorescent as the drug cargo escape the hydrogel network. To load cargo into Caf1 hydrogels by the "*melt*" approach **(Figure 2.14)**, aliquots of *native* Caf1 hydrogel were melted by heating at 100 °C for 1 min to afford a *sol*. Solutions of protein in PBS (20 µL) were then added immediately, and the solution was gently agitated to ensure mixing the sample tube was then put on ice to speed up regelation by removing excess heat and slowing down Caf1 protein unfolding, which resulted in affording the cargo-encapsulated hydrogel. The absence of a layer of liquid above the hydrogel suggested complete encapsulation of the protein cargos with the hydrogel network. To load model protein cargos into Caf1 hydrogels by the absorption method, aliquots of *refolded*-Caf1 hydrogels (420 µL) were lyophilised. Solutions of protein cargo in PBS were then added, and the hydrogel was left to absorb the protein solution into its matrix overnight, affording the cargo-loaded "*abs*" Caf1 hydrogels **(Figure 2.14)**. Again, the absence of a distinctive layer of water above the hydrogel suggests that all protein cargo was absorbed into the hydrogel network. To distinguish between the different cargo-loaded hydrogels, we use the notation which provides the name of the protein cargo, the method of cargo loading (by melting or absorption, and Caf1 concentration (5 %w/v) within the final hydrogel formulation).
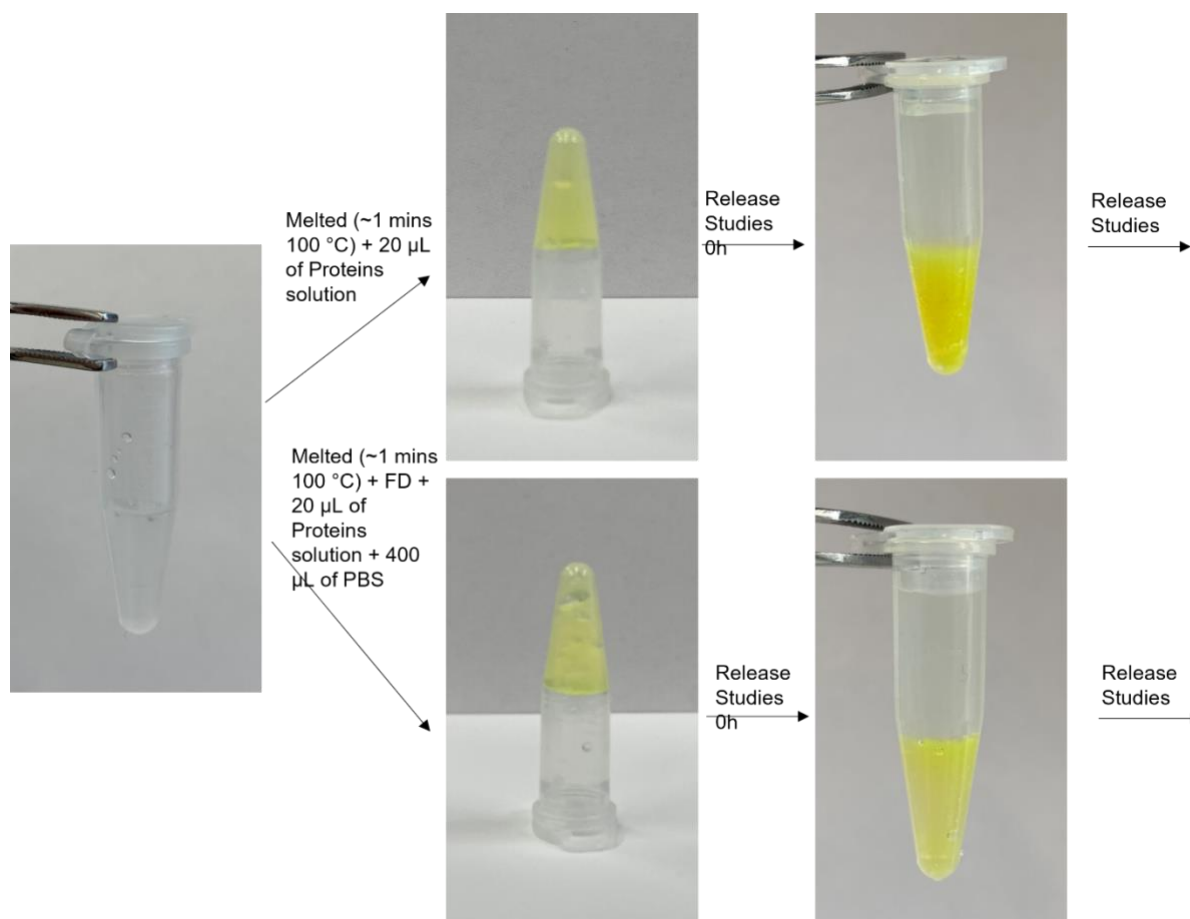
Figure 2.14, Images of fluorescence labelled protein cargos loaded into Caf1 hydrogels via "melt" or "abs" approach. Hydrogels were prepared by crosslinking Caf1 polymer with a PEG-SG crosslinker, it was then melted at 100 oC for 1 min, before 20 µL of the fluorescence labelled protein were added to the solution and allowed to cool overnight using the "melt" cargo loading approach before carrying out the release study. Cargo loaded via the "abs" approach was prepared in the same way as the "melt" approach, where Caf1 hydrogel was prepared and melted, and 20 µL of PBS buffer was added to the mixture before freeze-drying. 420 µL of protein cargo in PBS was added to the freeze-dried hydrogel and allowed absorption overnight before the release study.

Model protein cargos **(Figure 2.13) (Table 2.3)** Bovine Serum Albumin (BSA), Deoxyribonuclease (DNase) and Trypsin (Try) were chosen due to their differences in molecular weights and isoelectric charges which will provide a better insight to the drug loading efficiency via the two different cargo loading approaches. These protein cargos were loaded into the Caf1 hydrogels using both the "*melt*" and "*abs*" approach, the release kinetic studies were carried out at pH 7.4 and 37 ^{o}C to simulate body condition. The contains (cargo protein mixture) released from the Caf1 hydrogel network was analysed by UV spectrometry at predetermined time intervals (0.5, 1, 1.5,

2, 3, 4, 24, 48, 72, 96 h), the fraction of protein cargo release was plotted as cumulative release profiles shown in **Figure 2.15**. As a crude estimate of the release rate, the half-life ($t_{1/2}$) was determined in which half-life is defined as the time taken to release half the cargo **(Table 2.4)**.
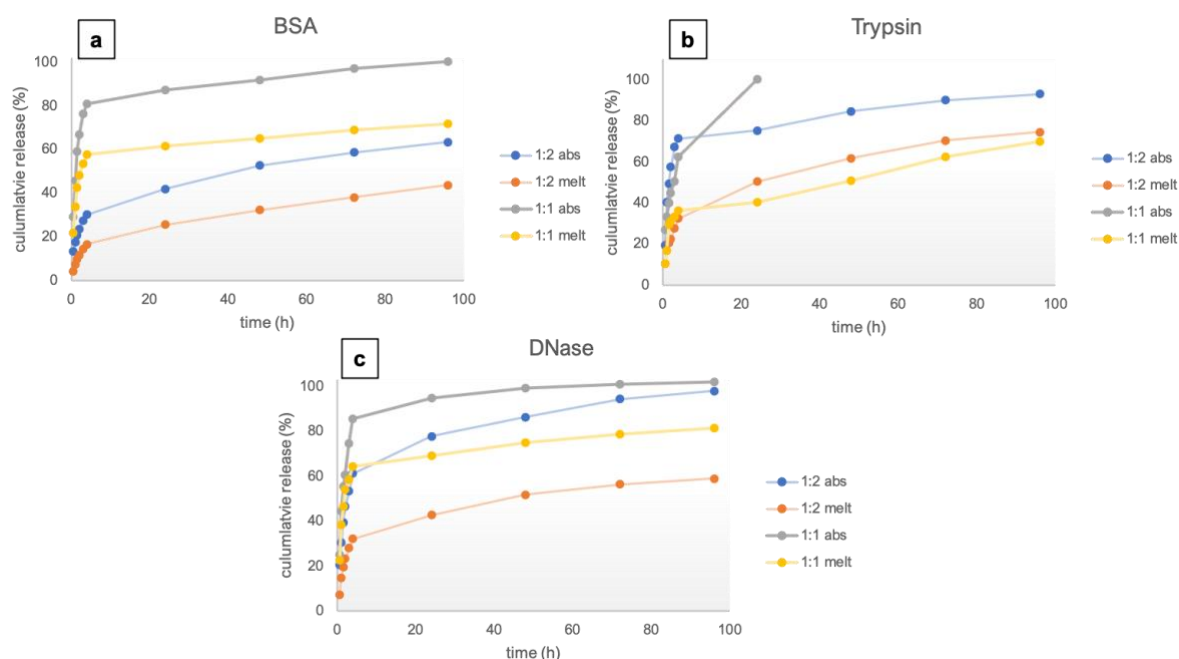
Figure 2.15, Cumulative release profiles of BSA **(a)**; DNase **(b)**; Trypsin **(c)** from 1:2 *abs* shown in **blue**; 1:2 *melt* in **orange**; 1:1 *abs* in **grey**; 1:1 *melt* in **yellow**. The ratio presented Caf1:PEG-SG in mass over volume (5:5 %w/v and 5:10 %w/v).

From release profiles **(Figure 2.15)** and half-life **(Table 2.4)**, it is clear that release is slower when protein cargos have been loaded via the "*melt*" approach when compared with the "*abs*" loading approach for the hydrogels of the same composition, i.e., 1:2 *melt* is slower (between 3.3 and 18.3 times slower) than 1:2 abs; 1:1 melt is slower (between 1.5 and 13.7 times slower) than 1:2 *abs* approach for all protein cargos. This observation suggests that they are more homogenously encapsulated throughout the hydrogels when loaded through the "melt" approach compared to the "*abs*" loading approach. It is speculated that the loading efficiency is poorer via the "*abs*" (absorption) approach than the "*melt*" approach; this is because cargos are likely to be found near the surface and did not travel through into the centre of the

50

hydrogel network (protein cargo enters through the door and tends to hang around the door), and thus, a faster release is anticipated.

Table 2.4, Half- life ($t_{1/2}$) determined from the BSA, DNase and Trypsin release profiles. The Half-life ($t_{1/2}$) were compared in the form of % reduction by comparing $t_{1/2}$ of "*abs*" hydrogel to its counterpart "*melt*" hydrogel.

		t1/2 (h)	% reduction
BSA	1:1 melt	2.57	2.1 times slower
	1:1 abs	1.22	
	1:2 melt	140.61	3.3 times slower
	1:2 abs	43.01	
DNase	1:1 melt	2.03	1.5 times slower
	1:1 abs	1.38	
	1:2 melt	47.01	18.3 times slower
	1:2 abs	2.57	
Trypsin	1:1 melt	35.42	13.7 times slower
	1:1 abs	2.59	
	1:2 melt	24.81	
	1:2 abs	1.74	14.3 times slower

As discussed previously in this chapter, an increase in the quantity of crosslinker in the formulation leads to increased crosslink density, resulting in a slower release over time. This was observed in all the release profiles **(Figure 2.15)**, that release from the 1:2 *abs* approach is slower than the 1:1 *abs approach*, likewise for the cargos loaded via the "*melt*" approach.

Closer analysis of the cumulative release profiles **(Figure 2.15)** comprising an initial fast release during approximately the first 4 h, followed by a slower release phase over the rest of the experiment. The fast-release phase of the release profiles sees significant levels of cumulative release (~15 – 85 % of the total protein mass), suggesting this is more complex than a burst-release phenomenon associated with proteins absorbed close to the surface of the hydrogel-water interface. To gain insight, the release profiles were fitted to the Korsmeyer-Peppas model **(Equation 2.4)**[44]:

$$M_t/M_\infty = kt^n \qquad \text{Equation 2.4}$$

where M_t/M_∞ represents the fractional release of the loaded protein, k is a kinetic constant, t is the release time, and n is the diffusional exponent that can be related to

the release mechanism of the entrapped molecules. If n = 0.5, the release is governed by Fickian diffusion. If n = 1, molecules are released by surface erosion, while both mechanisms play a role in the release if n has a value between 0.5 and 1. The initial 60 % of release data were fitted to the Korsmeyer-Peppas model **(Figure 2.16)**, and *n*-value were found to be mostly below 0.5, that indicates the release of these systems was mostly diffusion-controlled with the exception of BSA-abs-1:1 (n = 0.641) and DNase-abs-1:1 (n = 0.730)[45]. This was further investigated using Higuchi and Hixson-Crowell models **(Table 2.5)**, Higuchi model describes a release profile which is diffusion-controlled, whereas Hixson-Crowell is best fitted for drug release via dissolutions. Overall, the result shows that all the release profiles are diffusion-controlled, and the release is not due to dissolution as it is a better fit to Higuchi than the Hixson-Crowell model, where the coefficient of determination R^2 value is closer to 1 **(Table 2.5)**.
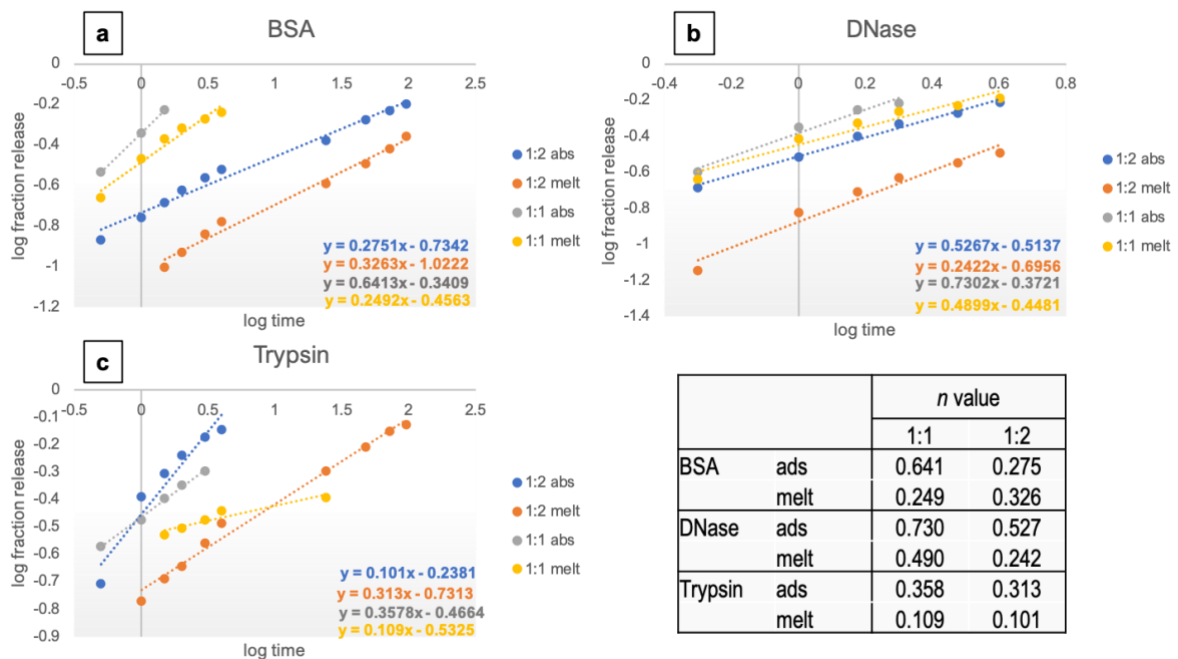
Figure 2.16, The initial 60% data of the release profiles (BSA, DNase and Trypsin) were fitted to the Korsmeyer-Peppas model. The n-value was determined from the gradient of the line of best fit.

Table 2.5, Coefficient of determination R^2 value determined from Higuchi and Hixson-Crowell model fitted by the release profiles of BSA, DNase and Trypsin up to 60 % of release.

		Coefficient of determination, R^2	
		Higuchi	Hixson-Crowell
BSA	1:1 melt	0.965	0.872
	1:1 abs	1.000	0.997
	1:2 melt	0.978	0.917
	1:2 abs	0.947	0.865
DNase	1:1 melt	0.985	0.932
	1:1 abs	0.994	0.976
	1:2 melt	0.909	0.780
	1:2 abs	0.989	0.945
Trypsin	1:1 melt	0.863	0.767
	1:1 abs	0.992	0.957
	1:2 melt	0.992	0.961
	1:2 abs	0.942	0.860

The mathematical analysis using the kinetic models (Korsmeyer-Peppas, Higuchi and Hixson-Crowell) indicated that the release is diffusion-controlled, however, it does not fully resolve the difference in release rate. The difference in release rate could be due to several factors, such as molecule size, static charges between the hydrogel matrix and the protein cargo, or the encapsulation method. To explore this possibility, the hydrogels' swelling, and degradation rates were investigated. The swelling and degradation rate are directly correlated to the release rate of the cargo as the swelling and degradation drive the release of cargo exponentially[46–49], thus, it was decided to investigate the swelling/degradation of the hydrogels. Chemically crosslinked Caf1 hydrogels are anticipated to uptake water up until its threshold and retain it for a period.[50] The Caf1 hydrogels of "*melt*" and "*abs*" were prepared using the same protocols as for the *in vitro* release studies, the sample hydrogels were allowed to be set over 2 d before the experiment. To start the experiment, the sample hydrogel was weighted (200 µl), then PBS (1mL) was added to each Caf1 hydrogel, excess PBS was removed, and Caf1 samples were then weighted at pre-determined times. Each 1 mL of PBS buffer taken was replaced with another 1 mL of PBS. Percentage swelling and degradation were calculated using **Equation 3** (see Experimental), and the data is presented in **Figure 2.17**. It was observed that *melt*-Caf1 hydrogel swelled notably from 0 h and dissolved gradually after 100 h. For the *abs*-Caf1 hydrogel, the

degradation rate is more progressive than the swelling rate, and the volume of the hydrogel reduced to approximately 82% of its original volume over 148 h. Thus, a faster release rate from *abs*-Caf1 hydrogel was observed as encapsulated cargos were released as the hydrogel degraded gradually. On the other hand, the *melt*-Caf1 hydrogel swells as time progresses, reducing the cargo release rate. This is because hydrogel swells, leading to an increase in hydrogel thickness and the length of the diffusion pathway, thus leading to a prolonged protein cargo diffusion time. This finding is painted a better insight into the release mechanism that took place for the latter phases of release, as shown in **Figure 2.16** less than 10 % of physical changes occurred before 24 h. The fast initial phase (0 – 4 h) and the subsequent slow phase (4 – 100 h) were both diffusion-controlled, as discussed above, it is anticipated that the difference in release rate is due to cargo sizes, static charges, and possible interaction with the matrix.
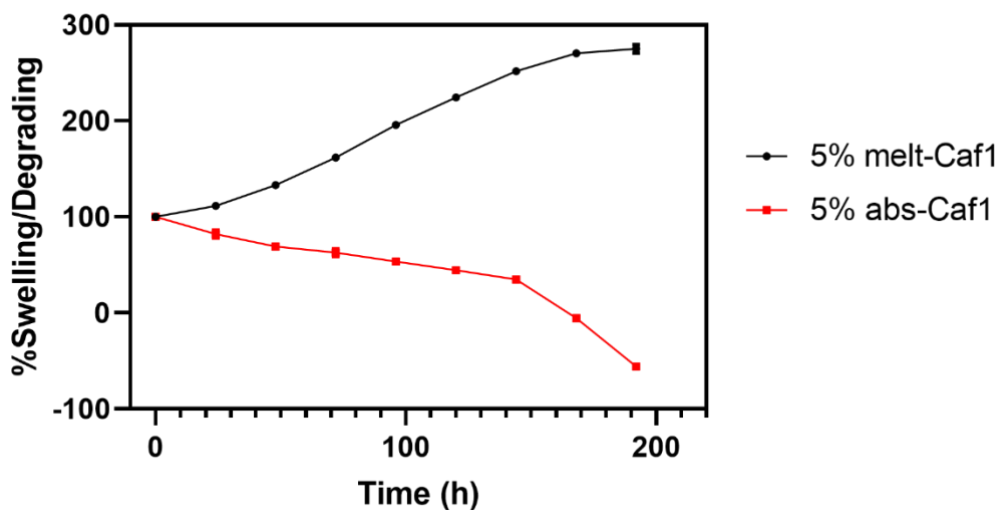
Figure 2.17, Swelling and degradation index of melt and abs 5 % Caf1 hydrogels (1:1).

In order to study the correlation between the release data, the diffusion coefficient **(Figure 2.18)** of BSA, DNase and Trypsin release experiments was calculated using an early-time approximation equation of Fick's second law **(Equation 2.5)**[31,39,45,51]. Where M_t/M_∞ is the fractional cargo release of the entrapped cargos, D is the diffusion coefficient, t is the release time and δ the diffusional distance, equal to the hydrogel thickness.

$$M_t/M_\infty = 4(Dt/\pi\delta^2)^{1/2} \qquad\qquad \textbf{Equation 2.5}$$
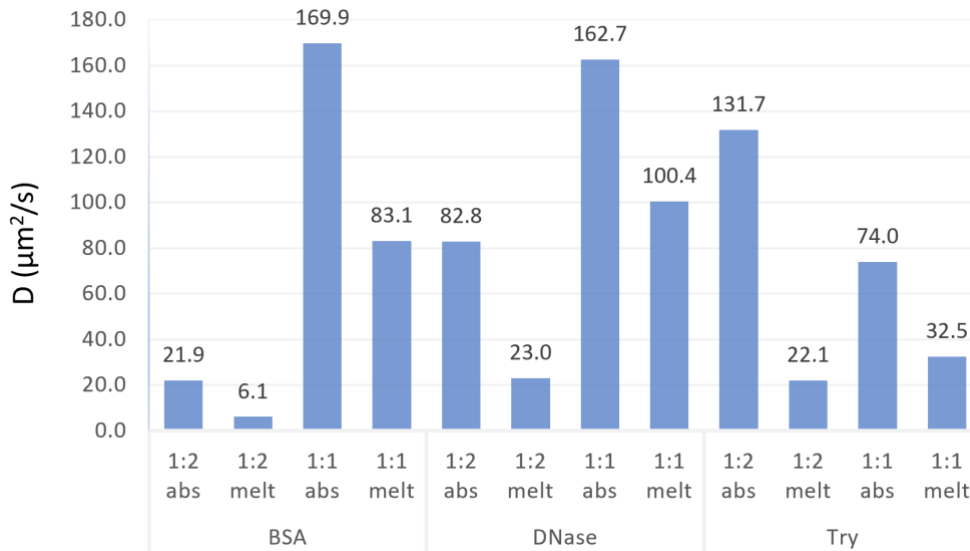
Figure 2.18, Diffusion coefficients of BSA, DNase and Trypsin release from "*melt*" and "*abs*" Caf1 hydrogels (1:1). The diffusion coefficients were calculated based on the fractional release of the protein cargos at 3 h and the hydrogel thickness of 4 mm.

The diffusion coefficients **(Figure 2.18)** revealed that the initial phase of BSA release is slower than DNase with most of the formulations, this is likely due to the size difference between the two biomolecules. BSA and DNase are similar in static surface charges, but different sizes (approximately 3 times smaller) **(Table 3)** which results in a faster release rate as it is less restricted by the hydrogel matrix. Interestingly, Trypsin which is slightly smaller than BSA in size, obtains a diffusion coefficient faster in the higher crosslinked formulations (1:2) using both cargos loading approaches and slower with the lower crosslinked formulations (1:1). It is anticipated this phenomenon is the result of the different in cargos loading approach, that the cargos are encapsulated/entrapped in different domain of the gel matrix.

Censi et al.[47] presented a thermosensitive hydrogel with a "biphasic" release kinetics comprising an initial fast release during the first five days, followed by a slower release phase highly influenced by the cross-link density. The "biphasic" appears to be attributed to hydrophobic and hydrophilic domains inside the hydrogel, the group observed rapid release of BSA during the initial stage localisation in the hydrophilic

domains of the hydrogel network as no change in BSA release was observed by the extent of methacrylate. The latter phase of release can then be attributed to cargos encapsulated in the hydrophobic domains of the hydrogel. It is therefore anticipated that Caf1-PEG hydrogel consists of both hydrophilic (PEG-SH) and hydrophobic (Caf1) domains. Proteins such as BSA also contain both hydrophobic and hydrophilic domains, which will likely interact with its Caf1-PEG counterpart and, thus, increase or reduce the release rate due to steric crowding. Steric crowding[52] is likely to be one of the factors causing the initial fast release, where there is no sufficient space inside the hydrogels and the "loose" protein cargos were being "squeezed out". Once the excess drug cargo has been released, a slower release gradually takes over in combination with the hydrogel swelling. Moreover, to overcome the rapid initial release, polymer-coated strategies have shown promising results in the literature, such as chitosan-coated, poly-lysine, and polyornithine have been used to tackle problems such as mechanical stability and controlled release rate.[53]

Taken together, the results suggest that there are compelling differences in the rate of cargo release protein cargos from *abs* and *melt* Caf1 hydrogels, it is due to the difference in cargo encapsulation/entrapment within the matrix. A well-encapsulated *melt* Caf1 hydrogel leads to a slower release, while proteins loaded via the *abs* approach failed to enter the hydrogel matrix's centre, resulting in a faster release. Both releases from melt Caf1 and abs Caf1 hydrogels were diffusion-controlled as most of the release took place at the initial phase, and slower release in the latter phase as swelling/degradation only occurred after 24 h. The difference in release rate is mostly due to molecule sizes and relative hydrogel pore size, as smaller biomolecules such as DNase obtained the fastest release rates compared with the larger biomolecule. In contrast, the larger molecules are controlled by static charges of the protein and the hydrogel matrix, where molecules in the hydrophilic domain are likely to be released first followed by those in the hydrophobic domain. This is evidenced as BSA has a faster rate when compared to Trypsin in the 1:1 Caf1:PEG-SG formulations for both approaches, as the extent of hydrophilic (PEG-SG) increases, BSA has a slower release rate against Trypsin in the 1:2 Caf1:PEG-SG formulations.

2.4. Conclusion

In summary, this chapter explored the possibility of Caf1 hydrogel used for drug delivery application by following the kinetic release of small molecules to large biomolecules. Caf1 hydrogel was synthesised by crosslinking Caf1 lysine residue with succinimidyl glutarate of PEG-SG to form amide bonds, the chemical crosslinked Caf1 hydrogel presented a well-defined network with good mechanical properties. Small molecule Rhodamine-B was selected as the model drug candidate, the molecule was encapsulated, and the release study shows a prolonged delivery of up to 50 h when it is loaded into the Caf1 hydrogel compared to Pluronic F-127 hydrogel with a higher polymer concentration. Both (Caf1 hydrogel and Pluronic F-127 hydrogel) diffusion-controlled systems differ in release rate due to differences in Rhodamine-B encapsulation and the space available for the Rhodamine-B to reside in the hydrophilic domains of the PEG domains of Pluronic F-127 hydrogel and Caf1 hydrogel before steric crowding occurs and forcing the molecules away from the hydrophilic domain of the hydrogel matrix. This effect was further investigated with the Caf1 formulations containing an increase of PEG-SG concentration, the results showed a hydrogel with improved mechanical properties as crosslink density increases and a slight improvement in retaining Rhodamine-B within the hydrogel network.

Macromolecule Bovine Serum Albumen (BSA) was the model protein for platform release studies. BSA was conjugated with FITC so that it could be easily detected using UV or fluorescence spectroscopy. The release data shows that BSA has a slower release rate when compared to Rhodamine-B because of the different sizes. As the size of the cargo molecule is close or near to the pore size of the hydrogel network, the cargo becomes less mobile to travel through the network, thus causing a slower release. However, this experiment needs to be revised due to competition between Caf1 and BSA to form amide bonds with the in-selective PEG-SG. Two new cargo loading approaches were developed to encapsulate model protein cargos with Caf1 hydrogels by utilising the unique reversible nature of Caf1 polymer, where the Caf1 polymer can switch between its polymeric form and monomeric form by thermal unfolding the Caf1 protein. Caf1 polymers were crosslinked with PEG-SG to form *native* Caf1 hydrogel, then the hydrogel undergoes a cycle of Caf1 refolding (proteins unfolding and refolding) to obtain *melt* Caf1 hydrogel. 1) Protein cargos were loaded into the hydrogel during the refolding stage via the "melt" approach, 2) while hydrogel

using the "abs" approach undergoes freeze-drying and cargo was loaded into the hydrogel during the rehydration stage of this method. The "melt" Caf1 hydrogel showed a lower mechanical strength when compared to native Caf1 hydrogel, due to short Caf1 polymer chains after refolding and therefore hydrogel containing 5 % Caf1 was formulated for this experiment. Three proteins, BSA, DNase and Trypsin, were selected to study the effect of cargo size and surface charges, the protein cargos were loaded into four different formulations (1:1 *melt*; 1:1 *abs*; 1:2 *melt*; 1:2 *abs*), which will provide insight into the approach loading efficiency. The results of all release profiles show that the cargo loaded via the "*melt*" approach has a slower release rate compared to the "*abs*" approach, Korsmeyer-Peppas model and Higuchi models suggest that the release is diffusion controlled for the majority of the cargo release (up to fractional 60 %). The release profiles show that all cargos were released with an initial fast release phase followed by a slow, gradual release in the latter phase, also known as the "biphasic" release system. The latter phase of the release is likely due to swelling, and degradation occurs after 24 h, while the early initial phase is governed by static interaction between the cargos and hydrogel matrix. The initial phase release is associated with the position of the protein molecule residing within the matrix, as Caf1 hydrogel is considered to contain both hydrophilic and hydrophobic domains, thus, the hydrophilic molecule will be released first, followed by the molecule in the hydrophobic region of the matrix. Therefore BSA has obtained a faster release rate than Trypsin at formulation containing 1:1 Caf1:PEG-SG using both approaches, and as the concentration of PEG-SG increases, BSA becomes less mobile, which resulted in a slower release than Trypsin as observed in the 1:2 formulations. Based on this knowledge, drug release for biomolecules can be tailored by altering crosslink density to achieve desired release rate, and further coating techniques can be applied to slow down release or strengthen mechanical properties, as shown in the literature. In conclusion, this chapter has laid out the fundamental groundwork for Caf1 hydrogel to be used as a drug delivery vehicle in the future.

2.5. Experimental

General Experimental

Fluorescein isothiocyanate (FITC) was purchased from Sigma-Aldrich. 4-arm Succinimidyl glutarate PEG (4-arm PEG) (20 kDa) was purchased from Creative PEGWorks. Sodium bicarbonate solution (0.05M, pH 8.2) was prepared by dissolving 4.2 g of sodium bicarbonate (Acros) in 1L of deionised water. The pH was adjusted to 8.2 with 1M HCl. Phosphate buffered saline PBS 100 mM sodium hypophosphite, 100 mM monosodium dihydrogen orthophosphate, 137 mM sodium chloride, 27 mM potassium chloride (Sigma-Aldrich), dissolving in 100 mL of deionised water. The pH was adjusted to 7.4 with 1M HCl. Rhodamine-B was purchased from Sigma-Aldrich. BSA, Try, and DNase was purchased from Sigma-Aldrich.

Instrumentation

pH measurements were made using a Hanna HI 90103 instrument which was calibrated using commercial buffer solutions (Sigma-Aldrich). UV-vis spectrometry was obtained using a Thermo Scientific NanoDrop One spectrophotometer with a pedestal that has a working range of up to 550.0 absorbance units (A) and 1.5 A with the use of a quartz cuvette. Rheological measurement was performed on an HR-2 Discovery Hybrid Rheometer from TA Instruments, with a standard steel parallel plate geometry (40 mm) and a 1 mm gap (volume of samples 1.2 ml).

Preparation of Caf1 protein

pGEM-T Caf1 plasmid was transformed into BL21 (DE3) competent E. coli cells. Terrific broth (TB) (500 mL) containing 100 μg mL-1 ampicillin in 2 L shake flasks was inoculated with single colonies and grown for 21 h at 35 °C, shaking at 180 rpm. The cell pellet was removed by centrifugation at 3000 rpm, 22 °C, 30 min (JA10 rotor, Beckman Coulter) followed by ultracentrifugation at 35,000 rpm, 22 °C, 60 min (45Ti rotor, Beckman Coulter) to collect the flocculent layer that forms above the cell pellet in Caf1 producing cells. This was resuspended in phosphate-buffered saline (PBS) (10 mM sodium phosphate, 137 mM sodium chloride, 2.7 mM potassium chloride, pH 8.0, 10 mL per flocculent). 5mg of DNase and RNase were added, and Caf1 polymer was extracted by incubation in a water bath at 48 °C for 3 h followed by overnight incubation at 22 °C, and the flocculants collected in the supernatant from 2 x 60 min ultracentrifugations at 22 °C, 35,000 rpm (Beckman 45 Ti rotor). Extracted Caf1

polymer was washed by tangential flow filtration using a Minimate TFF 500 kDa MWCO filter (Pall) and purified using HiScreen CaptoTM Core 70 columns (2 x 4.7 mL in series, GE Healthcare), with PBS as the running buffer. Polymer purity was analysed using Coomassie stained 15% SDS-PAGE.[29]

Preparation of Caf1-PEG hydrogel

Caf1 protein polymer (4 mg) was dissolved in PBS (200 µl, pH 7.4) at 37 °C for 3 min. 4-arm PEG (4 mg) was dissolved in sodium bicarbonate solution (0.05M, 200 µl) with some sonication (2 min). The solutions were then mixed by an aspiration for approximately 1 s before the onset of hydrogel formation and yielded 2 %w/v Caf1 hydrogel.

Rheology

Dynamic oscillatory studies were performed at a strain of 2% and frequency of 1Hz. The steady shear viscosity was measured at shear rates from 0.1 to 100 s^{-1} for samples 10, 20, and 30 mg mL^{-1}. The creep test was performed with a constant stress (0.2 Pa) applied over 30 s. After this time, the stress was removed whole, and the strain was monitored as a function of time for 120 s. The creep test measures the degree of elastic deformation and the rate of viscous flow on the application of small shear stress to the material and the complete recoverable point from elastic deformation upon removing that stress. The shear stress relaxation test was performed at 1% strain stress monitored as a function of time for 120 s. All measurements were performed at 25 °C. Shear stress tests were performed to measure the relaxation of stress to a material followed by an instantaneous change in deformation (strain), where a viscous material would instantaneously relax, and an elastic material would show zero relaxation over time.

Rhodamine-B UV absorbance calibration plot

Rhodamine-B (2 mg) was dissolved in 1 ml of PBS buffer, the solution was diluted accordingly down to 0.001 mg mL^{-1}. The prepared Rhodamine-B solutions were analysed via UV spectroscopy at 554 nm, the recorded absorbance values were plotted against the concentration (mg ml^{-1}) to yield a Rhodamine-B calibration plot **(Figure S2.3)**.

Release studies of Rhodamine-B from Caf1 hydrogel

2 %w/v of Caf1 Hydrogels were prepared using aqueous Rhodamine-B dye (0.01 mg ml-1) solution instead of deionised water using the same protocol as before. 300 μL dye loaded hydrogel was prepared in a GPC sample vial. PBS solution (1.0 mL, pH 7.4) was added to the hydrogel, to mimic phycological condition the experience was carried out at 25°C. The aqueous solutions were replaced at predetermined time intervals, the experiments were performed in triplicate. The collected aqueous solutions were analysed with UV-vis at 554 nm, and the concentration of Rhodamine-B was determined using a calibration curve **(Figure S2.3)**. Mass of Rhodamine-B in the aqueous solution was calculated and converted into mass fraction, mass fraction is plotted against time to produce the release profiles of Rhodamine-B. Release profiles were then fitted to several kinetic models mentioned below. All samples were measured in triplicate.

Release studies of Rhodamine-B from Pluronic F-127 hydrogel

The Pluronic F-127 hydrogel (80 mg) based were prepared using the cold method described by Schmolka.[54] The solid polymer was dissolved at the following concentration (20 %w/v) in phosphate buffer (400 µl, pH 7.4) to afford the hydrogel. Pluronic F-127 hydrogel was prepared in the same way, Rhodamine-B (0.01 mgmL^{-1}) solution was used to replace the aqueous PBS buffer solution (400 µl, pH 7.4). Rhodamine-B loaded hydrogel was prepared in a GPC sample vial. 1.0 mL of PBS buffer solution was then added on top of the hydrogel at time 0 h and the experiment was carried out at 25°C to mimic body condition. The aqueous buffer solution was replaced at predetermined time intervals, the experiments were performed in triplicate. The resultant aqueous solutions were analysed with UV-vis at 554 nm, and the concentration of Rhodamine-B was determined from a calibration curve **(Figure S2)**. The mass of the Rhodamine-B released was converted into the mass to be used in the calculation of the total released mass fraction, which was then plotted in cumulative release against time. Release profiles were then fitted to several kinetic models mentioned below. Samples collected at each time interval were analysed in triplicate via UV spectrology.

Preparation of model protein cargos with a fluorescence label

Aqueous solutions of BSA, DNase, and Trypsin (0.2 %w/v or 2 mg mL^{-1}) were mixed with fluorescein isothiocyanate (0.4 %w/v or 4 mg mL^{-1}) in a sodium carbonate buffer (0.05 M) pH 9.0 at a 20:1 volume ratio, incubated in the dark at 4 °C overnight. NH4Cl was added to a final concentration of 50 mM of ammonium chloride solution (5.88 mg), and the solution was incubated for a further 3 h. The solution was then dialysed in water to remove the unconjugated label, and the solution freeze-dried to obtain the labelled proteins.[55]

Model protein UV absorbance calibration plot

Fluorescence labelled – BSA, DNase, and Trypsin (5 mg) were dissolved in 1 ml of PBS buffer, and the solution was diluted accordingly down to 0.001 mg mL^{-1}. The prepared standard solutions were analysed via UV spectroscopy at 525 nm, the recorded absorbance values were plotted against the concentration (mg ml^{-1}) to yield BSA, DNase, and Trypsin calibration plots **(Figure S2.4)**.

Protein loading of Caf1 hydrogels by absorption "abs"

Caf1 hydrogels (2 %w/v, 400 µL) were melted at 100 °C for 2 min. The solution was allowed to cold in an ice bath (30 min) and allowed to stand at 8 °C overnight. The refolded hydrogel was freeze-dried to afford a white powder and then rehydrated by adding aqueous solutions of BSA or Trypsin in 420 µL of PBS buffer (28.95 µM) obtain protein-loaded hydrogel (*abs* Caf1).

Protein loading of 'meltable' "melt" Caf1 hydrogel

Caf1 hydrogels (2 %w/v, 400 µL) were melted by heating at 100 °C for 2 min, then mixed with aqueous solutions of BSA or Trypsin in 20 µL of PBS buffer (608 µM). The resulting solution was allowed to cool in an ice bath for 30 min and then allowed to stand at 8 °C overnight to afford the protein-loaded hydrogel was obtained (*melt* Caf1).

Protein release studies from Caf1 hydrogels

Protein-loaded Caf1 hydrogels were prepared as described above. PBS (1.0 mL, pH 7.4) was then added on top of the hydrogel and the in vitro study was carried out at 25 °C to mimic phycological condition. The aqueous solutions were carefully removed for spectroscopic analysis and replaced with fresh buffer at predetermined time intervals. The experiments were performed in triplicate. The collected aqueous solutions were analysed for protein concentration and related by measuring absorbance at 525 nm

based on a calibration curve **(Figure S2.4)** prepared using FITC-BSA/Try/DNase. Plots of protein release versus time were then fitted to Korsmeyer-Peppas and other kinetic models.

Swelling and degradation study

The % swelling and/or % degradation study of "abs" and "melt" Caf1 hydrogels was determined in PBS buffer (pH 7.4). The following equation calculated the swelling and/or degradation:

$$\%Swelling \ \& \ Degradation = [(W_t - W_i)/W_i] \ x \ 100 \quad \textbf{Equation 2.6}[56]$$

Where W_i is the initial weight and W_t is the weight of the hydrogel at a predetermined time.

Kinetics models

Release profiles that are independent of concentration gradient are defined as zero order release (Equation 2.7), where the fraction of mass release is calculated from mass at time t (hours) over initial mass (M_0), with k being zero order release constant.

$$M_t = M_0 + kt \quad \textbf{Equation 2.7}[35]$$

The first order **(Equation 2.8)** describes drug release that is dependent on the concentration remaining within the gel network, that initial mass (M_0) is subtracted from mass released at the time (M_t), and k is the first order release constant mentioned in time (t) in hours.

$$LogM_t = LogM_0 + kt/2.303 \quad \textbf{Equation 2.8}[35,36]$$

Drug release by dissolution by either change in gel network surface area or drug diameter can be fitted with the Hixson-Crowell model **(Equation 2.9)**. Hixson-Crowell measures the cube root of unreleased fraction ($M_0 - M_t$) (initial mass subtract mass at time interval) over time (t) in hours, with K_{HC} the Hixson-Crowell constant.

$$\sqrt[3]{M_0 - M_t} = K_{HC}t \quad \textbf{Equation 2.9}[36]$$

The Higuchi model describes drug release as a diffusion process based on Fick's law, which is square root time-dependent, as shown in **Equation 2.10** where K_H is the Higuchi constant.

$$F = K_H t^{\frac{1}{2}} \qquad\qquad \textbf{Equation 2.10}[36]$$

Korsmeyer-Peppas equation **(Equation 2.11)** describes the diffusion mechanism by which a drug diffuses from the hydrogel network. Diffusion exponent, n, defines the type of diffusion by Fick's law, the diffusion exponent can be determined by rearranging the Korsmeyer-Peppas equation from the gradient of Log fraction drug release against Log time (h) where F is the fraction of drug released at time t in hours, and K_m is the Kinetic constant.

$$F = K_m t^n \qquad\qquad \textbf{Equation 2.11}[57,58]$$

2.6. References

1. Balakrishnan, B., Mohanty, M., Umashankar, P. R. & Jayakrishnan, A. Evaluation of an in situ forming hydrogel wound dressing based on oxidized alginate and gelatin. Biomaterials 26, 6335–6342 (2005).
2. Bae, K. H. & Kurisawa, M. Emerging hydrogel designs for controlled protein delivery. Biomater Sci 4, 1184–1192 (2016).
3. Wang, Y. et al. Three-dimensional printing of shape memory hydrogels with internal structure for drug delivery. Materials Science and Engineering C 84, 44–51 (2017).
4. Buwalda, S. J. et al. Hydrogels in a historical perspective: From simple networks to smart materials. Journal of Controlled Release 190, 254–273 (2014).
5. Tiwari, G. et al. Drug delivery systems: An updated review. Int J Pharm Investig 2, 2 (2012).
6. Yin, L., Yuvienco, C. & Montclare, J. K. Protein based therapeutic delivery agents: Contemporary developments and challenges. Biomaterials 134, 91–116 (2017).
7. Delplace, V. et al. Controlled release strategy designed for intravitreal protein delivery to the retina. Journal of Controlled Release 293, 10–20 (2019).
8. Varghese, J. S., Chellappa, N. & Fathima, N. N. Gelatin-carrageenan hydrogels: Role of pore size distribution on drug delivery process. Colloids Surf B Biointerfaces 113, 346–351 (2014).
9. Lai, J. Biocompatibility of chemically cross-linked gelatin hydrogels for ophthalmic use. 1899–1911 (2010) doi:10.1007/s10856-010-4035-3.
10. Li, J. K., Wang, N. & Wu, X. S. Gelatin nanoencapsulation of protein/peptide drugs using an emulsifier-free emulsion method. J Microencapsul 15, 163–172 (1998).
11. Chen, H. et al. Covalently antibacterial alginate-chitosan hydrogel dressing integrated gelatin microspheres containing tetracycline hydrochloride for wound healing. Materials Science and Engineering C 70, 287–295 (2017).
12. Bakravi, A., Ahamadian, Y., Hashemi, H. & Namazi, H. Synthesis of gelatin-based biodegradable hydrogel nanocomposite and their application as drug delivery agent. Advances in Polymer Technology 1–11 (2018) doi:10.1002/adv.21938.
13. Li, J. K., Wang, N. & Wu, X. S. A novel biodegradable system based on gelatin nanoparticles and poly(lactic-co-glycolic acid) microspheres for protein and peptide drug delivery. J Pharm Sci 86, 891–895 (1997).
14. Appel, E. A., Forster, R. A., Rowland, M. J. & Scherman, O. A. The control of cargo release from physically crosslinked hydrogels by crosslink dynamics. Biomaterials 35, 9897–9903 (2014).

15.   Liu, H. et al. A functional chitosan-based hydrogel as a wound dressing and drug delivery system in the treatment of wound healing. RSC Adv 8, 7533–7549 (2018).

16.   Verma, V. S., Sakure, K. & Badwaik, H. R. Xanthan Gum a Versatile Biopolymer: Current Status and Future Prospectus in Hydro Gel Drug Delivery. Curr Chem Biol 11, 10–20 (2017).

17.   Bahrami, B. et al. Nanoparticles and targeted drug delivery in cancer therapy. Immunol Lett 190, 64–83 (2017).

18.   Mauri, E. et al. Double conjugated nanogels for selective intracellular drug delivery. RSC Adv 7, 30345–30356 (2017).

19.   de Jong, W. H. & Borm, P. J. a. Drug delivery and nanoparticles:applications and hazards. Int J Nanomedicine 3, 133–149 (2008).

20.   Lv, J. et al. Fluoropolymers for intracellular and in vivo protein delivery. Biomaterials 182, 167–175 (2018).

21.   Appel, E. A., Loh, X. J., Jones, S. T., Dreiss, C. A. & Scherman, O. A. Sustained release of proteins from high water content supramolecular polymer hydrogels. Biomaterials 33, 4646–4652 (2012).

22.   Zarzycki, R., Modrzejewska, Z., Nawrotek, K. & Lek, U. Drug Release From Hydrogel Matrices. Ecological Chemistry and Engineering S 17, 117–136 (2010).

23.   Mathew, A. P., Uthaman, S., Cho, K. H., Cho, C. S. & Park, I. K. Injectable hydrogels for delivering biotherapeutic molecules. Int J Biol Macromol 110, 17–29 (2018).

24.   Dash, S., Murthy, P. N., Nath, L. & Chowdhury, P. Kinetic modeling on drug release from controlled drug delivery systems. Acta Pol Pharm 67, 217–23 (2010).

25.   Waller, H., Ulusu, Y. & Lakey, J. H. Caf1 of Yersinia pestis Forms Complex Highly Stable Protein Polymers and Hydrogel Scaffolds. Biophys J 110, 339a (2016).

26.   Ulusu, Y. et al. Thermal stability and rheological properties of the 'non-stick' Caf1 biomaterial. Biomedical Materials 12, 051001 (2017).

27.   Picout, D. R. & Ross-Murphy, S. B. Rheology of biopolymer solutions and gels. ScientificWorldJournal 3, 105–121 (2003).

28.   Zuidema, J. M., Rivet, C. J., Gilbert, R. J. & Morrison, F. A. A protocol for rheological characterization of hydrogels for tissue engineering strategies. J Biomed Mater Res B Appl Biomater 102, 1063–1073 (2014).

29.   Dura, G., Waller, H., Gentile, P., Lakey, J. H. & Fulton, D. A. Tuneable hydrogels of Caf1 protein fibers. Materials Science and Engineering C 93, 88–95 (2018).

30.   Moore, T., Croy, S., Mallapragada, S. & Pandit, N. Experimental investigation and mathematical modeling of Pluronic(®) F127 gel dissolution: Drug release in stirred systems. Journal of Controlled Release 67, 191–202 (2000).

31.   Ye, F. et al. Real-time UV imaging of drug diffusion and release from Pluronic F127 hydrogels. European Journal of Pharmaceutical Sciences 43, 236–243 (2011).

32.   Franck, A. Understanding rheology of structured fluids. Book of TA instruments 1–11 (2004).

33.   Jeong, B., Bae, Y. H. & Kim, S. W. Drug release from biodegradable injectable thermosensitive hydrogel of PEG-PLGA-PEG triblock copolymers. Journal of Controlled Release 63, 155–163 (2000).

34.   Holowka, E. P. & Bhatia, S. K. Controlled-Release Systems. in Drug Delivery 7–62 (Springer New York, 2014). doi:10.1007/978-1-4939-1998-7_2.

35.   Jalababu, R., Veni, S. S. & Reddy, K. V. N. S. Synthesis and characterization of dual responsive sodium alginate-g-acryloyl phenylalanine-poly N -isopropyl acrylamide smart hydrogels for the controlled release of anticancer drug. J Drug Deliv Sci Technol 44, 190–204 (2018).

36.   Lin, H. et al. Transport and structural characteristics of crosslinked poly(ethylene oxide) rubbers. J Memb Sci 276, 145–161 (2006).

37. Karvinen, J., Ihalainen, T. O., Calejo, M. T., Jönkkäri, I. & Kellomäki, M. Characterization of the microstructure of hydrazone crosslinked polysaccharide-based hydrogels through rheological and diffusion studies. Materials Science and Engineering C 94, 1056–1066 (2019).

38. Naddaf, A. A., Tsibranska, I. & Bart, H. J. Kinetics of BSA release from poly(N-isopropylacrylamide) hydrogels. Chemical Engineering and Processing: Process Intensification 49, 581–588 (2010).

39. Salama, A. Chitosan based hydrogel assisted spongelike calcium phosphate mineralization for in-vitro BSA release. Int J Biol Macromol 108, 471–476 (2018).

40. Erickson, H. P. Size and shape of protein molecules at the nanometer level determined by sedimentation, gel filtration, and electron microscopy. Biol Proced Online 11, 32–51 (2009).

41. Kuijpers, A. J. et al. Characterization of the Network Structure of Carbodiimide Cross-Linked Gelatin Gels. Macromolecules 32, 3325–3333 (1999).

42. García De La Torre, J., Huertas, M. L. & Carrasco, B. Calculation of hydrodynamic properties of globular proteins from their atomic-level structure. Biophys J 78, 719–730 (2000).

43. Censi, R. et al. Photopolymerized thermosensitive hydrogels for tailorable diffusion-controlled protein delivery. Journal of Controlled Release 140, 230–236 (2009).

44. Delplace, V. et al. Controlled release strategy designed for intravitreal protein delivery to the retina. Journal of Controlled Release 293, 10–20 (2019).

45. Flory, P. J. & Rehner, J. Statistical mechanics of cross-linked polymer networks II. Swelling. J Chem Phys 11, 521–526 (1943).

46. Censi, R. et al. Photopolymerized thermosensitive poly(HPMAlactate)-PEG-based hydrogels: Effect of network design on mechanical properties, degradation, and release behavior. Biomacromolecules 11, 2143–2151 (2010).

47. Colombo, P., Bettini, R., Santi, P. & Peppas, N. A. Swellable matrices for controlled drug delivery: Gel-layer behaviour, mechanisms and optimal performance. Pharm Sci Technol Today 3, 198–204 (2000).

48. Yao, F. & Weiyuan, J. K. Drug Release Kinetics and Transport Mechanisms of Non-degradable and Degradable Polymeric Delivery Systems. Expert Opinion Drug Delivery 7, 429–444 (2010).

49. Hoare, T. R. & Kohane, D. S. Hydrogels in drug delivery: Progress and challenges. Polymer (Guildf) 49, 1993–2007 (2008).

50. Wilson, A. N., Blenner, M. & Guiseppi-Elie, A. Polyplex formation influences release mechanism of mono- and di-valent ions from phosphorylcholine group bearing hydrogels. Polymers (Basel) 6, 2451–2472 (2014).

51. Wu, S., Huang, X. & Du, X. Glucose- and pH-responsive controlled release of cargo from protein-gated carbohydrate-functionalized mesoporous silica nanocontainers. Angewandte Chemie - International Edition 52, 5580–5584 (2013).

52. Fan, M. et al. Covalent and injectable chitosan-chondroitin sulfate hydrogels embedded with chitosan microspheres for drug delivery and tissue engineering. Materials Science and Engineering C 71, 67–74 (2017).

53. Schmolka, I. R. Artificial Skin I . Preparation and Properties Treatment of Burns. J Biomed Mater Res 6, 571–582 (1972).

54. Barbero, N., Barolo, C. & Viscardi, G. Bovine Serum Albumin Bioconjugation with FITC. World Journal of Chemical Education, Vol. 4, 2016, Pages 80-85 4, 80–85 (2016).

55. Park, H. et al. Effect of Swelling Ratio of Intectable Hydrogel Composites on Chondrongenix Differentiation of Encapsculated Rabbit Marrow Mesenchymal Stem Cells In Vitro (Author Manuscript). Biomacromolecules 10, 541–546 (2010).

56. Ritger, P. L. & Peppas, N. A. A SIMPLE EQUATION FOR DESCRIPTION OF SOLUTE RELEASE II. FICKIAN AND ANOMALOUS RELEASE FROM SWELLABLE DEVICES. Journal of Controlled Release vol. 5 (1987).

57. Ritger, P. L. & Peppas, N. A. A simple equation for description of solute release I. Fickian and non-fickian release from non-swellable devices in the form of slabs, spheres, cylinders or discs. Journal of Controlled Release 5, 23–36 (1987).

58. Barron, V. et al. Development of chemically cross-linked hydrophilic-hydrophobic hydrogels for drug delivery applications. Eur Polym J 75, 25–35 (2016).

2.7. Appendix A
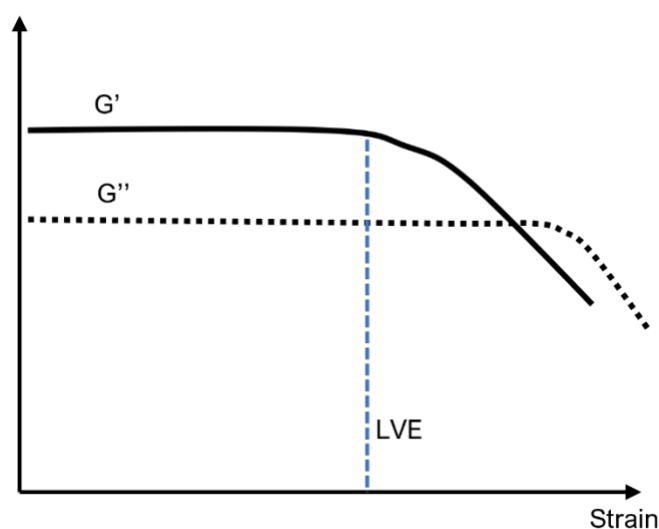
Figure S2.1, The linear viscoelastic region (LVE) describes the range in which a rheology test can be carried out without damaging the structure of the test sample. As shown in the blue line on the graph, the region is a constant value of storage modulus (G'), also known as the linearity limit.[28,59]
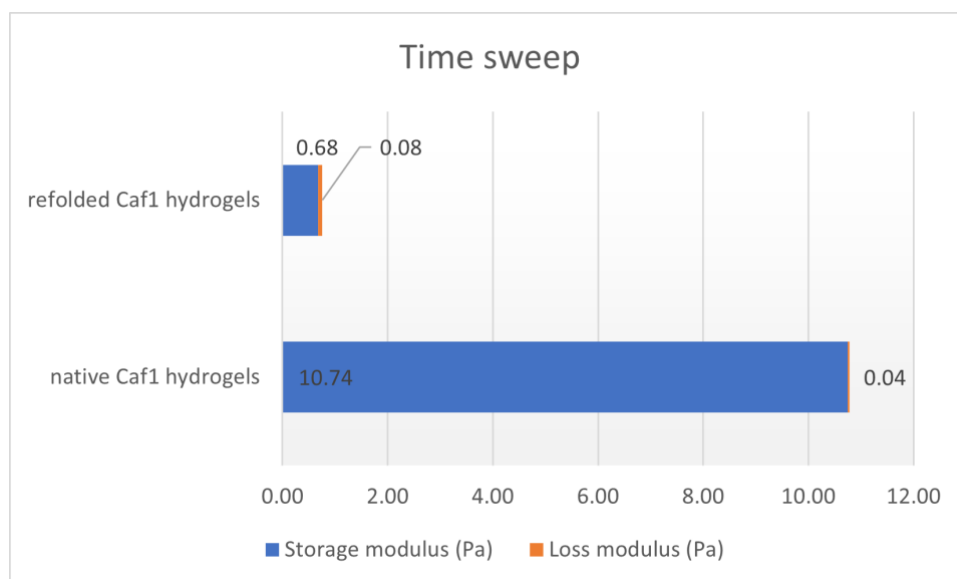
Figure S2.2, Rheological data of native Caf1 hydrogels (2 %w/v) and refolded Caf1 hydrogels (2 %w/v). Storage modulus (G') in **blue** and Loss modulus in **orange** (G''). Studies in our group show that the reduction in storage modulus also applied to other strengths of Caf1 hydrogels.[26]
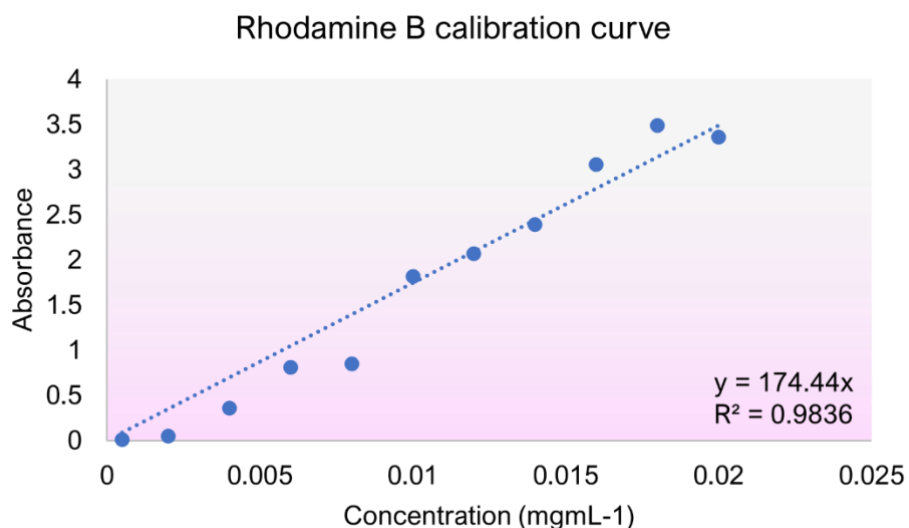
Figure S2.3, Rhodamine-B calibration curve of concentration (mgmL^{-1}) against absorbance at 554 nm via UV.
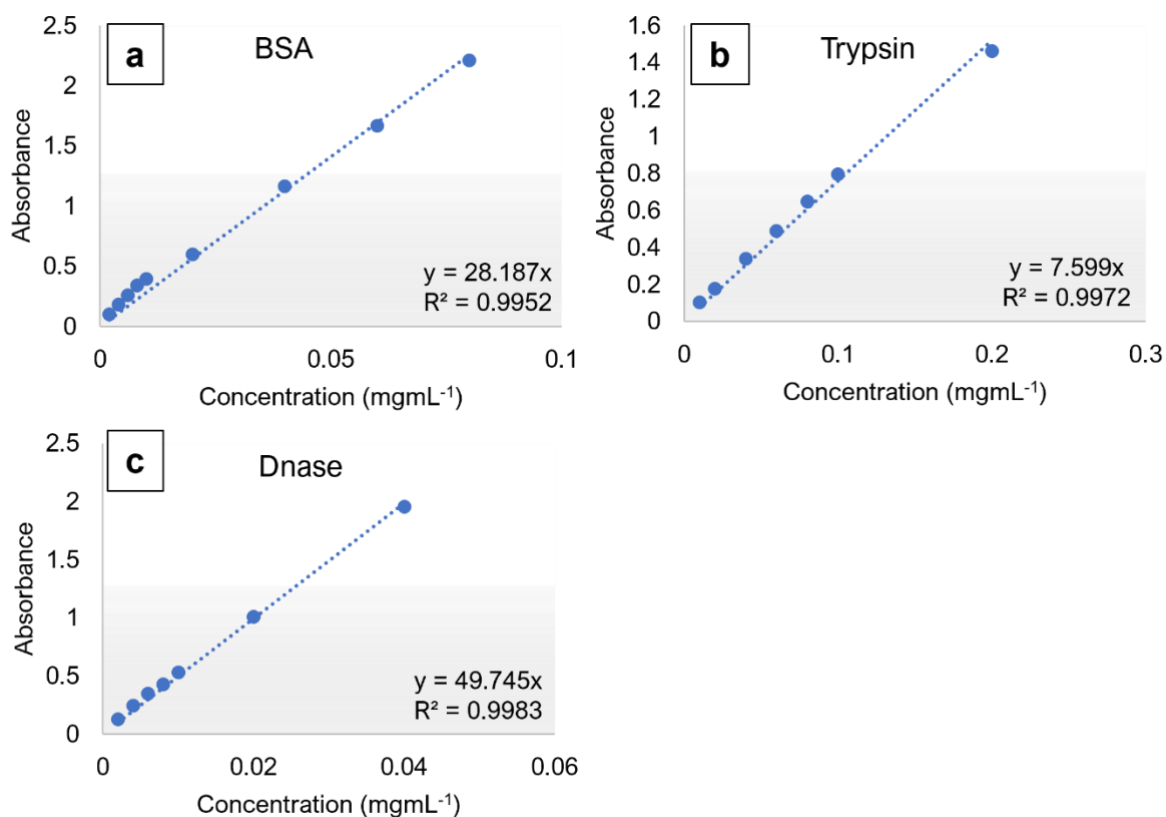
Figure S2.4 Calibration curve of **(a)** BSA, **(b)** Trypsin, **(c)** DNase concentration (mgmL⁻¹) against absorbance at 525 nm via UV.

Chapter 3

Stimuli-responsive hydrogels for drug delivery

Table of Contents

3.1. Overview

Work in Chapter 2 has demonstrated that controlled release of small and macromolecules from Caf1 hydrogels can be achieved, and the desired release rate can be tuned by increasing or decreasing the crosslinking density within the Caf1 hydrogels. Building upon this work, this chapter will explore the use of a stimulus to trigger rapid cargo release. This concept utilises disulfide bonds incorporated within the crosslinked hydrogels network as linkers that cleave upon reduction. This chapter explores Caf1-SS hydrogels prepared by reacting cysteine-modified Caf1 polymers with thiolated multi-arm PEGs, and the mechanical properties of these hydrogels was then evaluated with rheology. In particular, the reversible nature of disulfide bonds in Caf1-SS hydrogels was tested by physical breakage and oxidative cleavage.

Furthermore, this chapter reported a novel *mosaic* hydrogel prepared from Caf1 copolymers that contain both Caf1^{WT} and Caf1^{Cys} subunits. Two different approaches were employed to acquire the formation of the hydrogel, and the hydrogel was selected based on the mechanical properties that are best suited for controlled drug delivery application. The release of the cargo rhodamine-B was studied in different concentration dosages of the reducing agent GSH, which cleaves disulfide bonds to induce the cargo release from mosaic Caf1-SS hydrogels. The rate of rhodamine B release under different conditions was determined. The results from this study provided the groundwork needed further to develop this novel hydrogel as a drug cargo carrier.

3.2. Introduction

The current state-of-the-art in controlled delivery allows for the delivery of drugs with desired kinetic rates for extended periods, ranging from days to years.[1] Current oral and transdermal drug delivery systems can deliver drugs over 24 h, substantially improving drug efficacy and reducing side effects.[2] Implantable systems can deliver drugs locally for an even greater length of time, some of which can deliver drugs from months to years.[3] Despite such achievements, there are still areas where substantial improvements are required to address problems associated with systemic drug administration. Systemic drug administration describes different routes of

administration of substances into the circulatory system in the body. As discussed in the previous chapter, hydrogels are most commonly used as dermal, injection and infusion-based administration forms. Drug delivery using this class of hydrogels commonly exploits drug diffusion, as presented in Chapter 2, which can enhance drug half-life. It would be desirable, however, if there were more systematic control over when drugs are released. Stimuli-responsive drug carriers could be the solution to the problem, exploiting unique chemical environments to trigger cargo release and reduce potential side effects.

3.2.1. Stimuli-responsive hydrogels

Stimuli- responsive hydrogels are three-dimensional hydrophilic polymer networks formed via covalent bonds or self-assembly processes that can alter their networks' structural properties in the presence of an external stimulus.[4,5] The external stimuli used to trigger controlled delivery includes: pH, temperature, enzymes, light and magnetism.[6,7] Enzymes-responsive strategies have attracted a growing interest because enzymes can be used to specifically trigger cargo release by, e.g. cleaving a hydrogel network, and they can be tailored to specific targets. One example is protein disulphide isomerase (PDI), which catalyses thiol-disulphide exchange reactions to promote the formation or reduction of disulfide bonds.[8,9]

Disulfide bonds can be formed between two cysteine residues.[7,10–12] Cysteines can be found in most proteins, and they function to act as a guide in protein folding and enhance the stability of tertiary and quaternary protein structures **(Figure 3.1)**.[13] Moreover, disulfide bonds also play an important role as cellular redox switches, a biological process involved in signal transmission through the cascade reaction of thiol-disulfide conversion.[14]
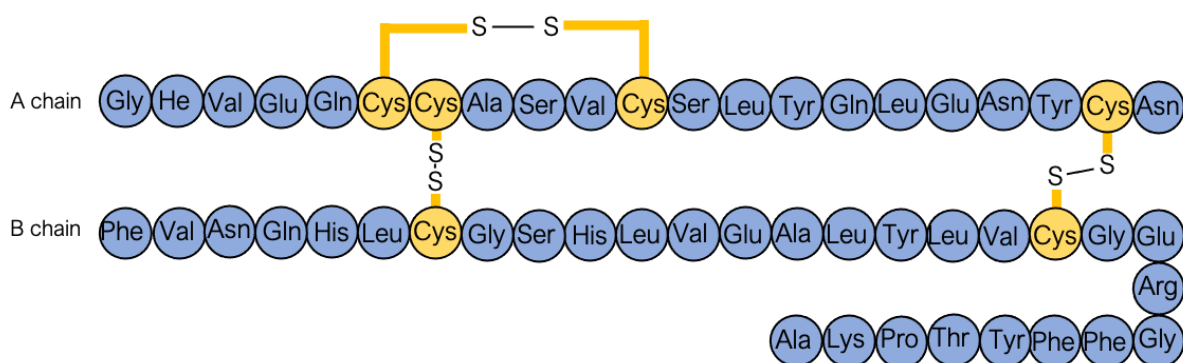
Figure 3.1, An example of disulfide crosslinks in Insulin consists of two peptide chains: A (21 amino acid residues) and B (30 amino acid residues). The amino acid cysteine (Cys) (yellow) has sulfhydryl groups (SH) in its side chain that can react to form disulfide (S-S) bonds in the presence of oxygen. Chains A and B are linked together by two disulfide bonds, and an intrachain disulfide directs amino groups to adopt the correct shape.[15]

The thiol- disulfide conversion redox process in *vivo* is regulated by the difference in concentration of thiol pools[16], which includes glutathione/glutathione disulfide (GSH/GSSG), cysteine/cystine (Cys/CySS), thioredoxin-1 (Trx1), glutaredoxin (Grx) and protein disulfide isomerase (PDI). The thiol-disulfide conversion depends on the thiol pool concentration, the disulfide bond is formed by oxidising two thiols groups and simultaneously,y disulfide bonds are being reduced to thiols. This redox nature of disulfide bonds allows them to be broken and reformed under mild conditions. Additionally, when disulfide bonds are incorporated into polymers, it allows access to stimuli-responsive and/or self-healing materials that exploit the redox nature of disulfide bonds.[17] For example, as disulfide bonds cleaved after being exposed to a cellular trigger such as Glutathione (GSH), Zhang et al. presented a dual stimuli-sensitive lipoic acid-modified poly(L-lysine) hydrogels/nanogels experience a rapid decrease of strength and elasticity in the presence of a reducing agent. [18]

Glutathione (GSH), a cysteine-containing linear tripeptide, has an average concentration of 1-10 mM in the cytoplasm.[19] Furthermore, active metabolic tumour cells typically exhibit an elevated production of GSH in the cytoplasm.[20] Therefore, polymer materials containing disulfide bonds have been identified as potential candidates for targeted tumour therapy.[21–23] In recent works, the application of disulfide-containing polymers has grown rapidly, leading to a wide range of new

dynamic materials, such as shape memory polymers, coating, adhesive, sensors, etc.[12,24] New emerging research for drug delivery involved multi-stimuli responsive polymer, which dramatically increases drug levels reaching a targeted area.[17,25,26]

This chapter explored the incorporation of disulfide bonds in Caf1 hydrogels. Caf1 wild type (Caf1[WT]) was modified with a cysteine group inserted at the N-terminal donor strand **(Figure 3.2a)**[27] to obtain Caf1[Cys], which allows the formulation of reversible disulfide bonds with PEG-SH crosslinkers which contain thiols at the termini of each arm. The mechanical properties of the resulting hydrogels (Caf1-SS hydrogel) were evaluated over a range of formulations with the aim to gain better insight through rheology studies. The reversible nature of disulfide bonds within the Caf1-SS hydrogel was explored by physical breakage and chemical cleavage. Moreover, two strategies have been applied to produce *mosaic* Caf1-SS hydrogels that consist of Caf1 copolymers containing both Caf1[WT] and Caf1[Cys] subunits. Finally, cargo release studies were carried out following the release of rhodamine-B to evaluate novel mosaic Caf1-SS hydrogel as a practical candidate for drug delivery.

3.3. Results and Discussion

Caf1 polymers consist of Caf1 subunits linked together via non-covalent linkages, where the donating subunit donates its N-terminal β-strand into the acceptor cleft of the adjacent subunit. The cysteine-modified Caf1[Cys] polymers were supplied by the Jeremy Lakey group at Newcastle University. In brief, Caf1[Cys] polymers were produced from *E. coli.* which was transformed with a pT7-COP plasmid containing a Caf1 operon and a pBad plasmid.[27] The modification of cysteine residue into the Caf1 subunit provides a thiol group for disulfide formation. The insertion site of mutation is located after the signal peptide (head) and before the N-terminal β-strand (tail), as shown in **Figure 3.2a**. Thus, the linkage between Caf1 subunits persists, and the Caf1 protein polymer chain structure is maintained **(Figure 3.2b)**.

3.3.1. Caf1-cysteine modification and disulfide bond formation
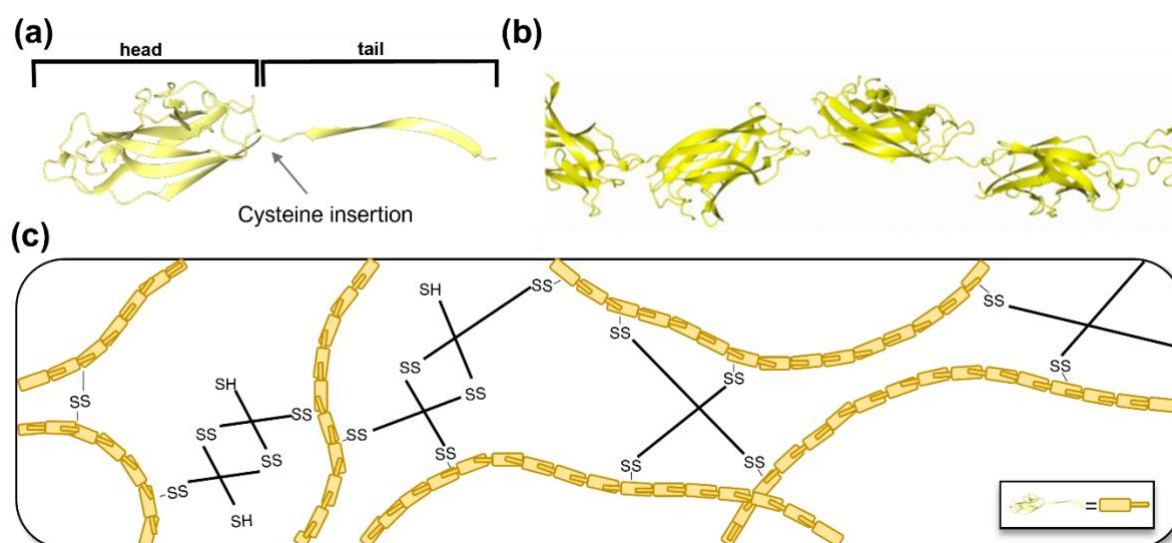
Figure 3.2, (a) Schematic representation of the Caf1 monomer featuring a cysteine insertion. The insertion of the cystine residue is targeted between the head and the tail of the monomer subunit. Schematic diagram **(b)** of Caf1 polymer presented in ribbon form. The Caf1 structure (PDB: 1P5U) was visualised using CCP4MG software. Schematic repetition **(c)** of reversible Caf1-SS hydrogel obtained from the formation of a disulfide bridge between Caf1-cystine and PEG-SH; Caf1-cystine and Caf1-cystine; PEG-SH and PEG-SH.

The introduction of a cysteine residue into the Caf1 protein allows for disulfide bond formation with free thiol (R-SH). A commercially available multi-arm PEG-SH **(Figure 3.3)** was selected as it was anticipated that its thiol end groups could react with the cysteine residue in Caf1^{Cys} protein, as well as its structure which acts as the building block for the hydrogel **(Figure 3.2c)**.[28]

Note that disulfide bond formation is not selective. Thus it was anticipated that disulfide bonds could also be formed between cysteine residue upon different Caf1^{Cys} subunits and between PEG-SH chains. To gain a better insight into the mechanical properties of hydrogels featuring these types of disulfide bonds, both Caf1-cystine and Caf1-cystine (Caf1-SS-Caf1) or PEG-SH and PEG-SH (PEG-SS-PEG) should be investigated separately. However, due to the low supply of Caf1^{Cys} polymers, this was not possible as a high quantity of Caf1^{Cys} proteins was required to carry out a rheology study to determine its mechanical strength. Nonetheless, as a control experiment, the mechanical properties of PEG-SS-PEG hydrogels were studied via rheological studies.

3.3.2. PEG-SS-PEG disulfide bonds studies
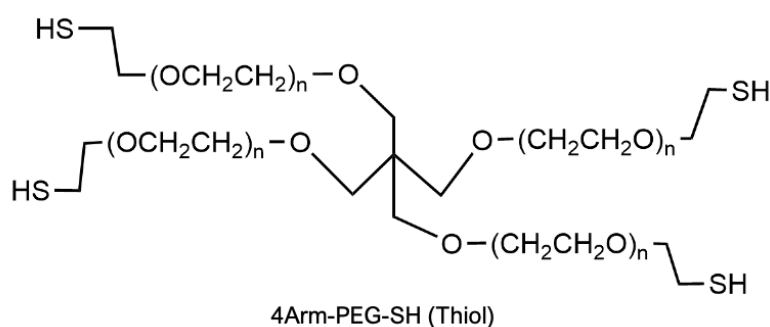
Figure 3.3, Structure of 4Arm-PEG-SH contains four thiol groups, which can be reacted with cysteine to form a disulfide bond.

PEG- SS-PEG hydrogels were synthesised by reacting 4-arm PEG-SH **(Figure 3.3)** in the presence of the oxidising agent H_2O_2, with the aim to exploit the mechanical properties of PEG-SS-PEG hydrogel crosslinked via disulfide bonds. The result **(Table 3.1, Entry 1)** shows that 5 % PEG-SS hydrogels achieved a storage modulus (G') of 1209 Pa and a gelation time of 10 min, while an increase in PEG-SH concentration to 10 % **(Table 3.1, Entry 2)** increased storage modulus to 3346 Pa and gelation time of 0.5 h. The improvement in mechanical strength is also evidenced by the increase in critical strain uptake, where the formulation at a higher concentration of PEG-SH **(Table 3.1, Entry 2)** obtained 501 % strain compared to 384 % for the lower concentration **(Table 3.1, Entry 1)**. This difference indicates increased cross-linking between the thiols. Moreover, an increase in cross-linking also reduces hydrogel flexibility, as shown by lowered LVE when comparing the results from the 5% PEG-SH formulation with the 10% PEG-SH formulation, the reduction in polymer flexibility also resulted in a longer gelation. Taken together, the results showed that PEG-SS-PEG hydrogels are obtained via disulfide bond formation in the presence of an oxidising agent.

Table 3.1, Formulation and mechanical properties of PEG-SS-PEG hydrogels.

Entry	PEG-SH (%w/v)	H_2O_2 (%w/v)	Gelation time	G' (Pa)	Mean LVE 0.1%- (%)	Critical strain (%)
1	5	8.75	10 min	1209	63	384
2	10	8.75	0.5 h	3346	40	501

3.3.3. Evaluation of Caf1-SS-PEG hydrogels by rheology

Caf1-SS-PEG were prepared by reacting Caf1^{Cys} (2 %) with 4Arm-PEG-SH (5 %) in the presence of the oxidising agent H_2O_2. The formulation **(Table 3.2, entry 1)** with 4.38 % H_2O_2 yielded a hydrogel in 28 h and a storage modulus (G') of 93 Pa. The slow reaction time also affected the overall network formation, as loosened Caf1 polymer chains cannot find free thiol to form the disulfide bonds as reaction time increases. This is evidenced in formulation two **(Table 3.2, entry 2)** as the concentration of H_2O_2 increases to 5.83 %, it drives the reaction and reduces the gelation time to 15 min, which results in hydrogel network with a G' of 442 Pa. Formulation three **(Table 3.2, entry 3)** yielded a hydrogel with the fastest gelation time of 5 min with a G' of 448 Pa. The fact that the storage modulus (448 Pa) is very similar to that when 5.58 % H_2O_2 is used suggests that no more than 8.75 % of H_2O_2 is required.

The results of formulation one **(Table 3.2, entry 1)** likely indicate that the hydrogel behaves more like a *sol* than *gel* where both LVE (100%) and critical strain (~500%) combine with a low G'. Both formulations two and three **(Table 3.2, entry 2 & 3)** have a lowered LVE (16%, 40%) and critical strain (163%, 306%) compared with **Entry 1 (Table 3.2)**, suggesting a more gel-like state, probably on account of a more fixated Caf1 network with limited loose chains.

Table 3.2, Formulation and mechanical properties of 2 % Caf1-SS hydrogels.

Entry	Caf1^{Cys} (%w/v)	Caf1^{WT} (%w/v)	PEG-SH (%w/v)	H$_2$O$_2$ (%w/v)	Gelation time	G' (Pa)	Mean LVE 0.1% - (%)	Critical strain (%)
1	2	-	5	4.38	28 h	93	100	~500
2	2	-	5	5.83	15 min	442	16	163
3	2	-	5	8.75	5 min	448	40	306
4	-	2	5	8.75	0.5 h	181	10	288

As a control experiment, *native* Caf1 (Caf1^{WT}) hydrogel **(Table 3.2, entry 4)** was prepared under the same conditions by reacting Caf1^{WT} (2 %w/v) and PEG-SH (5 %w/v) in the presence of H_2O_2 (8.75 %). Caf1^{WT} does not possess any thiol groups, and thus any cross-linking can only involve PEG-SH. The hydrogel **(Table 3.2, entry 4)**

was obtained in approximately 30 min and possessed a storage modulus of 181 Pa. The low LVE reading of 10 % and a critical strain of 288 % suggested that the hydrogel network is likely not well crosslinked. The results of this control experiment **(Table 3.2, entry 4)** showed that the increase in storage modulus of formulations two and three **(Table 3.2, entry 2 & 3)** must arise on account of cross-linking between Caf1[Cys] subunits and PEG-SH.

Formulation three **(Table 3.2, entry 3)** was selected from this point for further studies on account of its mechanical properties of a well-formed hydrogel network and high critical strain capacity.

3.3.4. Self-healing Caf1-SS-PEG macroscopic hydrogels
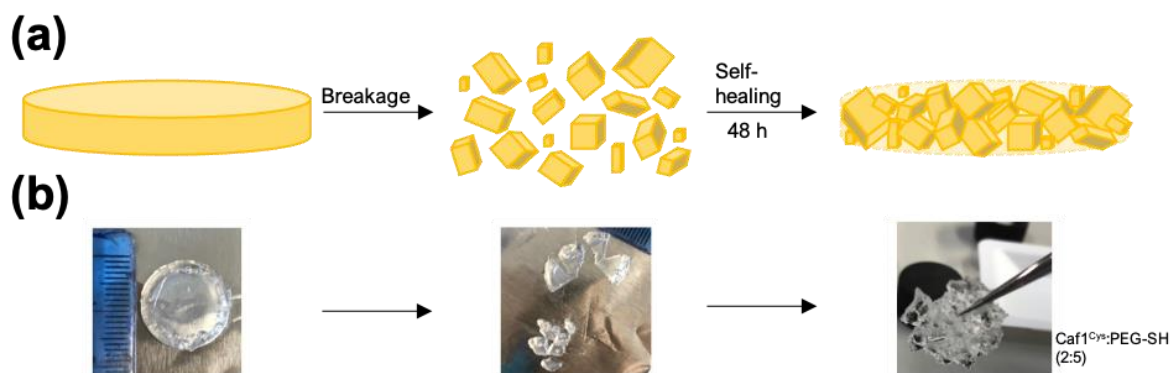
Figure 3.4,(a) Schematic illustration of Caf1-SS-PEG hydrogel mechanical breakage into small fragments. The hydrogel reassembled via disulfide bridges reformed at room temperature after 48 h. **(b)** Pictures of Caf1-SS-PEG hydrogel mechanical breakage and reformation.

It was speculated that on account of unreacted thiol groups 'trapped' inside the hydrogel network, these materials might possess self-healing properties. To investigate this, hydrogel prepared with formulation three **(Table 3.2, entry 3)** was broken into small fragments **(Figure 3.4a & b)**. The breakage allows the free thiols entrapped within the hydrogel network to react with other thiols neighbouring fragments to form a new disulfide bond. The hydrogel fragments were reassembled into a single continuous disk after 48 h. This observation demonstrated that self-repair could occur as new disulfide bonds become established from unreacted thiol groups within the hydrogels. This property of Caf1-SS-PEG hydrogel formation could be used in various applications, such as 3D printing and wound healing.

3.3.5. Reversible disulfide bonds in Caf1 S-S PEG hydrogels reformation

The The self-healing property of materials featuring disulfide bonds is driven by the redox process in which the disulfide bonds can be reductively cleaved by thiol-containing molecules such as glutathione (GSH) **(Figure 3.5)**[19], dithiothreitol (DTT) or β-mercaptoethanol. The disulfide bonds can then be reformed in the presence of an oxidant.
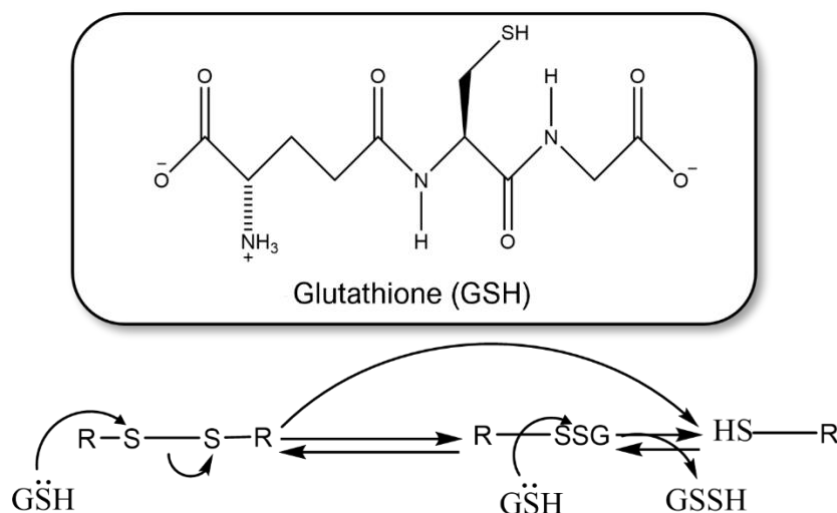
Figure 3.5, Glutathione (GSH) is a reducing agent that can cleave the disulfide bond. The addition of GSH is required to drive the reaction to completion, affording the corresponding thiols.[29]

This experiment investigated the reversible nature of disulfide bonds within the Caf1-SS-PEG hydrogel. The disulfide bond breakage/reformation process was monitored with SDS-PAGE and evaluated via rheology. A new hydrogel **(Gel 1, Figure 3.6a)** was made using the formulation shown in **Table 3.2, entry 3**. The formation of cross-links was monitored with SDS-PAGE **(Figure S3.1, Sample 1),** which showed bands present at a high molecular weight of 75+ kDa. The rheological study of Gel 1 measured a storage modulus of 262.6 Pa **(Figure 3.6b, Gel 1)** and LVE of 64% **(Figure 3.6b, Gel 1)**.

The disulfide bonds within hydrogel Gel 1 were then cleaved through a reaction with GSH to afford a *sol* material **(Figure 3.6a, Gel 2)**. The transformation into a *sol* was confirmed as the hydrogel material became liquid-like. The cleavage of disulfide bonds was supported by the absence of bands at high molecular weight (75+ kDa) in the

SDS-PAGE **(Figure S3.1, Sample 2)**. Hydrogen peroxide (8.75 % v/v) was then added to drive the reformation of the disulfide bonds to yield hydrogel Gel 3 **(Figure 3.6a, Gel 3)**. The bands above 75 kDa **(Figure S3.1, Sample 3)** reappeared as disulfide bridges reformed when the thiols were oxidised with H_2O_2. Gel 3 obtained a G' of 189.7 Pa **(Figure 3.6b, Gel 3)** and an LVE of 64% **(Figure 3.6b, Gel 3)**. These results were encouraging as they showcased the reversible characteristic of the disulfide bond within the Caf1-SS-PEG hydrogel. It is known that the refolded Caf1 chains in the refolded hydrogels are shorter in length than the Caf1 chains in native hydrogels. Therefore it is anticipated that gelation time and critical strain would increase while the storage modulus decreases as more cycles of deformation/reformation were to be performed.[30] Moreover, it demonstrated that disulfide bonds within the Caf1-SS-PEG hydrogel have the potential to act as a stimulus-trigger release mechanism for drug delivery application upon disulfide bond cleavage.
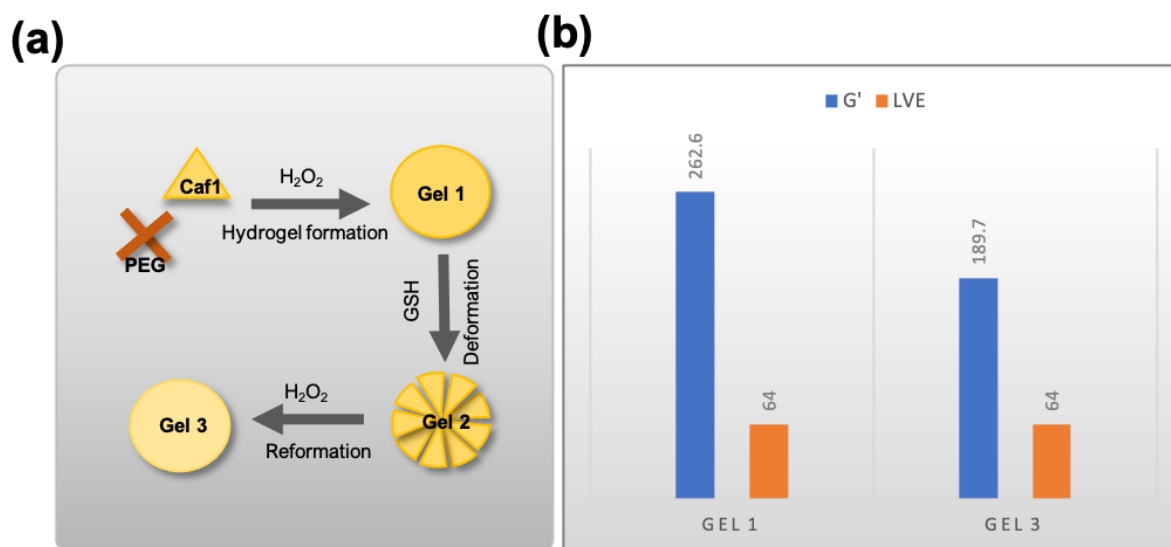
Figure 3.6, (a) Schematic representation of reversible hydrogel formation. Caf1^{Cys} reacted with PEG-SH in the presence of H_2O_2 to form **Gel 1**, **Gel 1** was broken down via cleavage of disulfide bonds with GSH into **Gel 2**. The resulting material was retained and allowed to reform in the presence of H_2O_2 to form into **Gel 3**. **(b)** The hydrogels were evaluated via rheology, disulfide bonds formation (**Gel 1**) and hydrogels with the reformation of disulfide bonds (**Gel 3**). Storage modulus (G') was recorded by the time sweep presented in **blue**, and the mean LVE region from 0.1% was recorded from the amplitude sweep in **orange**.

3.3.6. Reversible mosaic Caf1-SS-PEG hydrogels

Caf1^{WT} polymer and Caf1^{Cys} polymer are homopolymers as their polymer chains comprise identical subunits. However, subunits of different Caf1 subtypes can be polymerised to form a *mosaic* Caf1$^{Cys: WT}$ (copolymer) **(Figure 3.7a)** through the recently reported thermal unfolding process.[31] Both Caf1^{WT} polymer and Caf1^{Cys} polymer can be depolymerised into their monomers when heated above their melting temperature (approximately 85 to 90 °C). The monomer subunits then refold to reform the polymer chains upon cooling back to room temperature. This feature potentially allows cargo to be encapsulated within the hydrogel network (as discussed in Chapter 2). It also provides access to a new type of hydrogel based on mosaic copolymers.
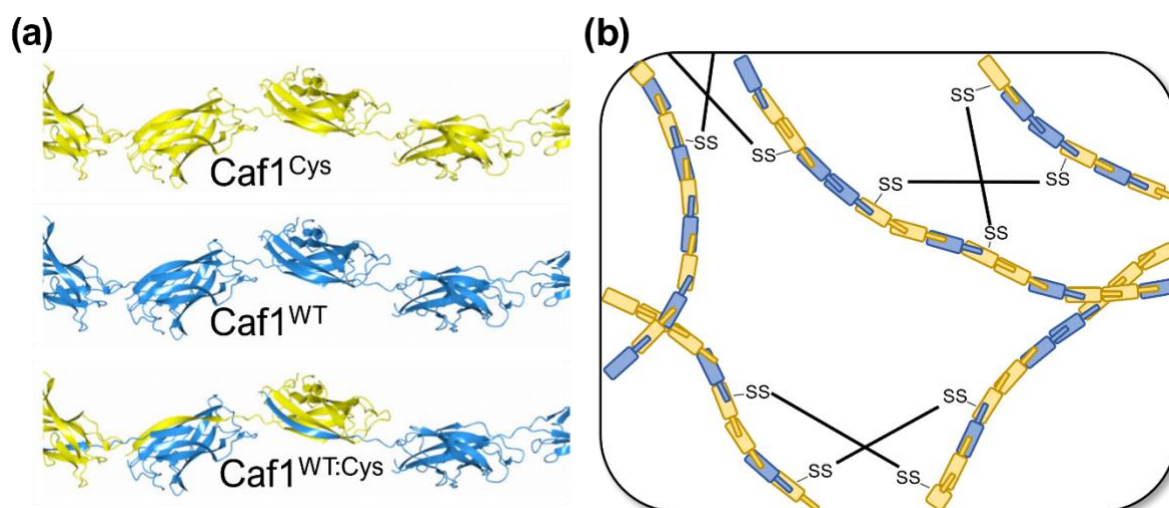
Figure 3.7, Structures **(a)** of Caf1 copolymers (Caf1$^{WT: Cys}$, Caf1^{WT}, Caf1^{Cys}) (PDB: 1P5U). The structure of Caf1^{Cys} monomers is highlighted in **yellow,** and Caf1^{WT} is highlighted in **blue**. The structures were visualised using CCP4MG software. **(b)** Crosslinked *mosaic* Caf1-SS hydrogels formed via disulfide bonds (SS) between Caf1^{Cys} monomers with PEG-SH in yellow.

Two strategies have been employed to produce *mosaic* Caf1$^{Cys: WT}$ hydrogels **(Figure 3.7b)**. Route one is a copolymer-crosslinking approach where the Caf1^{WT} and Caf1^{cys} polymers undergo a cycle of unfolding, mixing, and refolding to form *mosaic* copolymers that are then subsequently cross-linked. Route two involves a blending approach where both Caf1^{WT} and Caf1^{cys} subunits are cross-linked, and the resulting hydrogels are allowed to melt and then mixed, and the new network is allowed to reform, resulting in the formation of Caf1$^{Cys: WT}$ *mosaic* hydrogel.

3.3.7. Copolymer-crosslinking approach
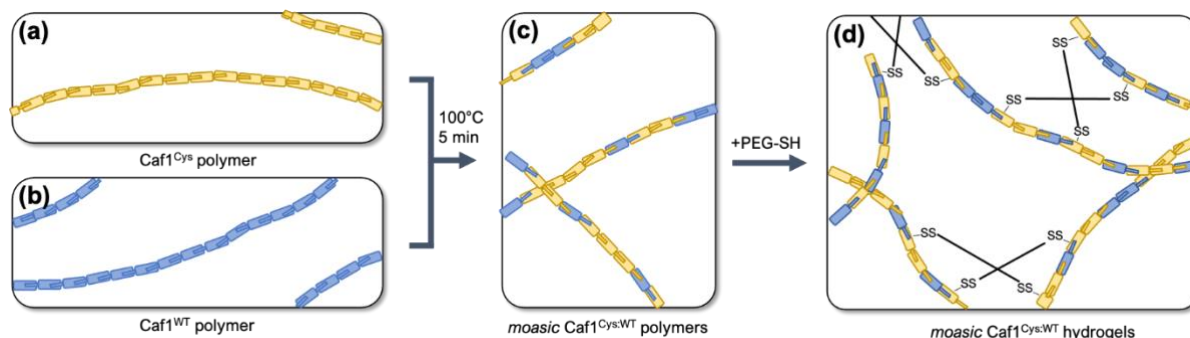
Figure 3.8, Schematic illustration of copolymer-crosslinking approach. Caf1^{Cys} **(a)** polymers are highlighted in **yellow,** and Caf1^{WT} **(b)** polymers are highlighted in **blue**. The Caf1^{Cys} and Caf1^{WT} polymers were added together, heated at 100°C for 5 min and allowed to cool to room temperature to form *mosaic* Caf1$^{Cys:\ WT}$ copolymers **(c)**. The *mosaic* Caf1$^{Cys:\ WT}$ copolymers were then crosslinked with PEG-SH with the addition of an oxidating agent to yield *mosaic* Caf1$^{Cys:\ WT}$ hydrogels **(d)**.

Mosaic Caf1-SS hydrogels were prepared via a "copolymer-crosslinking" approach **(Figure 3.8a & 3.8b)** where the Caf1^{Cys} polymer and Caf1^{WT} polymer were mixed in a single vessel, heated at 100 °C for 5 min and allowed to cool to room temperature to obtain *mosaic* Caf1$^{Cys:\ WT}$ copolymers **(Figure 3.8c)**. The Caf1^{Cys} subunits within the *mosaic* Caf1$^{Cys:\ WT}$ polymers were then crosslinked with 4-arm PEG-SH in the presence of an oxidising agent to yield *mosaic* Caf1$^{Cys:\ WT}$ hydrogels **(Figure 3.8d)**. Two *mosaic* Caf1$^{Cys:\ WT}$ hydrogels were prepared with overall Caf1 contents of 2% or 4% w/v. The relative quantity of Caf1^{Cys} polymer content will contribute most to the mechanical properties of the *mosaic* Caf1$^{Cys:\ WT}$ hydrogel network as the PEG-SH forms disulfide bonds with free -SH group of Caf1^{Cys} and not Caf1^{WT} subunits, leading to greater crosslinking of the Caf1 polymers.

The hydrogel with the lower Caf1^{Cys} content yielded a hydrogel **(Table 3.3, Entry 1)** in under 10 min with G' of 71 Pa and LVE of 63 %. The relatively low Caf1^{Cys} content mostly favours PEG-SS-PEG crosslinking and limited Caf1-SS-PEG cross-linking. This becomes evident as the ratio of Caf1^{Cys} increases **(Table 3, Entry 2)**. When the concentration of Caf1 increases to 1 % (w/v), the hydrogel **(Table 3, Entry 2)** obtained displays an improved storage modulus of 128 Pa and LVE was lowered to 40 %; this is because an increase in Caf1-SS-PEG crosslink density which reduces Caf1 polymer

flexibility, and thus, a lowered LVE. It also increased gelation time to 1 h (compared to 10 min previously); this increase is because hydrogel **Entry 1 (Table 3.3)** is predominately based on PEG-SS-PEG crosslinking when compared to hydrogel **Entry 2 (Table 3.3),** where there is a higher content of Caf1-SS-PEG formation. Despite this, these mosaic Caf1Cys: WT hydrogels' overall mechanical properties have significantly improved in terms of G' when compared with the control experiment **(Table 3.3, Entry 3 & 4)**. This hydrogel which features Caf1^{Cys} homopolymers cross-linked with PEGSH has a storage modulus of 21 Pa and an LVE of 158 %. Another control experiment was carried out with refolded Caf1^{Cys} polymers used to form Caf1-SS-PEG hydrogel **(Table 3.3, Entry 4)**. A gelation time of 35 min was observed, and a G' of 62 Pa and LVE of 63 % were measured. The shorter Caf1^{Cys} polymer chains resulted in an improved hydrogel in terms of mechanical properties compared to hydrogel **Entry 3 (Table 3.3),** probably due to its smaller pore size. This result shows that the addition of the Caf1^{WT} subunit has improved the mechanical properties of mosaic Caf1 hydrogels **(Table 3.3, Entry 2)** compared to hydrogels which are absent in Caf1^{WT} **(Table 3.3, Entry 4)**. This is an encouraging result as it confirms that *mosaic* hydrogels improved hydrogel mechanical properties even at low Caf1^{Cys} content **(Table 3.3, Entry 1)**, although the disulfide bonds formed are predominately PEG-SS-PEG instead of Caf1-SS-PEG.

A range of formulations of overall 4 % Caf1 content were prepared to investigate the effect of increases in Caf1^{Cys} content on the hydrogel mechanical properties.

Table 3.3, Formulation and mechanical properties of 2 %w/v mosaic Caf1-SS-PEG hydrogels.

Entry	Caf1^{WT} (%w/v)	Caf1^{Cys} (%w/v)	PEG-SH (%w/v)	Caf1^{Cys} : PEG-SH ratio	H$_2$O$_2$ (%w/v)	Gelation time	G' (Pa)	Mean LVE 0.1%- (%)
1	1.8*	0.2*	3	0.07:1	8.75	10 min	71	63
2	1*	1*	3	0.34:1	8.75	1 h	128	40
3	-	2	3	0.7:1	8.75	24 h	21	158
4	-	2*	3	0.7:1	8.75	35 min	62	63

* Refolded Caf1 polymer after heating at 100 °C for 5 mins.

It was anticipated that an increase in the composition of Caf1^{Cys} subunits should result in a rise in cross-linkages between Caf1^{Cys} and PEG-SH, thus enhancing the storage modulus. This was evidenced in formulation **Entry 1 (Table 3.4)**, where the hydrogel possessed a G' of 138 Pa, LVE of 40 % and the gelation time reduced to 10 min. This significantly improved compared to hydrogel **Entry 1 (Table 3.3)** formed with lower Caf1 concentrations. Interestingly, with an increase in Caf1^{Cys} content, the gelation time and LVE for **Entry 2 (Table 3.4)** remained unchanged, although the hydrogel did obtain a modest increase in storage modulus to 186 Pa. Further, the control experiments where there was a nearly negligible difference in G' between hydrogels obtained from long Caf1^{Cys} polymers (67 Pa) **(Table 3.4, Entry 3)** or refolded shorter Caf1^{Cys} polymers (64 Pa) **(Table 3.4, Entry 4)**. However, the gelation time has considerably shortened in formulation **Entry 4 (Table 3.4)** to 20 min compared to the 2 d observed for **Entry 3 (Table 3.4)**, probably as a result of using a shorter Caf1 polymer chain, that increases the likelihood of and a Caf1-SS-PEG disulfide bond formation.

Table 3.4, Formulation and mechanical properties of 4 %w/v mosaic Caf1-SS-PEG hydrogels.

Entry	Caf1^{WT} (%w/v)	Caf1^{Cys} (%w/v)	PEG-SH (%w/v)	Caf1^{Cys} : PEG-SH ratio	H$_2$O$_2$ (%w/v)	Gelation time	G' (Pa)	Mean LVE 0.1%-(%)
1	3.6*	0.4*	3	0.14:1	8.75	10 min	138	40
2	2*	2*	3	0.67:1	8.75	10 min	186	40
3	-	4	3	1.34:1	8.75	2 d	67	25
4	-	4*	3	1.34:1	8.75	20 min	64	40

* Refolded Caf1 polymer after heat treated at 100 °C for 5 mins.

These experiments have presented promising results for *mosaic* Caf1$^{Cys: WT}$ copolymer-based hydrogels using a "copolymer-crosslinking" approach, with the use of *mosaic* Caf1 copolymers enhancing hydrogel robustness by strengthening its mechanical properties.

3.3.8. "Blending" approach
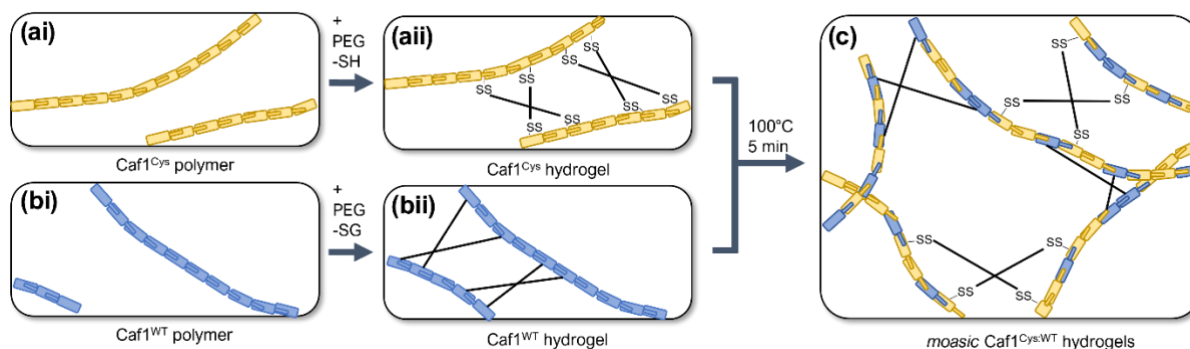
Figure 3.9,Schematic illustration of the "blending" approach. Caf1^{Cys} **(ai)** polymers are highlighted in **yellow,** and Caf1^{WT} **(bi)** polymers are highlighted in **blue**. The Caf1^{Cys} polymers were crosslinked with PEG-SH to form Caf1^{Cys} hydrogel **(aii)**; Caf1^{WT} polymers were crosslinked with PEG-SG to yield Caf1^{WT} hydrogel **(bii)**. Both hydrogels were heated at 100 °C for 5 min, then mixed via aspiration, and allowed to cool at room temperature to form *mosaic* Caf1$^{Cys: WT}$ hydrogels **(c)**.

The "blending" approach **(Figure 3.9)** was employed as an alternative method to form *mosaic* Caf1$^{Cys: WT}$ hydrogels. Hydrogel obtained via this approach was made from two types of covalent bond formation: crosslinking between the disulfide bond formed from Caf1^{cys}-SS-PEG and the amide bond formed from Caf1^{WT}-PEG. The Caf1^{Cys} hydrogel and Caf1^{WT} hydrogel were prepared separately. Caf1^{Cys} polymers **(Figure 3.9ai)** were

reacted with PEG-SH in the presence of H_2O_2 to form Caf1^{Cys} hydrogel **(Figure 3.9aii)**. Likewise, Caf1^{WT} polymers **(Figure 3.9bi)** were reacted with structural PEG-SG to form Caf1^{WT} hydrogel **(Figure 3.9bii)**. The two hydrogels were then heated at 100 °C for 5 min to unfold the polymer chains driving hydrogel melting. The resulting solutions were then mixed by aspiration, and the mixture was allowed to cool at room temperature to afford the *mosaic* Caf1$^{Cys:\ WT}$ hydrogel **(Figure 3.9c)** after 24 h **(Table 3.5),** as a demonstration shown in **Figure 3.10**.
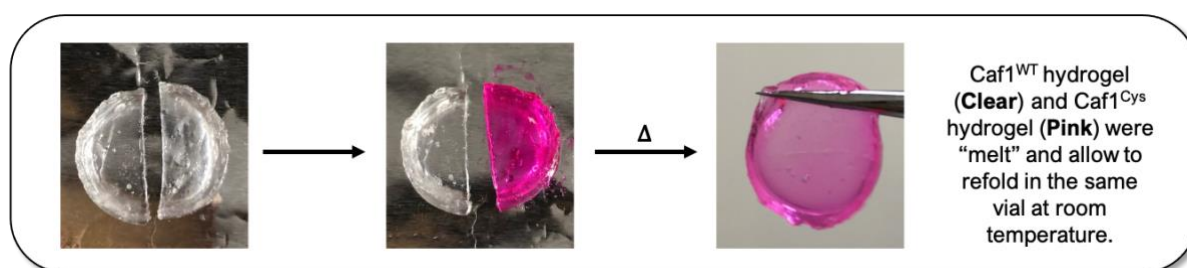
Figure 3.10, Picture demonstrations of Caf1^{WT} hydrogel pictured in **clear**, Caf1^{Cys} hydrogel pictured in **pink**. Both hydrogels were heated at 100 °C for 5 min to depolymerise, the Caf1 were then mixed and allowed to repolymerise at room temperature over 24 h to afford a *mosaic* Caf1-SS-PEG hydrogel.

The resulting hydrogel is speculated to be composed of the Caf1$^{Cys:\ WT}$ copolymers containing both Caf1^{cys} and Caf1^{WT} subunits. The mechanical properties of this hydrogel were measured to be G' of 296 Pa **(Table 3.5)**, with a critical strain of 3% strain **(Table 3.5)** and an LVE of 2% **(Table 3.5)**. The relatively high storage modulus and low LVE obtained for this hydrogel is likely the result of a combination of high crosslink density and shortened refolded caf1 polymer chains and, consequently, reduced structural flexibility.

Table 3.5, Formulation and mechanical properties of 2 %w/v mosaic Caf1-SS hydrogels.

Caf1WT hydrogel		Caf1-SS-hydrogel			Mosaic Caf1-SS-PEG hydrogel			
Caf1WT (%w/v)	PEG-SG (%w/v)	Caf1Cys (%w/v)	PEG-SH (%w/v)	H_2O_2 (%w/v)	Gelation time	G' (Pa)	Mean LVE 0.1%- (%)	Critical strain (%)
4	3	4	3	8.75	24 h	296	2	3
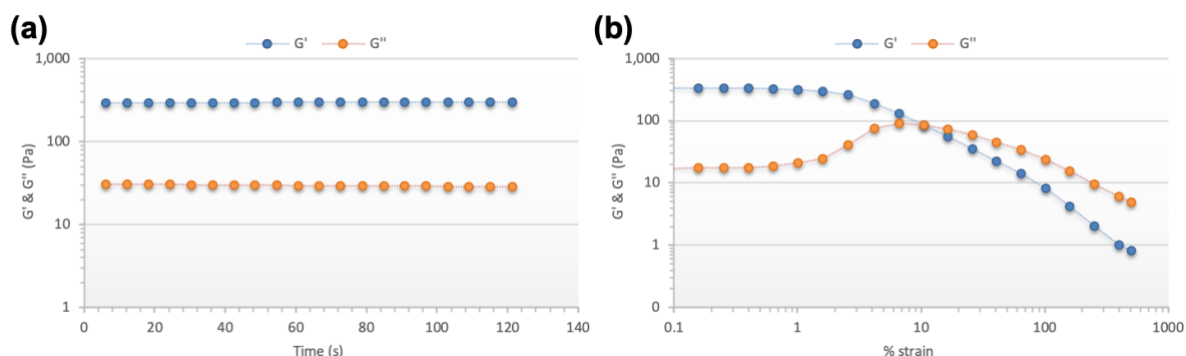
Figure 3.11, The mechanical properties were studied using rheology: **(a)** time sweep and **(b)** amplitude sweep. Storage modulus (G') is represented in **blue** and loss modulus (G'') is in **orange**.

The result shows that the 'blending' approach yielded a hydrogel with enhanced mechanical properties in terms of storage modulus (296 Pa) **(Figure 3.11a)** when compared with the copolymer-crosslinking approach (21-186 Pa) (**Table 3.3 & 3.4**). However, the LVE **(Figure 3.11b)** indicated that hydrogel yielded from the 'blending' approach is less flexible when compared to its copolymer approach counterparts. As discussed in the previous chapter, hydrogels with higher flexibility will be better candidates for controlled release applications. Hydrogels with low flexibility are more prone to degradation,[32] resulting in undesired fast, undesired release rates. Hydrogels with flexible polymer networks benefit from increased swelling in comparison to the rates of degradation. Thus, the copolymer-crosslinking approach was selected as a formulation strategy for hydrogel cargo delivery purposes.

3.3.9. Stimuli-responsive Caf1-SS-PEG Hydrogels for small molecule-controlled release
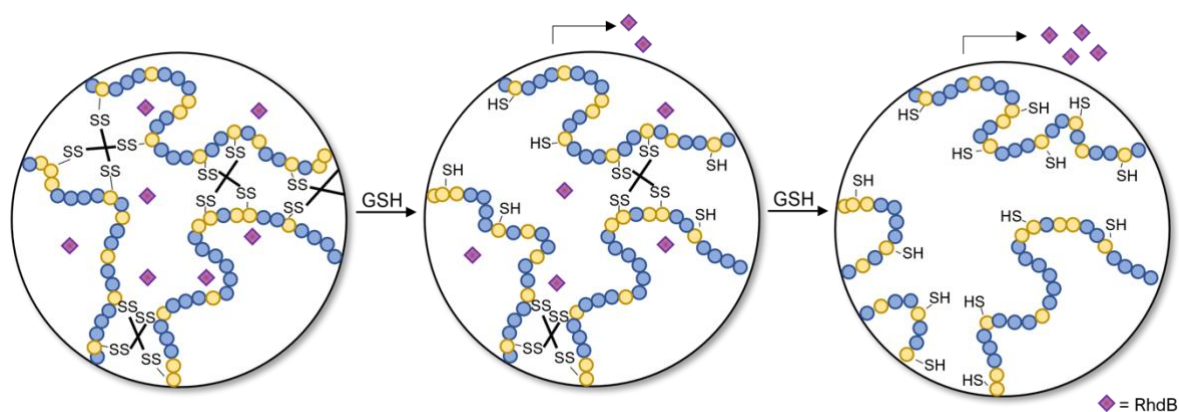
Figure 3.12, Schematic diagram of drug-loaded crosslinked *mosaic* Caf1-SS hydrogels that possess disulfide (SS) cross-linkages that include Caf1^{Cys} monomers as highlighted in **yellow** and Caf1^{WT} monomers presented in **blue**. Rhodamine-B in **purple** was loaded into the hydrogel as a model drug for release studies.

The 2 %w/v Caf1 $^{Cys:\ WT}$ *mosaic* hydrogel prepared by the copolymer crosslinking approach was selected to investigate disulfide stimulus-responsiveness as a trigger for the controlled release of a model drug **(Figure 3.12)**. Three *mosaic* Caf1-SS-PEG hydrogels were prepared via the copolymer-crosslinking approach, each with identical composition **(Table 3.6)**. The hydrogels (200 µL) were allowed to form at room temperature over 24 h before their dehydration by freeze-drying. Identical concentrations of rhodamine-B (2 %w/v) in PBS were loaded (>90 %) into the dried hydrogels using the absorption method described in Chapter 2. The gels were rested at room temperature overnight before the release studies.

Table 3.6, Formulation of 2 %w/v mosaic Caf1-SS hydrogels and RhdB release studies.

Entry	Caf1^{WT} (%w/v)	Caf1^{Cys} (%w/v)	PEG-SH (%w/v)	H$_2$O$_2$ (%w/v)	RhdB (% v/w)	GSH (mM)	1/2 life (h)
1	2	2	3	8.75	2	0	3.10
2	2	2	3	8.75	2	2.5	1.22
3	2	2	3	8.75	2	7.5	0.87

RhdB = Rhodamine-B in PBS buffer solution.
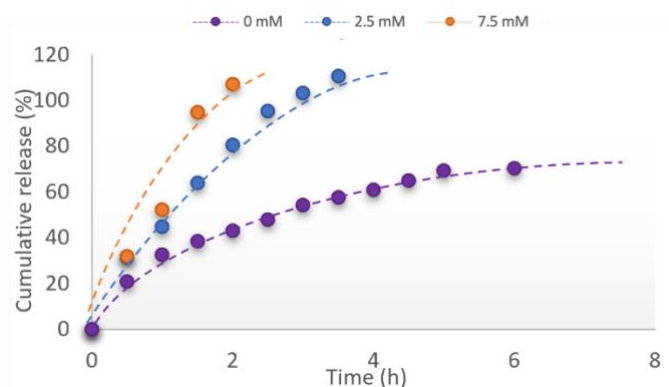
Figure 3.13,The release profile of rhodamine-B from mosaic Caf1-SS-PEG hydrogels in the presence of 0 mM, 2.5 mM, and 7.5 mM of GSH. Model cargo release over time. Additional GSH enhances the release of Rhodamine-B by cleaving the disulfide bonds of the hydrogel network, resulting in a faster release of Rhodamine-B.

PBS (500 μL) with GSH (0, 2.5 and 7.5 mM) was added to each hydrogel. It was anticipated that the rate of rhodamine-B release would increase as the concentration of GSH increased. The sample with 0 mM of GSH acts as a control. At predetermined time intervals, aqueous solutions containing Rhodamine-B were carefully removed from above the hydrogel for spectroscopic analysis to determine rhodamine-B concentrations and then replaced with a new PBS solution. The release profiles **(Figure 3.13)** of these samples were plotted as the cumulative release (%) versus time (h). The half-life of the RhdB released was calculated from the release profile **(Figure 3.13)**. Half-life is a measure of the time taken for drug release of 50 %. The sample with 0 mM of GSH obtained a half-life of 3.1 h **(Table 3.6, Entry 1)**, whereas the sample with 2.5 mM of GSH **(Table 3.6, Entry 2)** obtained a half-life of 1.22 h, which is 1.4 times faster compared to sample with 0 mM of GSH; the sample with 7.5 mM of GSH **(Table 3.6, Entry 3)** measured a half-life of 0.87 h which is 3.8 times faster than the sample with 0 mM of GSH.

The release profiles **(Figure 3.13)** showed significant differences between the three samples. After 2 h, approximately 38 % of rhodamine-B was released from the sample treated with 0 mM of GSH; this release is likely the result of rhodamine-B diffusion out from the hydrogel. As discussed in Chapter 2, molecules diffuse out from hydrogel networks when the molecule size is smaller than the pore size. The sample containing 2.5 mM of GSH induced approximately 60 % of RhdB release within 2 h; the increase in release rate is most likely driven by disulfide bond cleavage, which increases pore

size and, thus, a faster diffusion. This was also evidenced in the sample treated with 7.5 mM of GSH, which achieved 100 % of RhdB release within 2 h. These results supported the hypothesis that increases in the concentration of added GSH promote disulfide cleavage, leading to faster release due to increased pore size.

Kinetic modelling of the release profiles was performed to further investigate the release mechanism. Kinetic models were employed to study this release mechanism that occurred: first-order kinetic **(Figure 3.14a)**; Korsmeyer-Peppas **(Figure 3.14b)**; Higuchi **(Figure 3.14c)** and Hixson-Crowell **(Figure 3.14d)**. A 'good fit' to the model should obtain a coefficient of determination (R^2) near or close to 1. It is also important to note that these mathematical models are only valid for up to 60% of drug releases.[33] The first-order kinetics is described by a plot of the natural log of unreleased fraction vs time **(Figure 3.14a)**. This model is best at describing the rate of release when it is dependent on the concertation gradient. The R^2 derived from the first-order kinetic model were 0.9838, 0.8858 and 0.8513 (samples of 0, 2.5 and 7.5mM of GSH) **(Table 3.7)**. The relatively poor linear fit for the experiments with GSH probably arises because as these experiments progress, the pore size is always increasing (and thus, the diffusion constant is also changing).

91
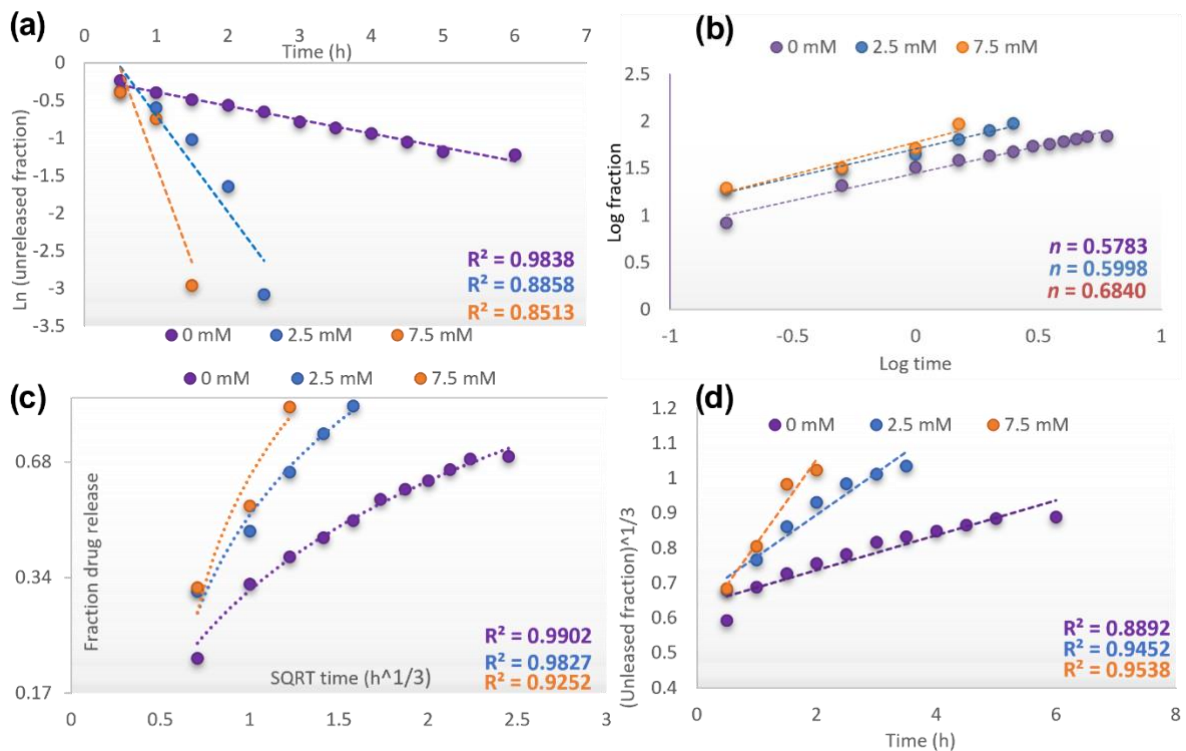
Figure 3.14, Release profiles transformed into the following kinetic models: fitted as **(a)** first-order kinetic plots; **(b)** Korsemyer-Peppas modelling of these profiles determined the diffusion exponent, *n*; **(c)** Higuchi plot and **(d)** Hixson-Crowell plot. Linear coefficient of determination (R^2) was determined for first-order kinetic, Higuchi, and Hixson-Crowell models.

Table 3.7, Coefficient of determination derived from kinetic models for RhdB release from mosaic Caf1-SS-PEG hydrogels.

	Coefficient of determination (R^2)		
GSH (mM)	0	2.5	7.5
First order	0.9838	0.8858	0.8513
Korsmeyer-Peppas	0.9923	0.9876	0.9587
diffusion exponent (n)	0.5783*	0.5998*	0.6840*
Higuchi	0.9902	0.9827	0.9252
Hixson-Crowell	0.8892	0.9452	0.9538

Kormeyer-Peppas model **(Figure 3.14a)** was used to evaluate whether the drug release follows Fick's Law. Diffusion exponent, *n* value, is derived from the Korsmeyer-Peppas models plot of log fraction released versus log t. The *n* values obtained were 0.5783, 0.5998 and 0.6840 **(Table 3.7)** for the samples. The results indicated that the drug release follows non-Fickian diffusion. In particular, the *n* values between 0.5 – 1 describe a system where both diffusion and swelling occur, and the drug release is time-dependent. To study whether the release was driven by cargo diffusion or released from swelling, Higuchi and Hixson-Crowell models were employed. The Higuchi plot **(Figure 3.14c)** (fraction release versus square root of t) describes drug release as diffusion driven. The coefficient of determinations obtained from this model were 0.9902, 0.9827 and 0.9252 (samples of 0, 2.5 and 7.5mM of GSH) **(Table 3.7)**. The Hixson-Crowell plot cube root of fraction against time **(Figure 3.14d)** describes drug release by hydrogel dissolution. The R^2 values were calculated as 0.8892, 0.9452 and 0.9538 (samples 0, 2.5 and 7.5mM of GSH) **(Table 3.7)**. Taken together, the results suggest the different release rates between samples with 0 mM GSH to samples with 2.5 or 7.5 mM of GSH were driven by disulfide bond cleavage, and it is

not due to gel dissolution or surface erosion. Swelling/degradation studies would need to confirm this finding, as well as further release studies utilising the reversible nature of disulfide bond in this type of hydrogel will be beneficial to this work.

The data obtained in this study showed encouraging results, and it demonstrated *mosaic* Caf1-SS-PEG hydrogels as a potential candidate for stimulus-responsive drug carriers. The drug release studies presented the effectiveness of drug release upon disulfide bond cleavage with a minimal concentration of reducing agents such as GSH. The mechanism by which the drug was released has been analysed by several mathematical models, and the results indicated that the overall release rate increases as the disulfide bonds are cleaved in the presence of reducing agents.

3.4. Conclusion

bonds incorporated into Caf1 hydrogels were exploited to trigger a stimuli-responsive cargo release. Thiol groups were introduced within the Caf1 N-terminal donor strand, allowing the potential for disulfide bonds to be formed between Caf1 and multi-arm PEG-SH crosslinkers. The gelation time and mechanical properties of the resultant hydrogels were studied at different formulation compositions in the presence of an increase in oxidising agent concentration that was added to drive disulfide bond formation. Despite that, the hydrogels will feature a substantial degree of crosslinking between the PEG-SS-PEG, but there is evidence to suggest Caf1-SS-PEG cross-linking.

The self-healing nature of these materials was studied by breaking the hydrogel into fragments; unreacted thiol groups within the hydrogel network, then thiol groups were then reacted to form new disulfide bonds and yield a new macroscopic hydrogel. The redox-driven reversible nature of disulfide bonds with these hydrogels was investigated with SDS-PAGE and rheology. Rheology studies indicated that during the reformation of disulfide bonds, suggested that Caf1[Cys] polymers have rearranged the Caf1-SS-PEG hydrogel network to yield a hydrogel with higher elasticity. With that in mind, prolonged gelation time and lower storage modulus were recorded with the hydrogels formed with refolded Caf1 polymer; this is most likely the result of a decrease in crosslink density combined with shorter Caf1 chains. *Mosaic* Caf1

hydrogels were fabricated with the aim of improving the mechanical properties of disulfide-bonded Caf1 hydrogels. Two approaches were employed to form mosaic Caf1 hydrogels; the hydrogel was yielded by crosslinking PEG-SH with *mosaic* Caf1$^{Cys:WT}$ (copolymers) via the copolymer crosslinking approach and the 'blending' approached by blending Caf1^{Cys} hydrogel with Caf1^{WT} hydrogel. In comparison, the 'blending' approach yielded hydrogel with improved storage modulus when compared to the copolymer crosslinking approach, this is because of the duo crosslinking between Caf1^{Cys}-SS-PEG and Caf1^{WT}-PEG. *Mosaic* Caf1-SS hydrogels formed via the copolymer crosslinking approach were selected to investigate their stimulus-responsive release properties further. The release profiles obtained showed strong evidence that the addition of GSH as a stimuli response triggered the release of the model drug rhodamine-B. First-order release kinetics in the absence of a reducing agent was observed, compared to the samples in the presence of a reducing agent. The comparative results from Higuchi and Hixson-Crowell indicated that drug releases were diffusion based in all three samples. Korsmeyer-Peppas model shows that all samples follow non-Fickian diffusion, with diffusion exponent n between 0.5 – 1.0, suggesting that the drug release is by diffusion and swelling. The difference in release rate in conjunction with the results of the mathematical models highlighted fast release is likely due to the cleavage of disulfide bonds in the presence of a reducing agent. This work demonstrated that the redox-responsive Caf1-SS hydrogels could be fabricated and used for stimulus release of model drug cargos.

3.5. Future Work

Caf1 polymer direct cross-linkage with drug cargo/nanoparticles via disulfide bonds

The interest in utilising disulfide bonds in drug delivery has increased significantly due to their redox nature.[34] As demonstrated, disulfide bonds can be easily established between two Caf1 protein subunits with cysteine residues. The same idea could also be applied to Caf1 polymer decorated with drug cargo via disulfide bonds (Caf1-SS-Cargo), provided the drug cargo or nanoparticles contain a thiol group as demonstrated by Guindani et al.[35]. This new hydrogel (Caf1-SS-Cargo) may provide

an improved cargo release mechanism in the presence of a reducing agent. In addition, it can act as a protective barrier for sensitive drug cargo.

3.6. Experimental

General Experimental

4-arm PEG-Succinimidyl glutarate (4-arm PEG-SG) (20 kDa) and 4-arm PEG – sulfhydryl mercapto (4-arm PEG-SH) (20 kDa) were purchased from Creative PEGWorks. Sodium bicarbonate solution (0.05 M, pH 8.2) was prepared by dissolving sodium bicarbonate (4.2 g) (Acros) in deionised water (1 L). The pH was adjusted to 8.2 with 1M HCl. Phosphate buffered saline (PBS) was prepared by dissolving salts in deionised water (100 mM sodium hypophosphite, 100 mM monosodium dihydrogen orthophosphate, 137 mM sodium chloride, 27 mM potassium chloride from Sigma-Aldrich, dissolving in 100 mL of deionised water). The pH was adjusted to 7.4 with dropwise addition of 1M HCl.

Instrumentation

Rheological measurements were performed using a Discovery HR-2 rheometer (TA Instruments, USA) with a parallel plate of 20 mm diameter and a gap of 1500 μm at 25 °C. UV-vis spectroscopy was performed using Thermo Scientific NanoDrop One[c]. pH measurements were made using a Hanna HI 90103 instrument (Hanna Instruments Ltd) which was calibrated using commercial buffer solutions (Sigma-Aldrich).

Caf1 protein expression and purification

Proteins were prepared by Dr Helen Waller and used as supplied. BL21 (DE3) E. coli cells (NEB) were transformed with pT7-COPΔR-Caf1^{Cys} plasmids as described by *Peters et al*. (2019).[27,36] Terrific broth (TB) 200 mL containing ampicillin (100 µg mL^{-1}) in 2 L shake flasks were inoculated with single colonies and grown for 21 h at 35 °C, with shaking at 180 rpm. The cell pellet was removed by centrifugation at 3000 rpm, 22 °C, 30 min (JA rotor) followed by ultracentrifugation at 35,000 rpm, 22 °C, 60 min (45 Ti rotor) to collect the flocculent layer that forms above the cell pellet. The product was then resuspended in PBS buffer (10 mM sodium phosphate, 137 mM sodium chloride, 2.7 mM potassium chloride, pH 8.0, 10 mL per flocculent). 5 mg of DNase and RNase were added, and Caf1 polymer was extracted by incubation in a water bath

at 48 °C 3 h. Followed by further overnight incubation at 22 °C, and the flocculant was collected in the supernatant by 2 x 60 min ultracentrifugations at 22 °C, 35,000 rpm (Beckman 45 Ti rotor). Extracted Caf1 polymer was purified with tangential flow filtration using a Minimate TFF 500 kDa MWCO filter (Pall) and purified using HiScreen Capto™ Core 70 columns (2 x 4.7 mL in series, GE Healthcare), with PBS as running buffer.

Preparation of reversible Caf1-SS-PEG hydrogels

Caf1-SS hydrogels were obtained by reacting 200 µL 4-arm PEG-SH (2 %v/v) and 200 µL Caf1^{cys} (2 %w/v) in PBS buffer in the presence of H_2O_2 of different concentrations (4.38, 5.83 and 8.75 %v/v) (2 µL). The samples were mixed with 5 seconds of the vortex and were left at room temperature to react further. The gelation time of the samples was estimated by the vial-inversion method. Rheological measurements were performed to gain further insight into the mechanical properties of these hydrogels.

Disulfide bond cleavage investigation

20 µL of GSH (20 %w/v) was added to 200 µL of Caf1-SS hydrogels, causing the transformation of the hydrogel into a solution. The sample was then oxidised with H_2O_2 (8.75 %w/v), transforming the solution into hydrogels. The latter hydrogels were studied by rheologies under the following conditions: The time sweep experiment was performed at a constant frequency (1 Hz) and strain (1 %). The frequency sweep experiment was conducted at a fixed strain of 1.0 % and the angular frequency from 0.1 to 100 rad s^{-1}. The amplitude sweep experiment was conducted at a fixed frequency (1 Hz), and the strain was from 0.1 % to 500%.

The chemical cleavage of the disulfide bonds was monitored using SDS-PAGE. Three identical Caf1-SS hydrogels (1, 2, 3) were prepared by reacting Caf1^{cys} (1 %w/v), 4Arm-PEG-SH (2.5 %w/v) and H_2O_2 (8.75 %w/v). The hydrogels were allowed to be set overnight. To cleave the disulfide bonds, 20 µL glutathione (10 mM) was then added to hydrogels sample **2** and sample **3**. Disulfide bond reformations were performed on hydrogel sample **3** by adding 20 µL of H_2O_2 (8.75 %w/v). Caf1^{cys} (1 %w/v) was dissolved in PBS buffer as the control sample. All the samples were stained with (Tris-HCl (125 mM) (pH 6.8), EDTA (5 mM), glycerol (5 % v/v), SDS (2 %w/v) and bromophenol blue (0.1 % v/v)) with no reductant. The samples were then heated at 100 °C for 5 min to

depolymerise the Caf1 polymer chains before loading onto SDS-PAGE gel.[37] The samples migrated in 15 % resolving gel under a constant voltage of 200 V for 60 min. The gel was removed from the cassette and stained with Coomassie blue (Generon). The gel was destained and scanned (Image Lab 5.2.1,, Biorad).

Preparation of 2nd generation reversible mosaic Caf1-SS hydrogels

Two approaches were employed to fabricate *mosaic* Caf1-SS hydrogels, consisting of copolymer chains comprising Caf1^{WT} and Caf1^{cys} monomers.

The copolymer crosslinking approach: Purified Caf1^{WT} and Caf1^{cys} polymers (2 %w/v)/ (4 %w/v) were dissolved in PBS (0.1 mM). The samples were then heated at 100 °C for 5 mins to depolymerise the Caf1 to its monomeric state. The samples were mixed in different concentrations (2 %w/v)/(4 %w/v) and allowed to cool at room temperature overnight. These new copolymers were then reacted in the presence of 1 μL of H_2O_2 (8.75 %v/v) with 4-arm PEG-SH (3 %w/v) to make up a 400 μL hydrogel.

The 'blending' approach: Two hydrogels were prepared: Gel 1 was formed by mixing 100 μL of Caf1^{cys} (4 %w/v), 100 μL 4-arm PEG-SH (3 %w/v) and 1 μL H_2O_2 (8.75 %w/v) at room temperature and allowed to rest for 24 h. Gel 2 was formed by mixing 100 μL of Caf1^{WT} (4 %w/v), 100 μL 4-arm PEG-SG (3 %w/v) and 1 μL H_2O_2 (8.75 %w/v) at room temperature, then allowed to rest for 24 h. The two hydrogels were then placed in a vial and heated at 100 °C for 5 min to cause both hydrogels to unfold. The resulting solution was left to gelate at room temperature for 24 h. Rheological measurements were performed on these hydrogels.

Drug loading of Caf1-SS-PEG hydrogels

Mosaic Caf1-SS hydrogels were prepared by dissolving Caf1^{WT} and Caf1^{Cys} protein polymer (2 %w/v) in phosphate-buffered saline (100 μL). 4-arm PEG-SH (3 %w/v) was dissolved in 0.05 M sodium bicarbonate solution (100 μL). 2 mg of Rhodamine-B (1 %w/v) was dissolved in PBS (200 μL) buffered solution. The solutions were mixed by aspiration, and 1 μL H_2O_2 (8.75 %w/v) was added to the samples. The drug-loaded *mosaic* Caf1-SS hydrogels were left to set at room temperature for 24 h.

Model drug release studies from reversible Caf1-SS-PEG hydrogels

Solutions of GSH (0, 2.5 and 7.5 mM) in phosphate-buffered saline (pH 7.4) were prepared. These solutions (500 μL) were then added on top of the cargo-loaded

mosaic Caf1-SS hydrogels (1, 2 and 3) **(Table 3.6)** prepared using the copolymer crosslinking approach, this in vitro study of drug release was carried out at 25°C. The aqueous solutions were replaced with fresh GSH solutions at predetermined time intervals. The collected aqueous solutions were analysed for rhodamine-B concentration using UV spectroscopy based on a calibration curve **(Figure S2)**, **which** was predetermined using UV-vis with absorbance at 554 mm, all samples were analysed in triplicate. The data was plotted as a cumulative release over time in the release profile and fitted to Korsmeyer-Peppas and other kinetics models, as mentioned in the Chapter, for better insight into the release mechanism.

3.7. References

1. Bae, K. H. & Kurisawa, M. Emerging hydrogel designs for controlled protein delivery. Biomater Sci 4, 1184–1192 (2016).
2. Bae, Y. H. & Park, K. Targeted drug delivery to tumors: Myths, reality and possibility. J Control Release. 153, 198–205 (2011).
3. Tiwari, G. et al. Drug delivery systems: An updated review. Int J Pharm Investig 2, 2 (2012).
4. Bawa, P., Pillay, V., Choonara, Y. E. & Du Toit, L. C. Stimuli-responsive polymers and their applications in drug delivery. Biomedical Materials 4, (2009).
5. Hoffman, A. S. Stimuli-responsive polymers: Biomedical applications and challenges for clinical translation. Adv Drug Deliv Rev 65, 10–16 (2013).
6. Tao, Y., Liu, S., Zhang, Y., Chi, Z. & Xu, J. A pH-responsive polymer based on dynamic imine bonds as a drug delivery material with pseudo target release behavior. Polym Chem 9, 878–884 (2018).
7. Chen, D. et al. Drilling by light: Ice-templated photo-patterning enabled by a dynamically crosslinked hydrogel. Mater Horiz 6, 1013–1019 (2019).
8. Delplace, V. et al. Controlled release strategy designed for intravitreal protein delivery to the retina. Journal of Controlled Release 293, 10–20 (2019).
9. Kar, M. et al. Responsive Nanogels for Anti-cancer Therapy. in Nanogels for Biomedical Applications vols 2018-Janua 210–260 (The Royal Society of Chemistry, 2017).
10. Saito, G., Swanson, J. A. & Lee, K. D. Drug delivery strategy utilizing conjugation via reversible disulfide linkages: Role and site of cellular reducing activities. Adv Drug Deliv Rev 55, 199–215 (2003).
11. Sun, M. et al. Cleavable cellulosic sponge for functional hepatic cell culture and retrieval. Biomaterials 201, 16–32 (2019).
12. Mackiewicz, M. et al. Degradable, thermo-, pH- and redox-sensitive hydrogel microcapsules for burst and sustained release of drugs. Int J Pharm 569, 118589 (2019).
13. Wang, Q., Guan, J., Wan, J. & Li, Z. Disulfide based prodrugs for cancer therapy. RSC Adv 10, 24397–24409 (2020).
14. Rosales, A. M. & Anseth, K. S. The design of reversible hydrogels to capture extracellular matrix dynamics. Nat Rev Mater 1, 1–15 (2016).
15. Chang, S. G., Choi, K. D., Jang, S. H. & Shin, H. C. Role of disulfide bonds in the structure and activity of human insulin. Mol Cells 16, 323–330 (2003).

16. Yan, X., Yang, X., Tong, X. & Huang, Y. A method to accelerate the gelation of disulfide-crosslinked hydrogels. Chinese Journal of Polymer Science (English Edition) 33, 118–127 (2015).

17. Liu, H. et al. Facile fabrication of redox/pH dual stimuli responsive cellulose hydrogel. Carbohydr Polym 176, 299–306 (2017).

18. Zhang, Y. X., Chen, Y. F., Shen, X. Y., Hu, J. J. & Jan, J. S. Reduction- and pH-Sensitive lipoic acid-modified Poly(l-lysine) and polypeptide/silica hybrid hydrogels/nanogels. Polymer (Guildf) 86, 32–41 (2016).

19. Forman, H. J., Zhang, H. & Rinna, A. Glutathione: Overview of its protective roles, measurement, and biosynthesis. Mol Aspects Med 30, 1–12 (2009).

20. Silva, M. M., Rocha, C. R. R., Kinker, G. S., Pelegrini, A. L. & Menck, C. F. M. The balance between NRF2/GSH antioxidant mediated pathway and DNA repair modulates cisplatin resistance in lung cancer cells. Sci Rep 9, 1–11 (2019).

21. Yao, Y. et al. Biodegradable multi-blocked polyurethane micelles for intracellular drug delivery: The effect of disulfide location on the drug release profile. RSC Adv 6, 9082–9089 (2016).

22. Abdullah-Al-Nahain, Lee, H., Lee, Y. S., Lee, K. D. & Park, S. Y. Development of Disulfide Core-Crosslinked Pluronic Nanoparticles as an Effective Anticancer-Drug-Delivery System. Macromol Biosci 11, 1264–1271 (2011).

23. Bingol, H. B. et al. Stimuli-responsive poly(hydroxyethyl methacrylate) hydrogels from carboxylic acid-functionalized crosslinkers. J Biomed Mater Res A 107, 2013–2025 (2019).

24. Hsieh, S.-R. et al. Exploring the Behavior of Bovine Serum Albumin in Response to Changes in the Chemical Composition of Responsive Polymers: Experimental and Simulation Studies. Polymers (Basel) 8, 238 (2016).

25. Monteiro, P. F., Travanut, A., Conte, C. & Alexander, C. Reduction-responsive polymers for drug delivery in cancer therapy—Is there anything new to discover? Wiley Interdiscip Rev Nanomed Nanobiotechnol 13, 1–16 (2021).

26. Wei, W. et al. Synthesis and characterization of a multi-sensitive polysaccharide hydrogel for drug delivery. Carbohydr Polym 177, 275–283 (2017).

27. Peters, D. T., Waller, H., Birch, M. A. & Lakey, J. H. Engineered mosaic protein polymers; A simple route to multifunctional biomaterials. J Biol Eng 13, 1–14 (2019).

28. Caliari, S. R. & Burdick, J. A. A practical guide to hydrogels for cell culture. Nat Methods 13, 405–414 (2016).

29. Delplace, V. et al. Controlled release strategy designed for intravitreal protein delivery to the retina. Journal of Controlled Release 293, 10–20 (2019).

30. Dura, G. et al. Exploiting meltable protein hydrogels to encapsulate and culture cells in 3D. Macromol Biosci doi:10.1002/mabi.202200134.

31. Solovyova, A. S. et al. Probing the oligomeric re-assembling of bacterial fimbriae in vitro: a small-angle X-ray scattering and analytical ultracentrifugation study. European Biophysics Journal 50, 597–611 (2021).

32. Young, S., Wong, M., Tabata, Y. & Mikos, A. G. Gelatin as a delivery vehicle for the controlled release of bioactive molecules. Journal of Controlled Release 109, 256–274 (2005).

33. Lisik, A. & Musiał, W. Conductomeric evaluation of the release kinetics of active substances from pharmaceutical preparations containing iron ions. Materials 12, (2019).

34. Qiao, Z. Y., Zhang, R., Du, F. S., Liang, D. H. & Li, Z. C. Multi-responsive nanogels containing motifs of ortho ester, oligo(ethylene glycol) and disulfide linkage as carriers of hydrophobic anti-cancer drugs. Journal of Controlled Release 152, 57–66 (2011).

35. Guindani, C. et al. Covalently Binding of Bovine Serum Albumin to Unsaturated Poly(Globalide-Co-ε-Caprolactone) Nanoparticles by Thiol-Ene Reactions. Macromol Biosci 19, (2019).

36. Li, M. Z. & Elledge, S. J. Harnessing homologous recombination in vitro to generate recombinant DNA via SLIC. Nat Methods 4, 251–256 (2007).

37. Dura, G., Waller, H., Gentile, P., Lakey, J. H. & Fulton, D. A. Tuneable hydrogels of Caf1 protein fibers. Materials Science and Engineering C 93, 88–95 (2018).

3.8. Appendix B

Figure S3.1, Preparation of reversible Caf1-SS hydrogels. SDS-PAGE studied cycles of the formation of disulfide bonds in the presence and absence of reducing agents.

Cycle	1 %w/v Caf1^{Cys} (µL)	2.5 %w/v PEG-SH (µL)	8.75 %w/v H2O2 (µL)	10 mM GSH (µL)	Gelation Time	Disulfide bonds
Std	200*	-	20	-	-	Form
1	100	100	20	-	1 d	Form
2	100	100	-	20	0.5 d	Deform
3	100	100	20	-	1 d	Reform

* Standard Caf1 polymer was prepared in 0.5 %w/v to match Caf1 contain with other samples.
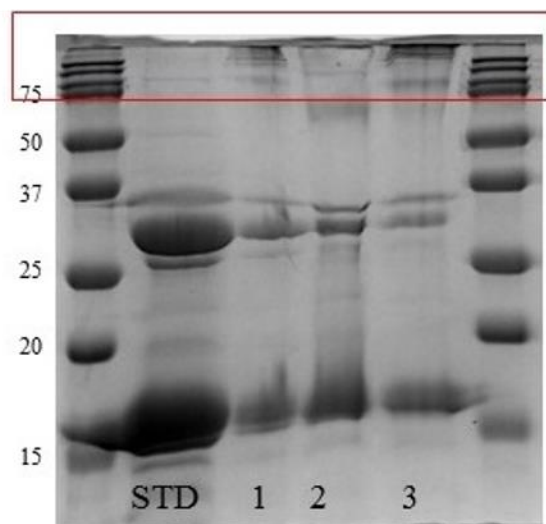
Figure S3.2, SDS-PAGE images **(a)** of a broken down Caf1^{Cys} polymer to monomers and dimers by the temperature at 100°C for 5 min. Caf1^{Cys} polymer standard (**STD**) (0.5 %w/v); Caf1-SS-PEG hydrogels as **Sample 1**; **Sample 2** contained materials of deformed Caf1-SS-PEG of **Sample 1** after disulfide cleavage by GSH; **Sample 3** is the reformation of **Sample 2** at the presence of oxidising agent H_2O. The molecular weight ladder ranges from 15 to 75+ kDa.
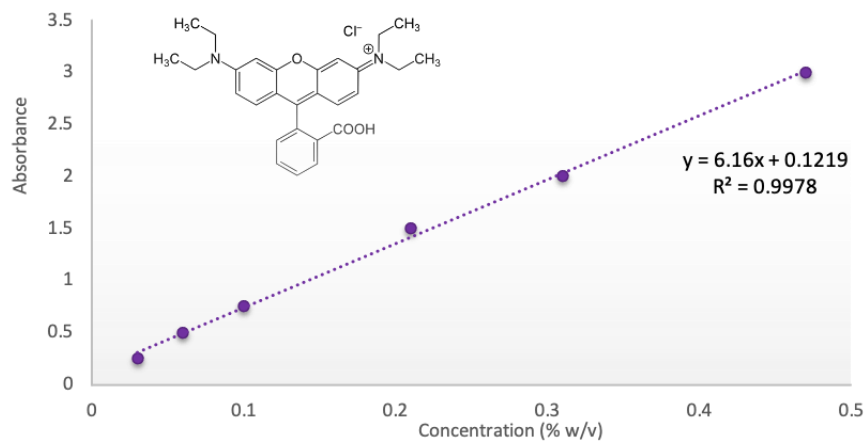
Figure S3.3, Standard absorbance curves against rhodamine-B concentration at 554 nm using UV-vis. Chemical structure of Rhodamine-B.

Chapter 4

Nanoscale Caf1 hydrogels

Table of Contents

4.1. Overview

In this chapter, synthetic approaches to produce Caf1 nanogels were explored with the intention of establishing a method that yields uniform and stable Caf1 nanogels. Caf1 nanogels were obtained via direct crosslinking with PEG-SG or glutaraldehyde by forming covalent bonds with Caf1 polymers. DLS analysis was used to determine the size of nanogels. The use of a mini-emulsion method to develop Caf1 nanogels was also attempted, which indicated possible nanogel aggregation due to Caf1-Caf1 linkage. Stable Caf1 nanogels were obtained via *refolded* Caf1 rearrangement approach where Caf1 polymer was thermally unfolded into its monomer form before crosslinking with PEG-SG to form Caf1 nanogels, the cross-linkage of Caf1 protein with PEG-SG was evidenced in SDS-PAGE.

A unique macroscopic hydrogel of Caf1 NGMG (nanogel reformed macro-gel) hydrogel was obtained by Caf1 nanogels aggregation, the characteristic of which was evaluated by rheology. Furthermore, Caf1 nanogels were decorated with FITC to form Caf1-FITC nanogels which demonstrates the potential use in cell encapsulation.

4.2. Introduction

Nanogels are an upcoming and innovative class of materials in the biomedical field because of their high drug encapsulation capacity, tuneable size, uniformity, limited toxicity, stability and potential for stimuli responsiveness.[1,2,3] Thus, they have attracted much interest in recent research in chemotherapy, diagnosis, sensing and drug delivery.[4,5] Nanogels are crosslinked polymeric hydrogel nanoparticles which share similar characteristics to macroscopic hydrogel, e.g. stimuli sensitivity, swelling capacity, customisable functionality, bioconjugation and encapsulation of bioactive substances.[1,6] Nanogels are characterised by their size from 1 up to 1000 nm.[7]

Nanogels can be prepared from a diverse range of natural polymers, synthetic polymers or a combination of both.[8] Like macroscopic hydrogels, the three-dimensional structure of nanogels are formed via chemical crosslinking with covalent bonds or physical crosslinking via non-covalent bonds (hydrogen bonds, electrostatic and/or hydrophobic interactions).[9]

In 1993, Akiyoshi and coworkers presented the findings of the first physical crosslinked nanogel composed of self-assembling cholesterol-bearing polysaccharides in water[10].

The group showcased the potential use of nanogels as nanocarriers for drug delivery. However, the term "NanoGel" was not introduced until 1999 in a publication by Vinogradov et al. [11]. Their work has captivated the interests of nanogels in pharmaceutical and biotechnological applications even to this day. The capacity to upload hydrophilic and hydrophobic drug molecules into the biocompatible and biodegradable nanogels, combined with its size factor allowing for administration via the parenteral and mucosal routes, has made nanogels a promising drug delivery tool.[12,13]

In this chapter, several approaches were investigated to fabricate uniform and stable Caf1 nanogels. Dilute aqueous solutions of Caf1[WT] polymers were crosslinked with PEG-SG or Glutaraldehyde (GA) in PBS buffer to form "minigels". A mini-emulsion approach was also studied to lower the polydispersity of nanogels' size. Another approach was explored utilising the unique refolding characteristic of the Caf1 protein. Refolded Caf1 polymers were crosslinked with PEG-SG crosslinkers to yield Caf1 nanogels, the resulting nanogels were analysed with DLS to determine the size. SDS-PAGE was used to verify Caf1-PEG cross-linking, and the nanogel size was confirmed by Atomic Force Microscopy (AFM) technique. This formulation of Caf1 nanogel was further studied to form a new type of macroscopic NGMG Caf1 hydrogel with a distinctive characteristic compared to *native* Caf1 hydrogel, that the NGMG Caf1 hydrogel is made up of a complexation of multiple Caf1 nanogels linked together via Caf1-Caf1 linkage.

Furthermore, fluorescein (FITC) was also conjugated onto Caf1 polymer, the modified Caf1 polymers were crosslinked with Caf1-PEG to obtain Caf1-FITC nanogels which then can be used for cell encapsulation.

4.3. Results and Discussion

Caf1 polymers display potential in drug delivery applications because of their ease of production, tunability and tailored stimuli-responsiveness. Research has provided the groundwork needed to produce macroscopic Caf1 hydrogels for drug delivery, with a goal now to develop Caf1 nanogels. Caf1 nanogels may have the potential for drug delivery applications as they could open doors to other drug administrative routes, such as oral, pulmonary uptake and injection.

This chapter will explore different methods to produce Caf1 nanogels **(Figure 4.1)**. Nanogels (Nanospheres) are nanoscale spherical hydrogels composed of a matrix system which has the potential to entrap, attach, or encapsulate cargo. The sphere's surface can be decorated with ligands or antibodies for targeting purposes.
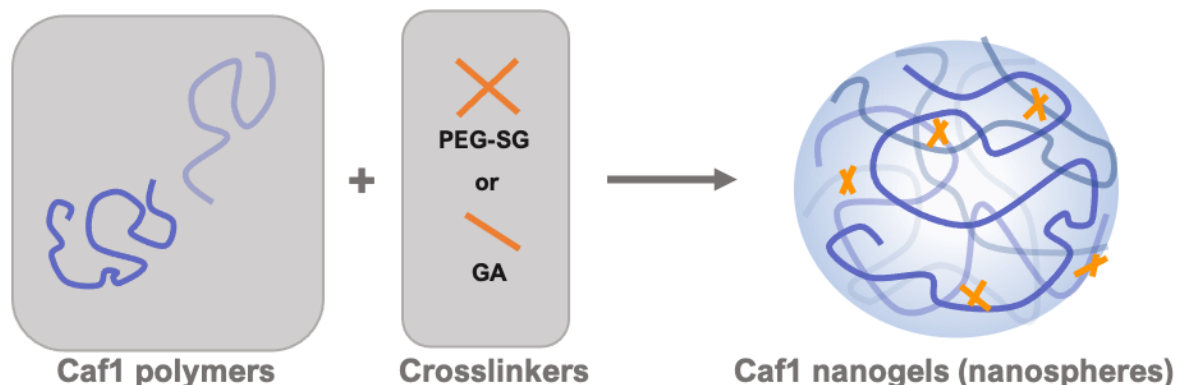
Figure 4.1, Schematic illustration of Caf1 nanogels formation by cross-linkage of a continuous Caf1 polymer chain or multiple Caf1 polymer chains with PEG-SG or GA crosslinkers.

4.3.1. Direct crosslinking approach

Previous work demonstrated that Caf1 hydrogels could be obtained by crosslinking the Caf1 protein polymers with PEG-SG in aqueous solutions. Nanogels are a scaled-down version of macroscopic hydrogels; therefore, it is possible to prepare nanogels simply by encouraging hydrogel formation at high dilution. The construction of nanogels is governed by thermodynamic and/or kinetic reactions or in combination, that leads to different final products or a mixture of product species. The distinction (Figure 4.2) between the two is that product A forms faster than product B due to the lower activation energy E_a, when compared to product A, that is thermodynamically more stable compared to product B. The reaction pathways are determined by energy input to the system, such as temperature, pressure, solvent or concentration. Hypothetically, a decrease in Caf1 and crosslinker concentration/ high dilution should drive the formation of nanogel species. However, these kinetic products may not be stable when concentrated. Likewise, the thermodynamically more favoured process will increase when the concentration is increased. Additionally, vacant Caf1's acceptor at the terminus of one Caf1 chain may be complex with the donor strand on another Caf1 chain, meaning the kinetic product can further react to form a thermodynamically

favourable product over time. Hence, the desired stable thermodynamic favoured nanogel formulation should be monodispersed with a low polydispersity index (PdI) and unchanged over time. Whereas kinetic products should obtain the characteristic of polydisperse and unstable particle size over time.[14]
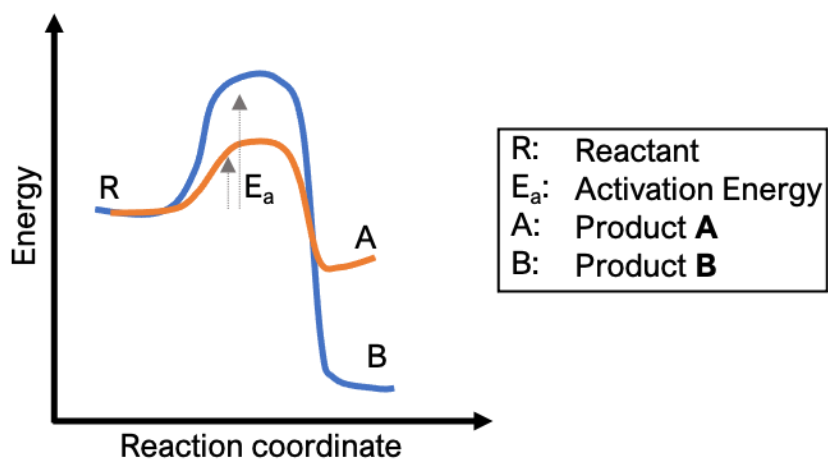
Figure 4.2, Illustration of energy vs reaction coordinate for reactant R. The difference in activation energy (E_a) can result in the formation of a kinetic product (**A**) or thermodynamic product (**B**).

Two preliminary conditions were investigated to produce Caf1 nanogels via a direct crosslinking approach, which includes altering reactant concentrations and differences in rotation speed. The results from these experiments provided some initial reaction conditions to produce stable and uniform nanogels.
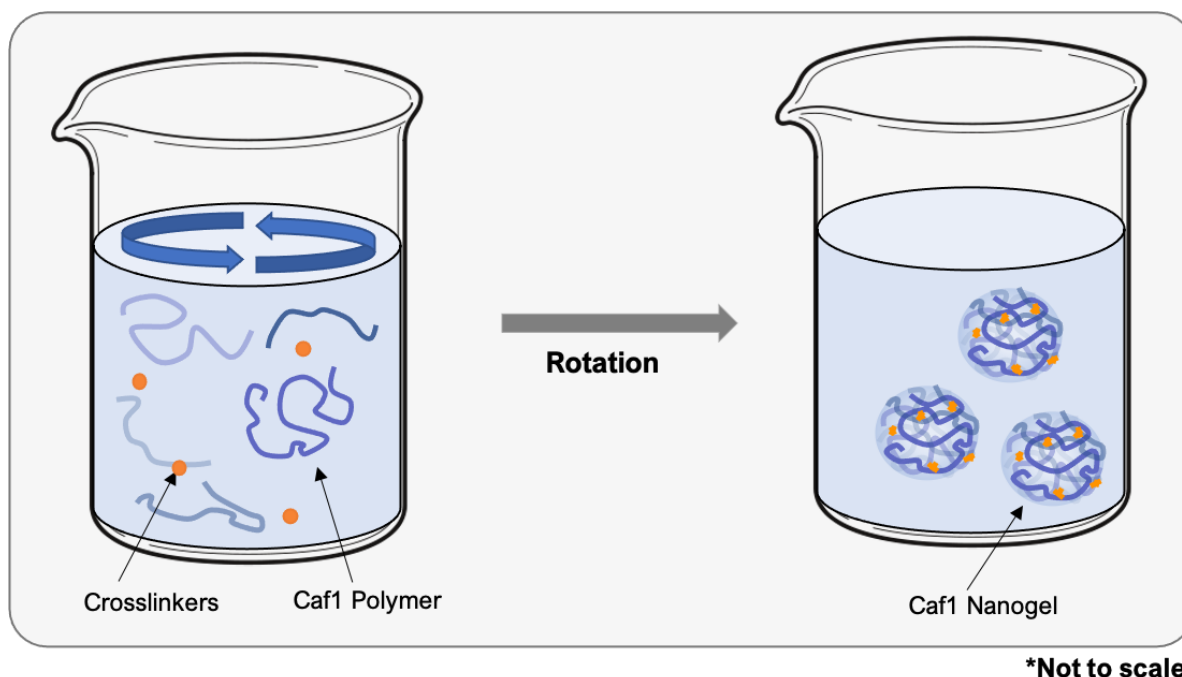
Figure 4.3, Caf1 nanogels reaction scheme via direct crosslinking approach. Caf1 polymer was crosslinked with PEG-SG crosslinkers to form Caf1 nanogels in diluted concentration. The agitation rotation speed was set at 200 and 500 rpm.

Caf1 nanogels **(Figure 4.3)** were prepared by mixing Caf1 polymers (15 kDa) (0.1, 0.2 %w/v) in 1 mL of PBS and 1 mL of 4-Arm PEG-SG (20 kDa) (0.1, 0.2 %w/v) in 0.05 M bicarbonate solution. The experiments were conducted at two different agitation speeds of 200 or 500 rpm at 25 °C. To determine the nanogel size, the resultant products (2 h and 24 h) were analysed with Dynamic light scattering (DLS). As reported in Table 1, **Sample 1 (Table 4.1)** shows little change in size between 2 h and 24 h. **Sample 2 (Table 4.1),** with high reactant concentration and high rotation speed yielded nanogels of 92 nm (0.404 PdI) at 2 h and 235 nm (0.388 PdI) at 24 h. **Sample 3 (Table 4.1)** which features lower reactant concentrations and lower rotation speed formed a product with 123 nm (0.345 PdI) in size at 2 h and 144 nm (0.478 PdI) at 24 h. Interestingly, **sample 3** is slightly larger in size when compared with **sample 1**, which featured a higher reactant concentration. **Sample 4 (Table 4.1)** yielded nanogels with 88 nm (0.463 PdI) at 2 h and 100 nm (0.548 PdI) at 24 h, the smallest nanogel compared with the other samples.

As a control experiment, the particle sizes of *native* Caf1 polymers were measured at different concentrations (0.001, 0.025, 0.05, 0.1 %w/v) and were also analysed by DLS

(**Figure S4.1**). Caf1 polymers have a hydrodynamics diameter of approximately 100 nm. All the measurements showed a broad histogram which indicates Caf1^{WT} polymers varies in polymer chain lengths. Interestingly, the results also suggest that nanogels formed using the direct crosslinking approach are similar in size to one Caf1 polymer chain.

Table 4.1, Samples of Caf1 nanogels formation via direct crosslinking approach, DLS measurement at 2 h and 24 h derived from **Figure S4.2** and **S4.3**.

Samples	Caf1 (%w/v)	PEG-SG (%w/v)	Rotation speed (rpm)	2 h Z-Ave (nm)	Pdl	24 h Z-Ave (nm)	Pdl
1	0.2	0.2	200	96	0.458	106	0.424
2	0.2	0.2	500	92	0.404	235	0.388
3	0.1	0.1	200	123	0.345	144	0.478
4	0.1	0.1	500	88	0.463	100	0.548

Mw: Caf1 polymer (15 kDa); 4 Arm PEG-SG (20 kDa)

The results in **Table 4.1** show that the most stable nanogels formed via the direct crosslinking approach is a low reactant concentration combined with lower rotation speed, and thus, rotation speed will be set at 200 rpm using this approach going forward.
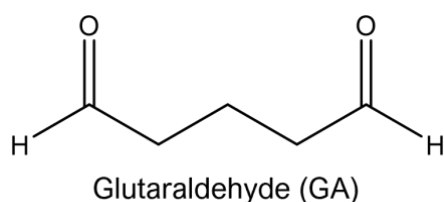
Glutaraldehyde (GA)

Figure 4.4, the chemical structure of glutaraldehyde.

To further explore the formation of Caf1 nanogels using the direct crosslinking approach, the crosslinker glutaraldehyde **(Figure 4.4)** was also investigated in this study. It was anticipated that the shorter crosslinker chain - glutaraldehyde might increase intramolecular Caf1 polymer cross-linking, that leads to the formation of Caf1 nanogels. Several formulations of Caf1: crosslinkers in different ratios were also explored to investigate the best reactant composition for Caf1 nanogels formation. Crosslinker PEG-SG was used initially, as previously shown in Chapter 2 shown the

crosslinking between Caf1 polymer and PEG-SG can be easily obtained by the formation of amide bonds, as well as, PEG-SG will act as a backbone for the Caf1 polymers and lead to a formation Caf1 nanogels.

The samples **(Table 4.2)** were prepared by reacting Caf1 polymers (0.1 %w/v) (1mL) with crosslinkers (0.1, 5 or 10 %w/v) (1 mL) (4-Arm PEG-SG or glutaraldehyde) with mild swirling (200 rpm). DLS analysed the resultant products at pre-determined time intervals (2, 72, 96, 120, 168, 192, 216, 240, 264, 288 h). **Figure 4.5, A1,** formulation of Caf1:PEG-SG (1:1) obtained a mixture of nano- and mini-scaled hydrogels as DLS measured polydisperse hydrogels in various shapes and sizes. **Figure 4.5, A2,** formulation of Caf1:PEG-SG (1:50) also resulted in the formation of a polydisperse product. **A1 (Figure 4.5, A1)** was the better formulation for producing a uniform nanogel, in which it recorded PdI of 0.373 and 0.337 (240 and 264 h). The polydispersity index (PdI) below 0.5 is widely accepted as a narrow-monodispersed model, and therefore PdI reading above 0.5 is considered polydisperse. **Figure 4.5, B1,** a formulation containing glutaraldehyde (1:1) yield a product of approximate size of 90 nm and PdI ranging from 0.262 to 0.512 during the 288 h period. **Figure 4.5, B2,** formulation of Caf1: glutaraldehyde (1:100) showed a nanogel species around 90 nm and a reasonable PdI (0.269 – 0.507). The results show that larger species are formed when reacted with 4-Arm PEG-SG, ranging from a diameter of approximately 90 to 120 nm (**Figure 4.5, A1 & A2**), compared to nanogels created from glutaraldehyde with a size of approximately 90 nm (**Figure 4.5, B1 & B2**). This is likely because 4-Arm PEG-SG is a larger molecule compared with glutaraldehyde. Importantly, this finding indicated that shorter cross-linkers lead to the formation of stable uniform Caf1 nanogels.

Table 4.2, Formulation of Caf1 nanogels formed via direct crosslinking approach by crosslink Caf1 polymer with PEG-SG or GA crosslinkers, and its relative size on 288 h.

Samples	Caf1 (%w/v)	PEG-SG (%w/v)	GA (%w/v)	Z-Ave (nm)	PdI
A1	0.1	0.1	-	176.6	0.509
A2	0.1	5	-	128.5	0.577
B1	0.1	-	0.1	84.73	0.262
B2	0.1	-	10	137.5	0.411

Mw: Caf1 polymer (15 kDa); 4 Arm PEG-SG (20 kDa); GA (100.11 Da)
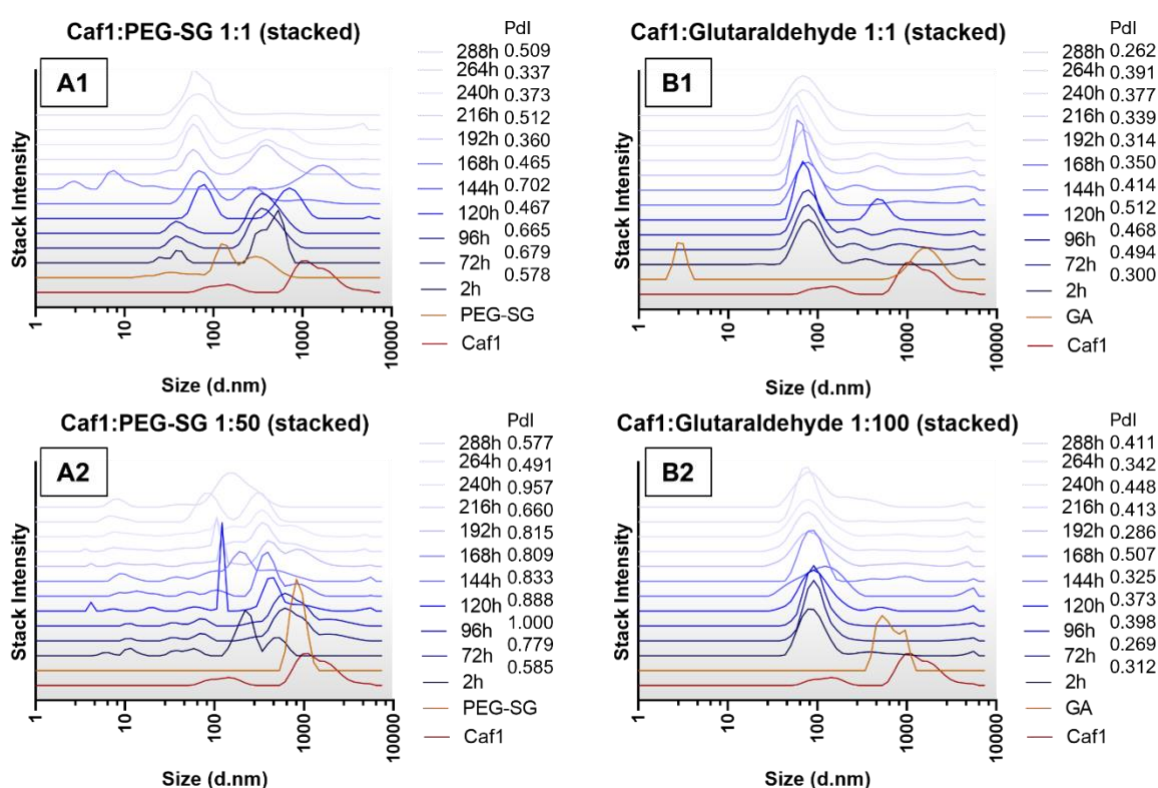
Figure 4.5, DLS measurements of Caf1 nano- and mini-gels at set time intervals (2, 72, 96, 120, 144, 168, 192, 216, 240, 264, 288 h) at 5°C. The plots of stack intensity against size (d. nm) in a range of different reactant compositions of Caf1:PEG-SG (1:1, 1:50) **(a1 and a2)** and Caf1:glutaraldehyde (1:1, 1:100) **(b1 and b2)**.

4.3.2. Mini-emulsion approach

Despite the promising results of using the direct crosslinking approach, the irregular polydispersity index (PdI) suggests more than one species (size) of Caf1 nano/mini-gels. Thus, the use of a mini-emulsion approach was considered.
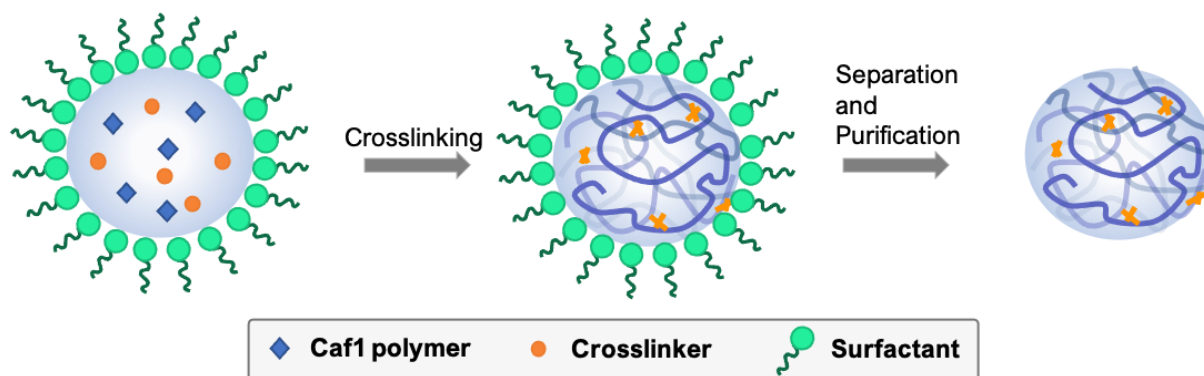
Figure 4.6, Schematic illustration of Caf1 nanogels formation via mini-emulsion approach. The reaction occurred within the micelles where Caf1 polymer and crosslinker were encapsulated.

Mini-emulsions are commonly used in polymerisation chemistry[15,16], where the technique speeds up reaction time and limits product size. Mini-emulsion is obtained by shearing a mixture of two immiscible liquid phases (organic and aqueous) with one or more surfactants to form micelles (Figure 4.6). The crosslinking chemistry took place within the micelles, which because of its limited volume, the reaction time reduces and yields a product with a size to that of the micelle.[17]

Surfactants Tween 80 and Span 80 were added to hexane (4 mL) to encourage micelle formation,[18] and the Caf1 polymer was dissolved in PBS. The two immiscible solutions were mixed by ultrasonication for 5 min before adding the crosslinker (4Arm PEG-SG) to the mixture. The solution further undergoes ultrasonication for 2 x 5 min, then stirred for 24 h at 350 rpm before centrifugation (7000 rpm, 1 min), and washed with water. The pellet obtained was later resuspended in PBS and analysed with DLS.

Table 4.3, Samples of Caf1 nanogels via mini-emulsion approach, DLS measurement at 2 h and 24 h derived from Figure S4.2 and S4.3.

			2 h		24 h	
Samples	Caf1 (%w/v)	PEG-SG (%w/v)	Z-Ave (nm)	PdI	Z-Ave (nm)	PdI
1	0.2	0.2	7846	1.000	3917	1.000
2	0.1	0.1	14790	1.000	12300	1.000

Mw: Caf1 polymer (15 kDa); 4 Arm PEG-SG (20 kDa)

Two samples with different reactant concentrations were prepared. **Sample 1 (Table 4.3)** with high reactant concentration yielded the Caf1 mini-gel of 7846 nm (1.000 PdI) at 2 h and 3917 nm (1.000 PdI) at 24 h. The combination of Z-average and PdI pointed to the formation of a very polydisperse hydrogel materials, evidenced by the results obtained from **Sample 2 (Table 4.3)**. The diluted formulation of **Sample 2 (Table 4.3)** shown crosslinked Caf1 material obtained with a size of 14790 nm at 2 h and 12300 at 24 h. Similarly, both results from **Samples 1 & 2 (Table 4.3)** show a reduction in Z-average after 24 h, which can be the results caused by the free NHS- group that is allowed to react with lysine residues from a Caf1 of another nanogel, resulting in crosslinking to form Caf1 mini-gels. The result indicated the need of an improved purification method where nanogel will remain separated during the purification step and does not result in undesirable aggregation. In conclusion, the results using the mini-emulsion approach did not yield a monodispersed nanogel. This is primarily due to nano-/mini-gel aggregation which forms a macroscopic hydrogel, the aspect of forming macroscopic hydrogels from nanogel will be further explored within this chapter.

4.3.3. Refolded Caf1 rearrangement approach

Caf1 polymers are made up of monomeric sub-units of Caf1 protein which are polymerised through a process called donor strand exchange,[19] where the Caf1 subunit donates its β-strand to the adjacent Caf1 subunit to complete the immunoglobulin-like fold of the next subunit in the chain. As discussed in previous chapters, the Caf1 polymer possesses the ability to refold after complete thermal unfolding, a feature that allows the Caf1 polymer to switch between its polymeric and monomeric forms. The ability to undergo reversible thermal refolding even when crosslinked allows Caf1 hydrogels to rearrange their networks.
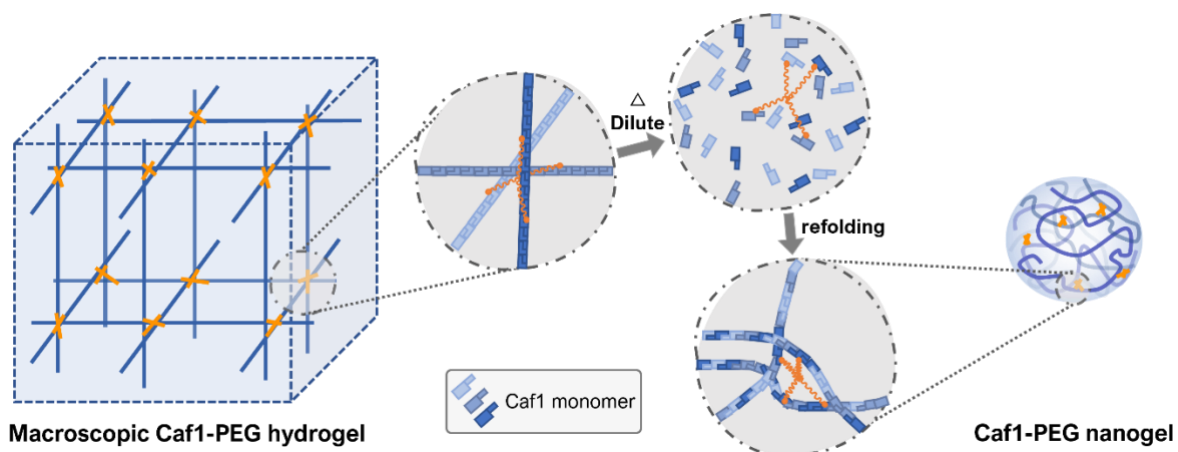
Figure 4.7, Schematic illustration of Caf1-PEG nanogel formation by rearranging a macroscopic Caf1-PEG hydrogel network. Macroscopic Caf1-PEG hydrogel was obtained by crosslinking Caf1 polymer with 4-Arm PEG-SG, the material was later melted, diluted, and allowed to refold.

The *refolded* Caf1 rearrangement approach uses the unique property of Caf1 to form new Caf1 nanogels by transforming from its macroscopic state into a nanogel state **(Figure 4.7)**. Two samples were prepared to test this hypothesis. Caf1 polymers (1 or 2 %w/v) were crosslinked with 4-arm PEG-SG at 1:1 to form Caf1-PEG macroscopic hydrogels. The hydrogels were then melted at 100 °C for 5 min until the Caf1 protein had completely unfolded and a solution was obtained. Learning from the results observed from the direct crosslinking approach, the solution of melted material was diluted with buffer by a factor of 10, reducing the overall concentration of Caf1. The solution was allowed to react slowly at room temperature overnight under mild swirling at 200 rpm. DLS analysed the resultant products to determine nanogel size and Pdl **(Figure 4.8)**. The Pdl of the nanogels formed from 1% Caf1 hydrogel **(Figure 4.8a)** shows a polydisperse species with a value of 0.415 at 216 h. The broad peak highlights this conclusion. Nanogels formed from 2 %w/v Caf1 hydrogels **(Figure 4.8b)** showed a sharp narrow peak at 110 nm at 216 h with a Pdl of 0.249. The results show a monodisperse Caf1 nanogels species formed using 2 % Caf1 hydrogels suggesting the product is thermodynamically stable, as the peak remained unchanged from 72 h to 216 h, meaning the reaction came to completion after 72 h and no further aggregation processes to the nanogels occurred.

Melted Caf1 polymers (Figure S4.4) were studied with DLS as a control experiment. Two peaks were observed for all three (*melt* Caf1 after 4 d, low and high shear rotation speed) of the sample's concentration with sizes approximately 15 nm to 110+ nm. The

result compared to the original long chained Caf1 polymer **(Figure S4.1)** is shown to be significant, as the peak of 15 nm likely pointed to Caf1 monomers given the size recorded **(Figure S4.1)** and the larger species 110+ nm is the *refolded* Caf1 material. The results **(Figure 4.8)** observed from the samples using the *refolded* Caf1 rearrangement approach supported this finding, as the smaller peak disappeared over time and only one peak at 110+ nm was displayed.
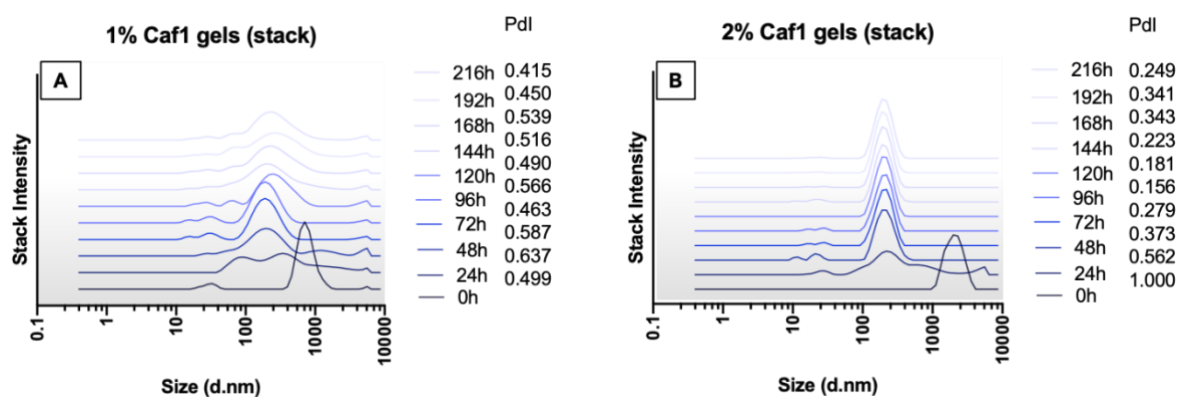
Figure 4.8, DLS measurement of Caf1 nanogels at set time intervals (24, 48, 72, 96, 120, 144, 168, 192, 216 h) at 5°C. The plots of stack intensity against size (d. nm), and the associated PdI values were determined. Caf1 nanogels formed from 1% (w/v) Caf1 hydrogel (a) and 2% (w/v) Caf1 hydrogel (b).

SDS-PAGE **(Figure 4.9)** was also used to demonstrate that Caf1-PEG cross-linkages within the Caf1 nanogel remain intact after rearrangement. SDS-PAGE separated the components of the Caf1 nanogels into a ladder of different molecular weights. In the sample of Caf1 polymer only one band was observed at ~15 kDa, which is associated with the Caf1 monomer. Multiple bands at the molecular weight of 75+ kDa were observed in the sample containing only Caf1 nanogels due to crosslinked Caf1 subunits complex where two or more Caf1 subunits are linked together. The bands observed above 75 kDa likely correspond to multiple Caf1 monomers linked by PEG crosslinkers.
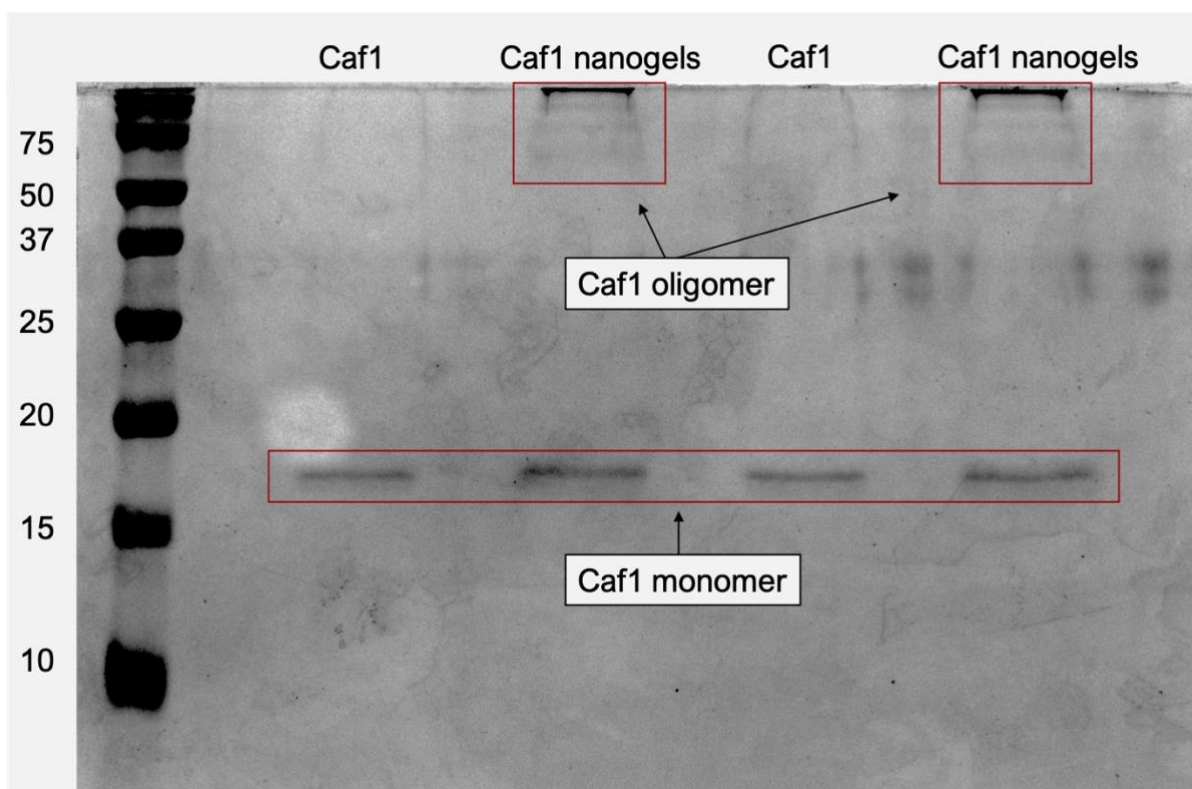
Figure 4.9, Image of SDS-PAGE of broken-down Caf1 monomer and Caf1 oligomer from Caf1 polymer and Caf1 nanogels.

Atomic Force Microscopy (AFM) was used in an attempt to visualise Caf1 nanogels, a mechanical probe will tap the surface of the material surface which will translate into reading via the piezoelectric elements and thus into precise scanning images.[20] The sample was prepared by overnight drying aqueous nanogels droplets in 1 %w/v of concentration on a silicon wafer. A cantilever then scanned the sample, and the results were transformed into an AFM image **(Figure 4.10)**. The image **(Figure 4.10)** shows that there are small individual dispensed Caf1 nanogels with an average diameter of 143 nm near the size recorded by DLS.

It is noted that the experimental protocol is to dry the nanogels on the silicon wafer. The size determined from this experiment can only be used as a guide due to nanogel flattening as the nanogel structure collapses. A Liquid Cell should be adopted to reduce this limitation. Alternatively, transmission electron microscopy (TEM) could possibly be used.

Sample	Diameter (nm)
1	150
2	141
3	182
4	148
5	125
6	130
7	132
8	138
Ave	**143**
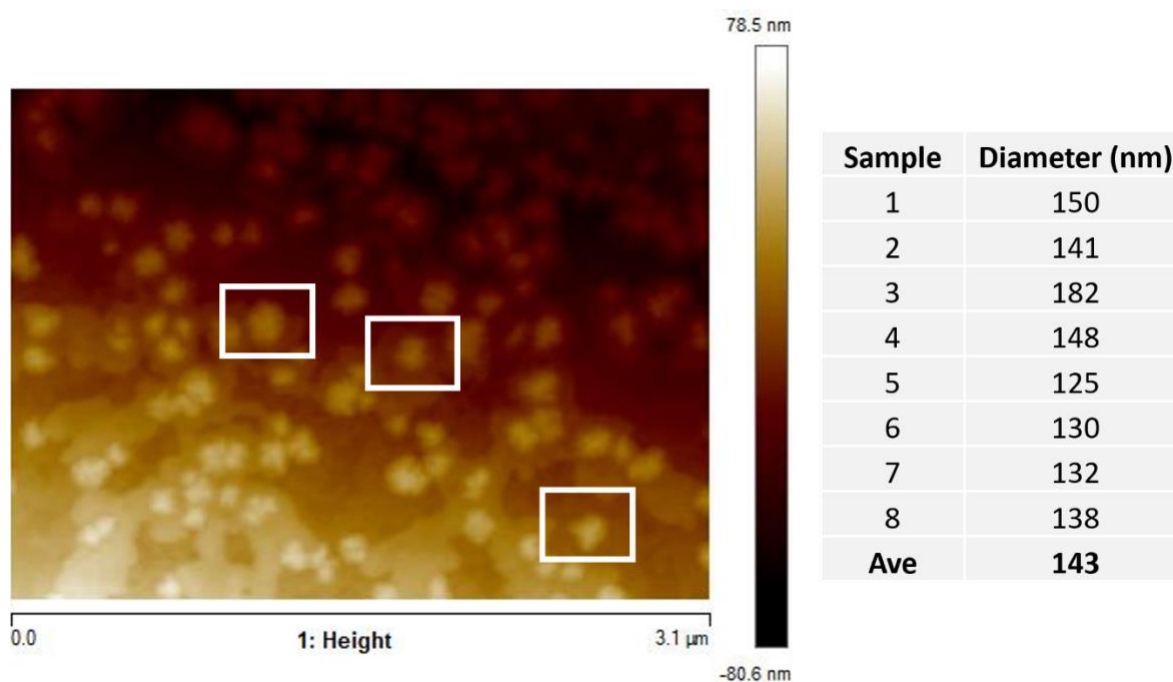
Figure 4.10, AFM Image of nanogel at the edge of the droplet which resulted in a height gradient. Caf1 nanogels can be seen as highlighted in boxes, and some of the diameters were measured with the size average recorded at 143 nm.

4.3.4. Novel Caf1 NGMG (nanogel reformed macro-gel) hydrogel

The macroscopic hydrogels formed via the mini-emulsion approach suggested that Caf1 nanogels may be able to link together provided vacated Caf1 donor strand is allowed to interact with another vacated Caf1 acceptor terminus. It was postulated that a new type of macroscopic Caf1 NGMG (nanogel reformed macro-gel) **(Figure 4.11)** could be formed by linkage occurring between free Caf1 polymer on the surface of the nanogel reacted with another free Caf1 polymer from another nanogel. The idea that Caf1 nanogels can crosslink together to form macroscopic Caf1 NGMG hydrogel is explored in this session.
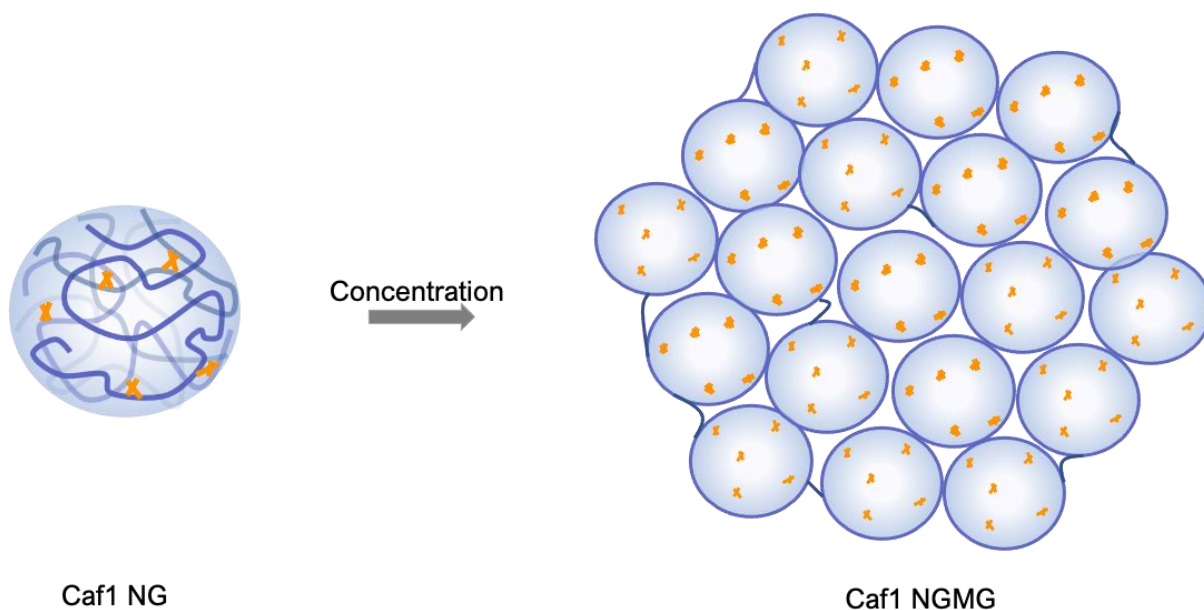
Figure 4.11, Schematic representation of Caf1 NGMG (nanogel reformed macro-gel) hydrogel formation by concentrating Caf1 NG (nanogel).

Caf1 nanogels (NG) were freeze-dried to remove the water inside and outside the hydrogel network while maintaining the matrix intact. The freeze-dried materials **(Figure 4.12a)** were rehydrated at a volume of 200 μL to reform hydrogel **(Figure 4.12b)**. The macroscopic Caf1 NGMG hydrogel was obtained after approximately 24 h, the hydrogel was then analysed with rheology to gain better insight into its mechanical properties. As a control, a 1 % *Native (Nat)* Caf1 hydrogel was selected by reacting Caf1 polymer (1%) with 4-Arm PEG-SG (1%). The storage modulus (G') **(Figure 4.12c)** recorded from this gel was 4.6 Pa, and a loss modulus (G'') of 0.15 Pa. Caf1 NGMG hydrogel **(Figure 4.12c)** registered a G' of 7.49 Pa and a G'' of average 1.95 Pa. As a control, the 1 % *melt* Caf1 hydrogel **(Figure 4.12c)** recorded a G' of 1.12 Pa and a G'' of an average of 0.06 Pa. In conjunction with the results recorded from the angular frequency experiments **(Figure 4.12d)** Caf1 NGMG matrix is entirely different from the 1 % *melt* Caf1 hydrogel in terms of mechanical properties, in comparison it is closer to 1 % *Native (Nat)* Caf1 hydrogel than 1 % *melt* Caf1 hydrogel. Moreover, the storage modulus and loss modulus of the Caf1 NGMG **(Figure 4.12c)** are relatively close when compared to 1 % *Native (Nat)* Caf1 hydrogel **(Figure 4.12c)**, this is likely the result of the difference in the hydrogel structure which made up the network of cross-linked nanogels.
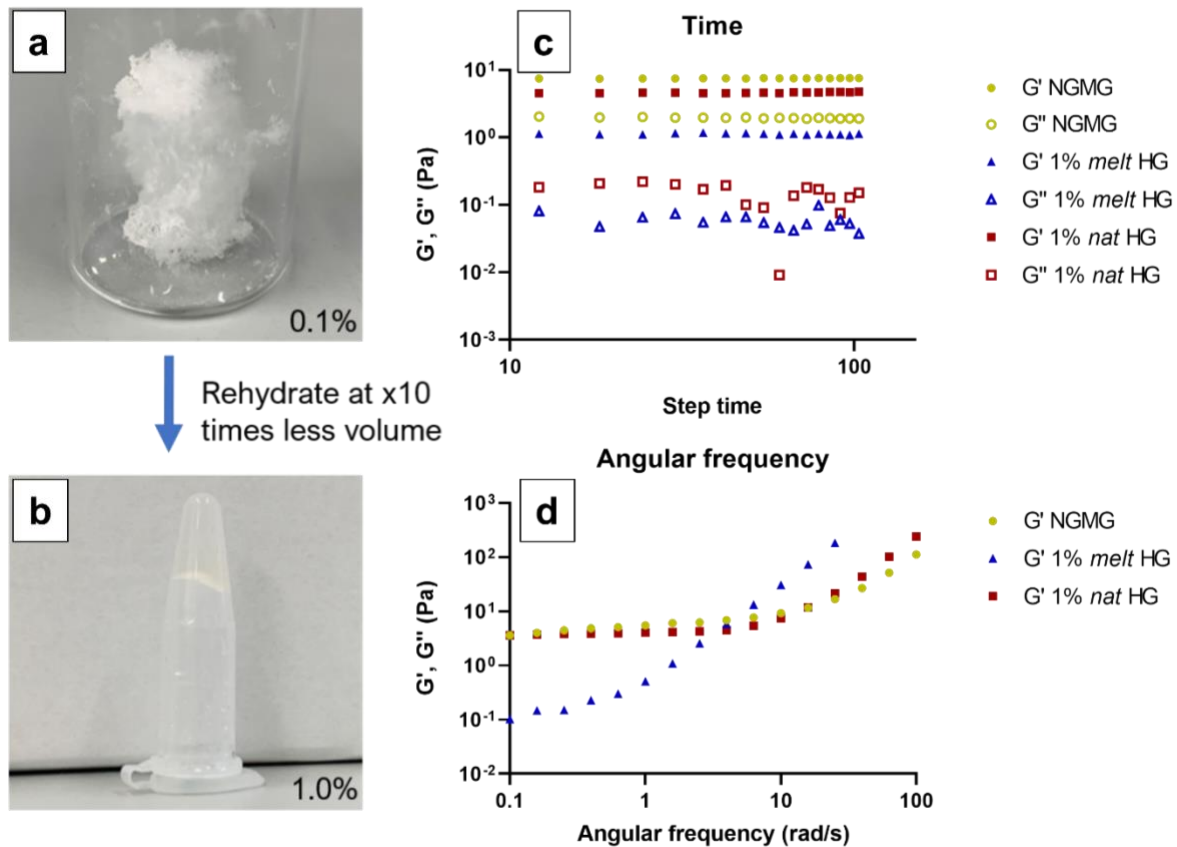
Figure 4.12, Image A **(a)** taken of freeze-dried Caf1 nanogels, image B **(b)** new macro-gel formed after 24h of rehydration at 1 % (w/v) Caf1 NGMG. **(c)** Rheology time sweep and **(d)** angular frequency experiments of 1 % (w/v) Caf1 NGMG hydrogel in **yellow**, 1 % (w/v) *melt* HG hydrogel in **blue** and 1 % (w/v) *nat* Caf1 hydrogel in **red**.

Macroscopic Caf1 hydrogels are formed by Caf1 polymer crosslinking with PEG-SG to give rise to an extensively cross-linked macroscopic network, Caf1 NGMG hydrogel is likely created by multiple Caf1 nanogels linked together via Caf1-Caf1 linkage and perhaps some degree of non-covalent bonding, e.g., mechanical interlocking of polymer chains. This phenomenon can be described as "double network gels" which are hydrogels composed of two types of networks (crosslinked and interconnected networks).[21] This property of Caf1 nanogels transforms the material from nanoscale into a macroscopic material which could be useful in cell work applications as a culture medium or as a method to encapsulate cells within the hydrogel materials. Also, this work suggests that the C-terminal subunit of a Caf1 chain is always assembly competent, forming a complex with a donor strand.

4.3.5. The aggregation of fluorescently labelled Caf1 nanogels

This work will briefly explore a potential application for Caf1 nanogels. The unique ability to transform Caf1 nanogel into Caf1 NGMG hydrogel via concentration-induced self-assembly can be used for cell encapsulation.[22,23] Introducing the RGDS motif into the Caf1 polymer endows it with a cell adhesion property similar to fibronectin[24]. This feature can provide a mechanism for Caf1[RGDS] nanogels to bind to the surfaces of cells. As the nanogels deposit onto the cell's surface, the Caf1 subunit may crosslink with the adjacent vacant Caf1 subunit to form a film of Caf1 NGMG around the cell and essentially encapsulates the cell **(Figure 4.13).**
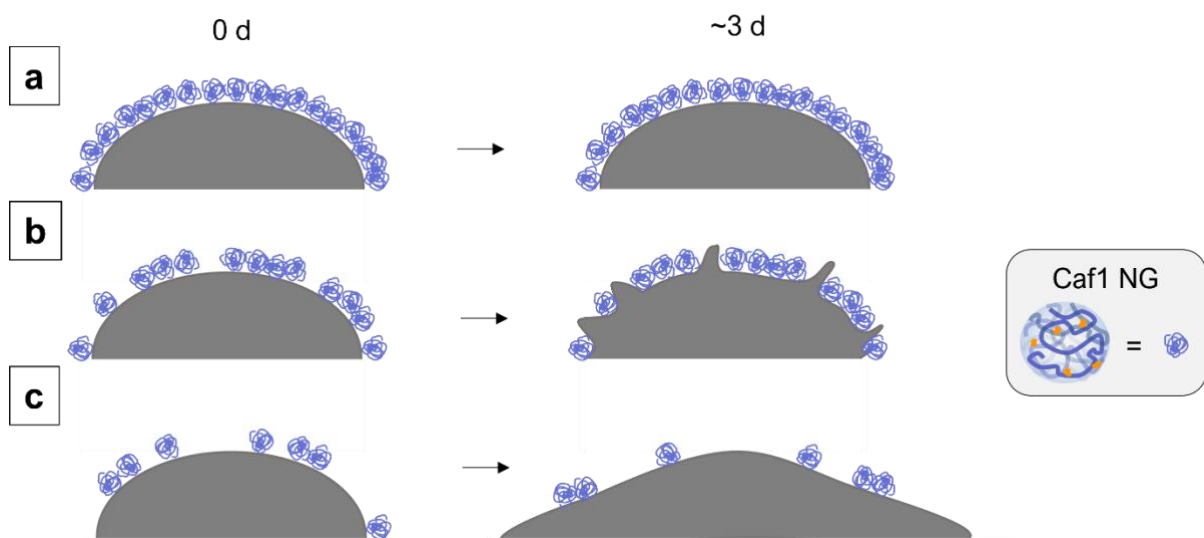
Figure 4.13, Schematic diagram of cell encapsulation with Caf1-RGDS nanogels, represents the cells in **grey** and the Caf1 nanogels in **blue**. It is speculated that the shape of a cell fully covered in nanogels **(a)** would likely remain unchanged over time. In contrast, the partially covered cell **(b)** will possess growth due to insufficient hydrogel coverage which results in cell leakage. Lastly, a poorly covered cell **(c)** will not restrain cell growth over time, that results in total leakage.

Fluorescein isothiocyanate (FITC) was used to attach a fluorescent group to Caf1 via reaction with an amine group on the subunit to yield a Caf1[FITC] polymer. Caf1[FITC] nanogels were prepared using the *refolding* rearrangement approach. The nanogels were then observed with a fluorescence microscope over 3 d **(Figure 4.14),** the fluorescence images show that small objects of individual nanogels can be seen at day 0 **(Figure 4.14a)** and the fluorescence objects grow in size over a period of three days 0 **(Figure 4.14b, c & d)**. This shows that the cross-linkage between Caf1 nanogels occurred as it aggregates and links with the adjacent nanogel to form a microscopic

Caf1 NGMG hydrogel. The success of this can be used in conjunction with Caf1[RGDS] protein to provide cell adhesiveness to the Caf1[FITC] nanogels. Success will obtain both characteristics of cell adhesive property and fluorescence sensitivity that can be used for cell encapsulation. Cell encapsulation is a strategy to isolate cells such as allogeneic and xenogeneic cells from the host immune response[24] and protect the cell.
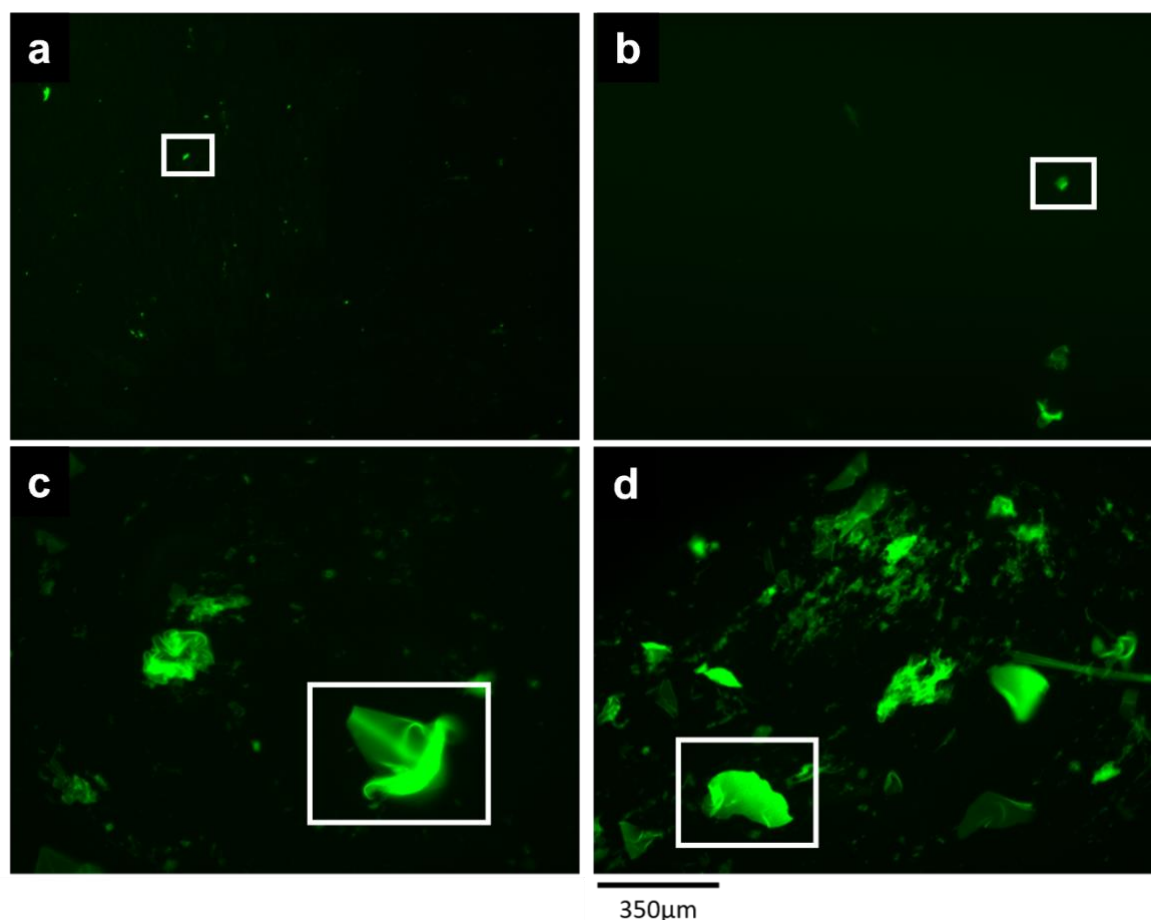
Figure 4.14, Fluorescence image of Caf1FITC nanogels over time. (a) 0 d; (b) 1 d; (c) 2 d; (d) 3 d.

4.4. Conclusion

Different approaches were explored to produce Caf1 nanogels. Caf1 nanogels were obtained using the direct crosslinking approach, in which the components made up of Caf1 hydrogels were allowed to interact at high dilution to form nano-sized hydrogel species, the size of the nanogels was analysed with DLS. The results indicated that the most stable nanogels were created when a combination of low reactant content and low energy input (rotation speed) were used. Further investigations were conducted

to determine the conditions required to form uniform nanogels using a smaller crosslinker (glutaraldehyde). Caf1 nanogels obtained from crosslinking with a small crosslinker (GA) yield a monodisperse sample of nanogels with a low PdI, whereas the nanogels formed from the reaction of Caf1 polymer chain with a large crosslinker (4-Arm PEG-SG) yield a polydisperse sample of nano-/mini-gels. A mini-emulsion approach was also studied. The concept of this approach was to force uniform nanogel formation in a limited space within a micelle, however, this method was unsuccessful in macroscopic hydrogels being formed.

Another approach was explored by utilising the reversible unfolding of the Caf1 protein. Caf1 nanogels were obtained via the *refolded* Caf1 rearrangement approach where Caf1 polymer was first crosslinked with a crosslinker to form a macro hydrogel, the Caf1-Caf1 linkages were then cleared in thermal unfolding before being allowed to refold in a diluted environment to form Caf1-PEG nanogels. The result of the 2% Caf1 hydrogels formulation showed that the sample is monodisperse and stable even after 216 h, maintaining a low PdI of 0.249. The retention of the Caf1 and PEG-SG cross-links was supported by results from SDS-PAGE, where bands of Caf1-PEG oligomers were observed at >75 kDa. An AFM image was taken of this sample, and individual nanogels can be seen. This idea was further explored to form Caf1 NGMG (nanogel reformed macro-gel) hydrogels which are formed nanogels cross-linked by Caf1-Caf1 interaction. Rheological data shows that the matrix system made up of this new Caf1 NGMG hydrogel is different from *native* Caf1 hydrogel, where the mechanical properties have improved.

The ability of macroscopic hydrogel (marcogel) formation from nanogels was considered a potential use in cell encapsulation work Caf1[RGDS] polymers may drive the concentration of Caf1 nanogels upon the surfaces of cells. Their crosslinking would then lead to cell encapsulation.

4.5. Future Work

This work has demonstrated a successful method to produce Caf1 nanogel, it is anticipated that Caf1 nanogel can be used for drug delivery. The measurement of drug release will be an experimental challenge as it has a greater surface than its relative size, which may lead to rapid drug release. One way to reduce this is to conjugate the drug molecule of interest with the Caf1 polymer network by introducing a modified Caf1 subunit into the system, as shown in Chapter 3. Alternatively, a coating could be applied to the nanogel to retain drug release.[25,26]

4.6. Experimental

General Experimental

4-arm Succinimidyl glutarate PEG (4-arm PEG-SG) (20 kDa) was purchased from Creative PEGWorks. Sodium bicarbonate solution (0.05 M, pH 8.2) was prepared by dissolving 4.2 g of sodium bicarbonate (Acros) in 1L of deionised water. The pH of the solution was adjusted to 8.2 with 1M HCl. Phosphate buffered saline (PBS) is made up of 100 mM sodium hypophosphite, 100 mM monosodium dihydrogen orthophosphate, 137 mM sodium chloride, and 27 mM potassium chloride (Sigma-Aldrich), dissolved in 100 mL of deionised water. The pH was adjusted to 7.4 with 1M HCl.

Instrumentation

DLS measurements were performed on a Malvern Instruments Nano ZS. Rheological measurements were performed using a Discovery HR-2 rheometer (TA Instruments, USA) with a parallel plate of 20 mm diameter and a gap of 1500 μm at 25 °C. AFM measurements were performed using a multimode 8-atomic force microscope with a Nanoscope V controller and an "E" scanner (Bruker, Germany). Fluorescence microscopy images were obtained using Zeiss Axiskop 2 Plus. The pH measurements were made using a Hanna HI 90103 instrument calibrated using commercial buffer solutions (Sigma-Aldrich).

Preparation of Caf1 protein

pGEM-T Caf1 plasmid was transformed into BL21 (DE3) competent E. coli cells. Terrific broth (TB) (500 mL) containing 100 µg mL^{-1} ampicillin in 2 L shake flasks was inoculated with single colonies and grown at 35 °C for 21 h, shaking at 180 rpm. The

cell pellet was removed by centrifugation at 3000 rpm, 22 °C, 30 min (JA10 rotor, Beckman Coulter) followed by ultracentrifugation at 35,000 rpm, 22 °C, 60 min (45Ti rotor, Beckman Coulter) to collect the flocculent layer that forms above the cell pellet in Caf1 producing cells. This was resuspended in phosphate-buffered saline (PBS) (10 mM sodium phosphate, 137 mM sodium chloride, 2.7 mM potassium chloride, pH 8.0, 10 mL per flocculent). 5mg of DNase and RNase were added, and Caf1 polymer was extracted by incubation in a water bath at 48 °C for 3 h followed by overnight incubation at 22 °C, and the flocculant was collected in the supernatant from 2 x 60 min ultracentrifugation at 22 °C, 35,000 rpm (Beckman 45 Ti rotor). Extracted Caf1 polymer was washed by tangential flow filtration using a Minimate TFF 500 kDa MWCO filter (Pall) and purified using HiScreen Capto™ Core 70 columns (2 x 4.7 mL in series, GE Healthcare), with PBS as the running buffer. Polymer purity was analysed using Coomassie stained 15% SDS-PAGE.[27]

Preparation of Caf1 nanogel via direct crosslinking approach

Caf1 nanogels were obtained by reacting Caf1 polymers (0.48, 0.96 %w/v) with 4-Arm PEG-SG (5, 10 %w/v) or Glutaraldehyde (0.1, 10 %w/v). Solutions of 1 mL of Caf1 polymer and 1 mL of crosslinker were mixed at a rotation speed of 200 or 500 rpm. DLS measurement was taken at 2 h and 24 h. In addition, a control experiment was carried out to obtain the approximate size of Caf1 polymers (0.001, 0.025, 0.05, 0.1 %w/v) via DLS **(Figure S4.1)**.

Preparation of Caf1 nanogel via mini-emulsion approach

Surfactants Tween 80 (2.5 %w/v) and Spam 80 (1.2 %w/v) were added to 4 mL of hexane and swirled at 350 rpm. Surfactants were used to form a bilayer and separate the organic solvent (hexane) from the aqueous solution (PBS). Caf1 polymers (0.48, 0.96 %w/v) were dissolved in 500 μL of BPS solution mixed for 10 min. The Caf1 solution was then added to the organic solution and ultrasonicated for 5 min at 30 % power for a 9 x 3 s cycle. 500 μL of Crosslinker 4-Arm PEG-SG (5, 10 %w/v) was dissolved in 0.05 M aqueous bicarbonate solution (pH 8.5) before being added to the mixture and ultrasonicated for a further 2 x 5 min. The mixture was then stirred on the magnetic plate at 350 rpm for 24 h and purified by centrifugation at 7000 rpm for 1 min. Three washes of centrifugation were carried out to extract Caf1 nanogels, to

remove the remaining Hexane, it was resuspended in PBS and sonicated for 24 h. DLS analysed the samples.

Preparation of Caf1 nanogel via Refolded Caf1 rearrangement approach

Caf1 hydrogels were obtained by crosslinking 100 μL of Caf1 polymer (1, 2 %w/v) with 100 μL of 4-Arm PEG-SG (1, 2 %w/v). The hydrogels were heated at 100 °C for 5 min to unfold the Caf1 inter-subunit linkages and then diluted with 1800 μL of PBS. Caf1 nanogels were obtained after 24 h with mild swirling at 200 rpm. The nanogel sizes were analysed by DLS. SDS-PAGE was used to verify the presence of Caf1-PEG cross-links, and AFM was employed to visualise the size and shape of Caf1 nanogels. A control experiment was carried out to obtain the approximate size of *melt* (refolded) Caf1 polymer (0.1%w/v) at different rotational speeds (200 or 500 rpm) via DLS **(Figure S4.1)**.

Preparation of Caf1 NGMG (nanogel reformed macro-gel) hydrogel

Caf1 hydrogels were obtained by crosslinking 100 μL of Caf1 polymer (1 %w/v) with 100 μL of 4-Arm PEG-SG (1 %w/v). The hydrogels were heated at 100 °C for 5 min to unfold the Caf1 inter-subunit linkages and then diluted with 1800 μL of PBS. Caf1 nanogels were obtained after 24 h with mild swirling at 200 rpm. The Caf1 nanogels were then freeze-dried using Heto PowerDry LL3000 (Thermo) overnight to remove water content inside and outside the nanogel mixture, the freeze-dried nanogels were rehydrated in 200 μL of PBS. The newly obtained Caf1 NGMG hydrogels were allowed to be set at room temperature for 24 h before carrying out the rheological experiment. As a control, *native* Caf1 hydrogel and *melt* Caf1 hydrogel were prepared. *Native* Caf1 hydrogel was prepared by 100 μL of Caf1 polymer (1 %w/v) with 100 μL of 4-Arm PEG-SG (1 %w/v), *melt* Caf1 hydrogel was prepared in the same way using *melt* Caf1 polymers that have gone through a cycle of thermally unfolding.

Preparation of FTIC-labelled Caf1-FTIC

Caf1^{FITC} polymers were obtained by conjugating Caf1^{WT} polymers with 2 μL of FITC, 2 mL of Caf1^{WT} (1 %w/v) was dissolved in 0.05 M of bicarbonate solution (pH 8.5) and then mixed with FITC (2 %w/v) dissolved in DMSO. The resulting solution was mixed at 200 rpm overnight in an ice bath. 50 mM of ammonium chloride solution (5.88 mg)

was added to terminate the reaction. Caf1[FITC] was purified by dialysis in 500 mL PBS for 24 h before freeze-drying.

Preparation of Caf1-FITC nanogel via refolded Caf1 rearrangement approach

The Caf1-FITC nanogels were then obtained via the *refolded* Caf1 rearrangement approach, by reacting Caf1-FITC hydrogel 100 μL of Caf1-FITC polymers (1 %w/v) with = 100 μL of 4-Arm PEG-SG (1 %w/v). The hydrogels were then heated at 100 °C for 5 min to unfold the Caf1 inter-subunit linkages and then diluted with 1800 μL of PBS, the Caf1[FITC] nanogels were obtained after 24 h with mild swirling at 200 rpm. The transformation of Caf1[FITC] nanogels into Caf1[FITC] NGMG hydrogel was followed by fluorescence microscopy (0, 1, 2, 3 d), and the test samples were stored at 5 °C during the experiment.

Dynamic light scattering (DLS)

Particle sizes of the nanogels were evaluated on a Malvern Instruments Nano ZS. Data were analysed with Bruker NanoScope Analysis particle sizing software according to the Stoke-Einstein equation. The size of the particle was calculated from the absorbance intensity measured. The experiment was carried out using the low-volume disposable cuvette at the temperature of 25 °C for the duration of 10 s at the measurement position of 2 nm and a count rate of 179.2. All test sample was analysed in triplicate, stored at 5°C in between measurement.

Rheology

Rheological measurements were performed with a Discovery HR-2 rheometer (TA Instruments, USA) with a parallel plate of 20 mm diameter and a gap of 1600 μm at 25 °C. Time sweep experiments were performed at a constant frequency of 1 Hz and strain of 1.0 %.

SDS-PAGE

20 μL of Caf1 polymers (1 %w/v) and Caf1 nanogels (1 %w/v) were stained with loading dye and heated at 100°C for 5 min to depolymerise Caf1 polymer chain. The samples migrated in 15 % resolving gel under a constant voltage of 200 V for 60 min. The gel was then removed from the cassette and stained by Coomassie Blue (Generon).[27] The

gel was then destained to remove excess Coomassie Blue before being scanned (Image Lab 5.2.1, Biorad)

Atomic force microscopy (AFM)

One drop of the nanogel dispersion (~10 µL) was placed on the surface of fresh silica and air-dried at room temperature. The AFM observations were performed in tapping mode (ScanAsyst) at ultra-low force to minimise damage to the material. An isolation table/acoustic enclosure (Veeco Inc, Metrology Group) decreased vibrational noise. Silicon tips on V-shaped silicon nitride cantilevers (ScanAsyst-Air, Bruker) were used for imaging. The nominal tip radius was set to approximately 2 nm, the resonant frequency of 70 kHz, and spring constant k ~0.4 N/m. The AFM height images obtained were analysed with NanoScope Analysis 1.5 Software (Bruker).

Fluorescence microscopy

Fluorescence images of Caf1^{FITC} nanogels and Caf1^{FITC} NGMG hydrogels were captured using Zeiss Axiskop 2 Plus. Images of the sample were taken at 0, 1, 2, and 3 d stored at 5°C between image taken.

4.7. References

1. Neamtu, I., Rusu, A. G., Diaconu, A., Nita, L. E. & Chiriac, A. P. Basic concepts and recent advances in nanogels as carriers for medical applications. Drug Deliv 24, 539–557 (2017).
2. Liu, P., Pearce, C. M., Anastasiadi, R. M., Resmini, M. & Castilla, A. M. Covalently crosslinked nanogels: An NMR study of the effect of monomer reactivity on composition and structure. Polymers (Basel) 11, (2019).
3. Yallapu, M. M., Jaggi, M. & Chauhan, S. Design and engineering of nanogels for cancer treatment. Drug Discov Today 16, 456–463 (2011).
4. Buwalda, S. J., Vermonden, T. & Hennink, W. E. Hydrogels for Therapeutic Delivery: Current Developments and Future Directions. Biomacromolecules 18, 316–330 (2017).
5. Hamidi, M., Azadi, A. & Rafiei, P. Hydrogel nanoparticles in drug delivery. Adv Drug Deliv Rev 60, 1638–1649 (2008).
6. Sung, B., Kim, M. H. & Abelmann, L. Magnetic microgels and nanogels: Physical mechanisms and biomedical applications. Bioeng Transl Med 6, 1–18 (2021).
7. Akiyama, E. et al. Self-assembled nanogels of cholesteryl-modified polysaccharides: Effect of the polysaccharide structure on their association characteristics in the dilute and semidilute regimes. Biomacromolecules 8, 2366–2373 (2007).
8. Dorwal, D. Nanogels as novel and versatile pharmaceuticals. Int J Pharm Pharm Sci 4, 67–74 (2012).
9. Vashist, A. et al. Chapter 1: Journey of Hydrogels to Nanogels: A Decade after. RSC Smart Materials 1–8 (2018) doi:10.1039/9781788010481-00001.

10. Akiyoshi, K., Deguchi, S. & Moriguchi, N. Self-Aggregates of Hydrophobized Polysaccharides in Water. Formation and Characteristics of Nanoparticles. Macromolecules 26, 3062–3068 (1993).

11. Vinogradov, S., Batrakova, E. & Kabanov, A. Poly(ethylene glycol)-polyethyleneimine NanoGel(TM) particles: Novel drug delivery systems for antisense oligonucleotides. Colloids Surf B Biointerfaces 16, 291–304 (1999).

12. Zeb, A. et al. Potential and applications of nanocarriers for efficient delivery of biopharmaceuticals. Pharmaceutics vol. 12 (2020).

13. Sharma, A. et al. Nanogel - An advanced drug delivery tool: Current and future. Artif Cells Nanomed Biotechnol 44, 165–177 (2016).

14. Campos, M. P. et al. Growth kinetics determine the polydispersity and size of PbS and PbSe nanocrystals. Chem Sci 13, 4555–4565 (2022).

15. Lovell, P. A. & Schork, F. J. Fundamentals of Emulsion Polymerization. Biomacromolecules 21, 4396–4441 (2020).

16. Siegwart, D. et al. Cellular uptake of functional nanogels prepared by inverse miniemulsion ATRP with encapsulated proteins, carbohydrates, and gold nanoparticles. Biomacromolecules 10, 2300–2309 (2009).

17. Hamzah, Y. et al. Synthesis of polyethylene glycol diacrylate nanogel using irradiation of inverse micelles technique. e-Polymers 12, (2012).

18. Asua, J. M. Miniemulsion polymerization. Progress in Polymer Science (Oxford) 27, 1283–1346 (2002).

19. Waksman, G. & Hultgren, S. J. Structural biology of the chaperone– usher pathway of pilus biogenesis. Nat Rev Microbiol. 2 7, 765–774 (2010).

20. Giessibl, F. J. Advances in atomic force microscopy. Rev Mod Phys 75, 949–983 (2003).

21. Nakajima, T. et al. True chemical structure of double network hydrogels. Macromolecules 42, 2184–2189 (2009).

22. Kharkar, P. M., Kiick, K. L. & Kloxin, A. M. Designing degradable hydrogels for orthogonal control of cell microenvironments. Chem Soc Rev 42, 7335–7372 (2013).

23. Zhao, F. et al. Composites of Polymer Hydrogels and Nanoparticulate Systems for Biomedical and Pharmaceutical Applications. Nanomaterials 5, 2054–2130 (2015).

24. Takahashi, S. et al. The RGD motif in fibronectin is essential for development but dispensable for fibril assembly. Journal of Cell Biology 178, 167–178 (2007).

25. Hsiao, L. W. et al. Cross-linked polypeptide-based gel particles by emulsion for efficient protein encapsulation. Polymer (Guildf) 115, 261–272 (2017).

26. Wang, Y., Tu, S., Pinchuk, A. N. & Xiong, M. P. Active drug encapsulation and release kinetics from hydrogel-in-liposome nanoparticles. J Colloid Interface Sci 406, 247–255 (2013).

27. Dura, G., Waller, H., Gentile, P., Lakey, J. H. & Fulton, D. A. Tuneable hydrogels of Caf1 protein fibers. Materials Science and Engineering C 93, 88–95 (2018).
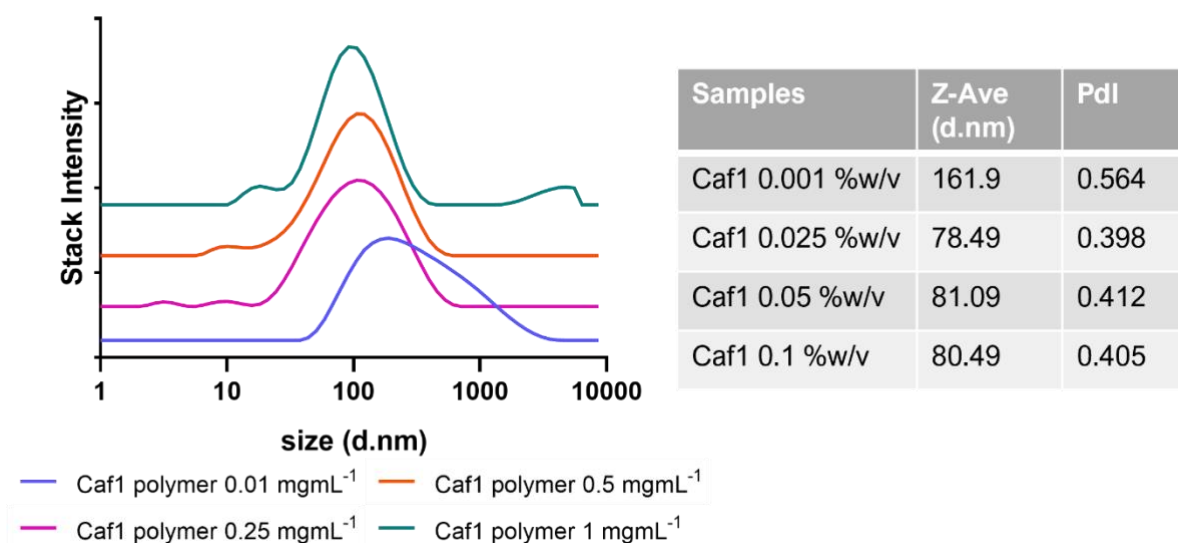
4.8. Appendix C

Samples	Z-Ave (d.nm)	PdI
Caf1 0.001 %w/v	161.9	0.564
Caf1 0.025 %w/v	78.49	0.398
Caf1 0.05 %w/v	81.09	0.412
Caf1 0.1 %w/v	80.49	0.405

Figure S4.1, Figure S4.1, Size distribution of Caf1 polymers chain (0.01, 0.25, 0.5 and 1 %w/v) in PBS, plotted as intensity vs size.

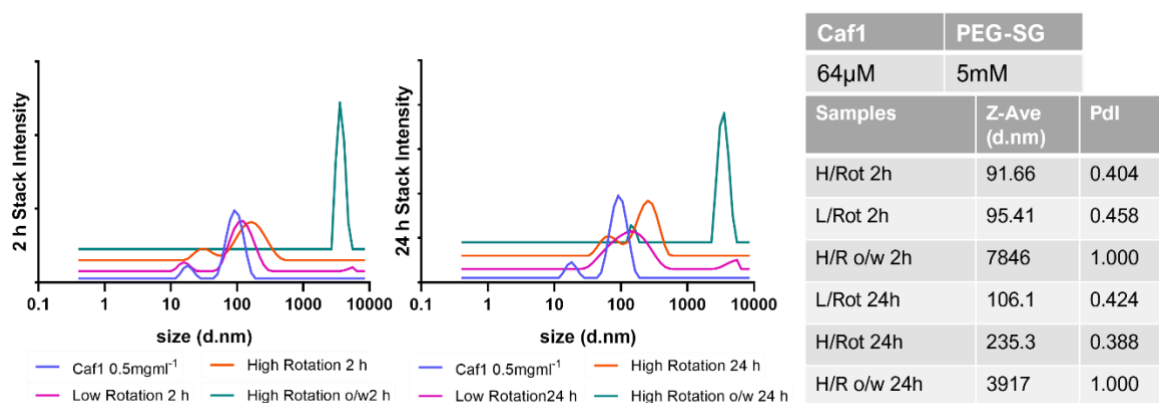| Caf1	PEG-SG	
64µM	5mM	
Samples	**Z-Ave (d.nm)**	**PdI**
H/Rot 2h	91.66	0.404
L/Rot 2h	95.41	0.458
H/R o/w 2h	7846	1.000
L/Rot 24h	106.1	0.424
H/Rot 24h	235.3	0.388
H/R o/w 24h	3917	1.000

Figure S4.2, Figure S4.2, Size distribution of Caf1 nano- and mini-gels formed from Caf1 polymer (64 μM) with PEG-SG (5 mM) in PBS, plotted as intensity vs size. DLS measurement of samples from high (500 rpm) and low (200 rpm) rotation speed, and sample formed in mini-emulsion (o/w). Z-average was recorded, and the PdI value was determined shown in the table. Two DLS measurements were measured at 2 h and 24 h for all samples.

Caf1	PEG-SG	
32µM	2.5mM	
Samples	**Z-Ave (d.nm)**	**PdI**
H/Rot 2h	87.54	0.463
L/Rot 2h	123.0	0.345
H/R o/w 2h	1.479e5	1.000
L/Rot 24h	143.9	0.478
H/Rot 24h	100.4	0.548
H/R o/w 24h	1.230e5	1.000

Figure S4.3, Size distribution of Caf1 nano- and mini-gels formed from Caf1 polymer (32 µM) with PEG-SG (2.5 mM) in PBS, plotted as intensity vs size. DLS measurement of samples from high (500 rpm) and low (200 rpm) rotation speed, and sample formed in mini-emulsion (o/w). Z-average was recorded, and the PdI value was determined shown in the table. Two DLS measurements were measured at 2 h and 24 h for all samples.
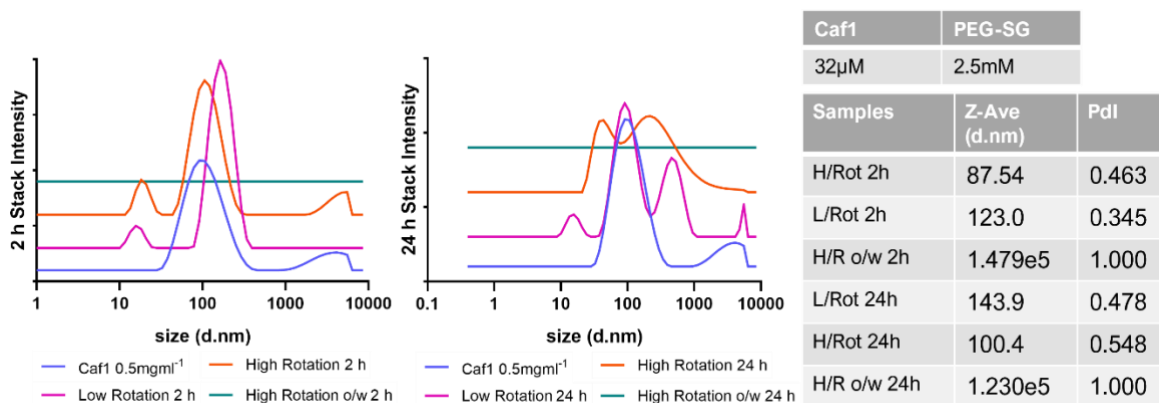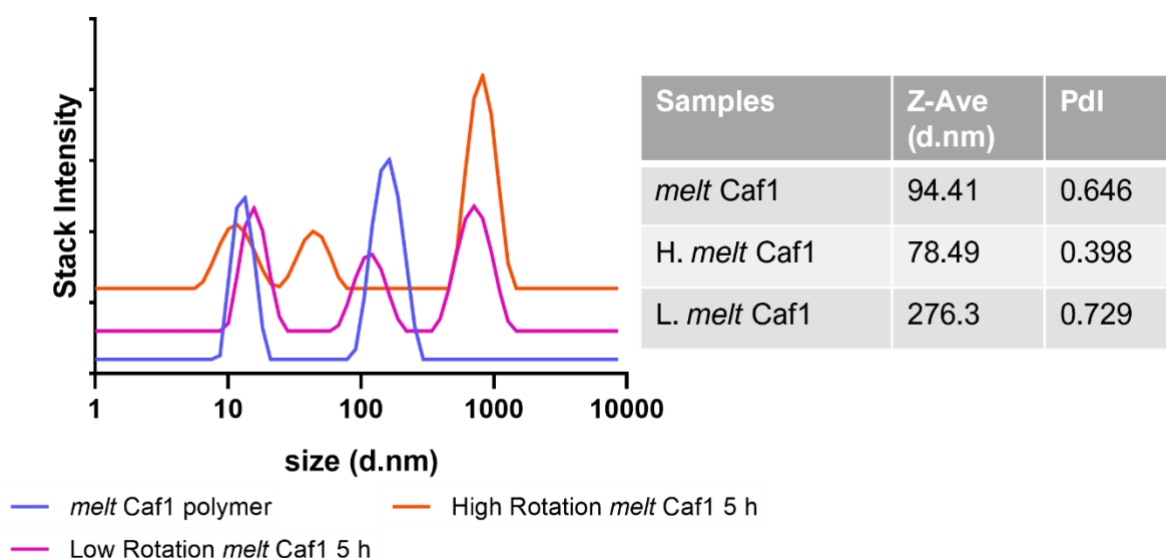

Samples	**Z-Ave (d.nm)**	**PdI**
melt Caf1	94.41	0.646
H. *melt* Caf1	78.49	0.398
L. *melt* Caf1	276.3	0.729

Figure S4.4, Size distribution of refolded (melt) Caf1 polymers chain (1 %w/v) in PBS plotted as intensity vs size. DLS measurement of refolded (melt) Caf1 polymers chain after 4 d, at low rotation speed (shear) (200 rpm) and high rotation speed (shear) (500 rpm) after 5 h.

Chapter 5
Research Outlook

Great progress has been made in the development of Caf1 polymer for drug delivery applications. This thesis explores the different aspects of Caf1 protein polymer to formulate chemically crosslinked hydrogel for drug delivery. In chapter 2, drug release kinetic and the mechanic of cargo release from crosslinked hydrogel were studied. The work showed small and large molecules released from the Caf1 hydrogels are diffusion-controlled biphasic release, where model drug molecules are released initially from the hydrophilic domains then followed by those in the hydrophobic domains of the gel matrix. By utilising the reversible nature of Caf1 proteins a new drug loading "*melt*" approach was developed, which has shown great efficiency in encapsulation of large biomolecules. Further, this work has demonstrated it is possible to achieve the desired release rate by altering the crosslink density. Chapter 3 demonstrates how disulfide bonds were incorporated into Caf1^{Cys} hydrogels, which triggered a stimuli-response in the presence of the reducing agent GSH, and hence a faster release rate was observed. Moreover, the mechanical properties of Caf1^{Cys} hydrogel can be improved by using the "blending" approach to form *mosaic* Caf1$^{Cys:WT}$ hydrogel. The formulation of chemically crosslinked Caf1 nanogel were investigated in Chapter 4, the nanogels formed using "refolded Caf1 rearrangement approach" were monodisperse in population and were stable over a period of 216 h. These nanogels possess a property to reform into a microscopic Caf1 (NGMG) hydrogel by accessing the vacant Caf1 C-terminal which would compile with the nearby donor strand. It is hypothesised that this Caf1 nanogel can be used for cell encapsulation by modifying Caf1 protein with RGDS group and later forming a film of Caf1 NGMG hydrogel.

This work act as a building block for future work in drug delivery application with key fundamental findings showcasing drug loading, release kinetics and hydrogels formation, from nanogel to stimuli-responsive of macroscopic Caf1 hydrogels.